NUMERICAL AND EXPERIMENTAL STUDY OF FLASH EVAPORATION PHENOMENON AND RESULTING SHOCK WAVE

By

Ahmad Mansour

A DISSERTATION

Submitted to
Michigan State University
in partial fulfillment of the requirements
for the degree of

Mechanical Engineering - Doctor of Philosophy

2020

ABSTRACT

NUMERICAL AND EXPERIMENTAL STUDY OF FLASH EVAPORATION PHENOMENON AND RESULTING SHOCK WAVE

By

Ahmad Mansour

Flash evaporation or flashing is an evaporation phenomenon caused by a sudden pressure drop sufficiently below the saturation pressure. Due to this sudden drop in pressure, the liquid undergoes a quick phase transition, and the sensible heat of the liquid converts into latent heat of evaporation. An accidental release of pressurized liquid from supply pipelines or liquid storage tanks can generate a flashing jet with violent phase change. This fast phase change can cause rapid mixture with an oxidant like air, and if the liquid is flammable, disastrous effects such as explosions, fires, and damage to industrial equipment can occur. On the other side, flash evaporation can be beneficially employed in industrial applications. It can have a significant effect on the performance of many devices (e.g. injectors and reactors). The understanding of the fluid behavior of the flash evaporation and the resultant shock waves can help to prevent disastrous consequences that may occur due to accidental fluid release as well as can be useful to further develop the phenomena's industrial and technological applications such as utilize resulting shock waves in creating useful compression.

This work investigates spray flashing evaporation phenomena and resulting shock waves experimentally and numerically, considering superheated liquid water as working fluid. 2D transient Ansys Fluent simulation was utilized to present and prove the occurrence of shock waves generated by a flashing water jets when superheated water is injected through a nozzle into a low-pressure water vapor zone. The Mixture model was applied using the concept of slip velocities to model multiphase flows as non-homogeneous multiphase model where the phases (liquid water

and water vapor) move at different velocities. In addition, a rectangular vacuum chamber connected to a circular nozzle was used in the experiments. A z-type Schlieren technique with a Photron high-speed camera was used to observe the propagation of the moving shock wave and the flow. The numerical simulation results show that once the superheated water is injected in the low-pressure environment, the flashing phenomenon occurs, and a shock wave is induced. This shock wave is a moving shock wave, and it travels forward into the vacuum chamber. The two-phase mixture expands behind the moving shock wave that travels faster into the water vapor. The entire flow characteristics such as pressure, velocity, Mach number, speed of sound, density, and volume fraction are discontinuous across the shock wave. After the moving shock wave strikes the end of the vacuum chamber, it reflects from the wall as reflected shock wave that propagates back into the chamber, further increasing the pressure behind it.

An experimental work was carried out with injected liquid water having an initial temperature ranging between 40 and 100°C and vacuum pressure ranging between 4000 Pa and 10000 Pa. To show the shock wave structure, the Schlieren technique was used and Schlieren photographs were mathematically filtered using the Image Processing and Analysis in Java (ImageJ). The experimental results were in good agreement with the numerical results, confirming that once the superheated water is injected in the vacuum chamber, it flashes directly and can induce a shock wave. The results confirm that with increasing superheat of the injected water, the flash evaporation accelerates. At low vacuum pressure, full flashing occurs, and a shock wave is induced especially with a high initial liquid temperature.

ACKNOWLEDGMENTS

In the name of Allah, the most merciful, the most beneficent. All the thanks be to Allah, the Lord of the universe. I would like to thank almighty Allah for giving me the blessing, strength, knowledge, ability, and opportunity to undertake this dissertation.

I would like to express my deep sense of gratitude and indebtedness to my advisor, Prof. Norbert Mueller, for providing me the opportunity and guidance throughout my PhD study. His keen interest and personal involvement during this study is beyond words of gratitude.

Many thanks go to Prof. Charles Petty, Prof. Abraham Engeda, and Prof. Neil Wright for their helpful criticisms and suggestions as members of the supervisory committee.

I gratefully acknowledge Sebha University and the Ministry of Higher Education in Libya for the unique opportunities given to me, allowing me to pursue my PhD degree.

I would like to express my thanks to other individuals who contributed, in some way, to the completion of this research especially my colleagues in the Turbomachinery Lab at Michigan State University.

My deepest thanks go to my family members. Words cannot express how grateful I am to my father, my mother, brothers, and sisters whose dreams for me have resulted in this achievement. Without their love, support, and encouragement, I would not have been where I am today. May Allah bless them all.

I would like to express my indebtedness, appreciation, and gratitude to my great companion my beloved wife, who has contributed to this dissertation an enormous amount of love, support, and sacrifice. For this, I will always be grateful. She has stood by me as my best friend and loved, supported, encouraged, entertained, and helped me get through this difficult time in the most

positive way. I ask Allah to reward her the best in this life and in the hereafter. Last but not least, I would like to acknowledge the patience of my beloved daughter Meral, and my sons Moaad and Mohamed, for their smile, moral support, and endless love that kept me going.

TABLE OF CONTENTS

LIST OF FIGURES

KEY TO SYMBOLS

P	Pressure $[Pa]$
P_i	Initial condition $[Pa]$
T	Temperature $[k]$
T_i	Initial temperature $[k]$
A	Area $[m^2]$
r	Radius $[m]$
$\vec{v}$	Velocity $[m/sec]$
$\vec{v}_m$	Mass-averaged velocity $[m/sec]$
$\vec{v}_k$	velocity of phase k $[m/sec]$
$\vec{v}_{dr,k}$	Drift velocity for secondary phase k $[m/sec]$
$\vec{v}_l$	Liquid velocity $[m/sec]$
$\vec{v}_l$	Vapor velocity $[m/sec]$
$\vec{v}_{lv}$	Relative or the slip velocity $[m/sec]$
M	Mach Number
s	Speed of sound $[m/sec]$
n	Number of phases
$\vec{a}$	secondary-phase particle's acceleration $[m/sec^2]$
d_v	diameter of the particles (or droplets or bubbles) of secondary phase $[mm]$
$\vec{g}$	Gravity acceleration $[m/sec^2]$
f_{drag}	drag function

k_{eff}	The effective conductivity [w/m. k]
k	Thermal conductivity [w/m. k]
k_t	Turbulent thermal conductivity [w/m. k]
$E_k = h_k$	The sensible enthalpy for an incompressible phase k [j/kg]
S_E	volumetric heat sources $[m^3/sec]$
c	specific heat capacity, with unit [j/kg. k]
ρ_m	mixture density $[kg/m^3]$
ρ_k	Density of phase k $[kg/m^3]$
ρ_v	Density of vapor $[kg/m^3]$
ρ_l	Density of liquid $[kg/m^3]$
$\dot{m}$	Mass transfer rate $[kg/m^3 s]$
α	volume fraction
α_k	volume fraction of phase k
α_l	Liquid volume fraction
α_v	Vapor volume fraction
μ	Viscosity $[kg/m.sec]$
μ_m	Viscosity of the mixture [kg/m. sec]
μ_l	Viscosity of the liquid [kg/m. sec]
μ_v	Viscosity of the vapor [kg/m. sec]
ε	dissipation rate
τ_{lv}	Particulate relaxation time $[sec]$

CHAPTER 1

Flash evaporation phenomenon

1.1 Introduction

Flash evaporation is a phase change phenomenon observed when a liquid is exposed to a sudden pressure drop below its saturation pressure. Flash evaporation, often called flashing phenomenon, is sometimes caused by a large pressure difference between upstream and downstream when pressure decreases suddenly where the liquid temperature at the upstream is kept constant before the evaporation begins. Therefore, the liquid temperature becomes higher than the saturation temperature; thus, evaporation of the liquid occurs. During a sudden drop in pressure, the liquid undergoes a fast phase transition process and the sensible heat of the liquid converts into the latent heat of vaporization [1]. This fast phase change could happen inside the fluid released generating a flashing jet that could produce destructive consequences, such as explosions, fires, damage to industrial equipment, or toxic exposure in the environments [2, 3, 4, 5, 6]. In addition, it may also be a source of intense noise as the flashing mechanisms occurs in the expansion devices of refrigeration cycles [7]. On the positive side, flashing jets or spray systems can be useful for industrial and technological applications. For example, by using water as a working fluid, NASA has been developing an open-loop spacecraft spray evaporative heat sink for use in space [8]. In addition, flashing is used in geothermal power plants to produce steam, which is used to power the turbines. The flash steam power plant illustrated in Figure (1.1) is the most common type of power plant that utilizes hot liquid water to produce the steam. By pumping this hot water under high pressure from the ground to the plant on the surface, where the pressure is suddenly reduced and with this the boiling point, which causes flash evaporation of the hot water into steam, which in turn is used to drives the turbine connected to a generator generating electricity [9]. The flashing phenomenon is used in many chemical plants and biochemical industry, such as absorption, oxidation. It also has a significant effect on the performance of many

devices like the expansion devices of refrigeration cycles and injectors [10, 11]. In addition, flash evaporation is also one of the main processes in the production of alumina where after dissolution the slurry is processed through pressure and temperature reduction in the flash vessel [12].

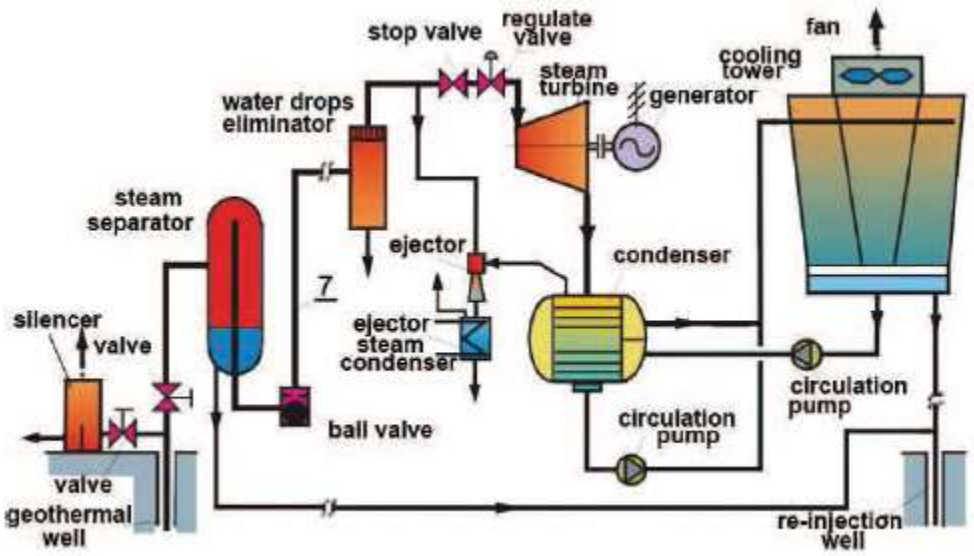

Figure 1.1 Schematic diagram for the single flash steam power plant system with condensing turbine.

There are many useful industrial applications of flash evaporation, including the steam generation processes, chemical processes, and water desalination for drinking water [13, 14, 15, 16, 17, 18]. Desalination is the process used to produce fresh water for drinking from salty water, where fresh water is separated from brine through flash evaporation. About 20% of desalinated water production worldwide is produced from a Multiple-Stage Flash desalination plant (MSF), which may reach up to 20 stages or more [19]. The hot steam from a steam generator powers a brine heater before the first stage to heat the liquid to the desired inlet temperature. The higher the temperature, the higher is the distillation rate, and a larger amount of vapor can be extracted from the brine. In MSF, the pressure in each stage is maintained below the corresponding saturation temperature of the heated brine. When the heated brine enters the stage, its temperature falls below

the saturation temperature at that pressure and the flash evaporation occurs separating the fresh water from the brine. The unflashed brine passes from one stage to the next stage for further flashing so that the brine can be evaporated repeatedly without adding more heat [19, 20, 21]. Figure (1.2) shows a schematic of a first MSF stage that contains a brine heater, a demister to minimize carryover of brine droplets into the distillate, and a distillate tray that collects the produced distillate in each stage which is the then cascaded from stage to stage in parallel with the brine and pumped into a storage tank.

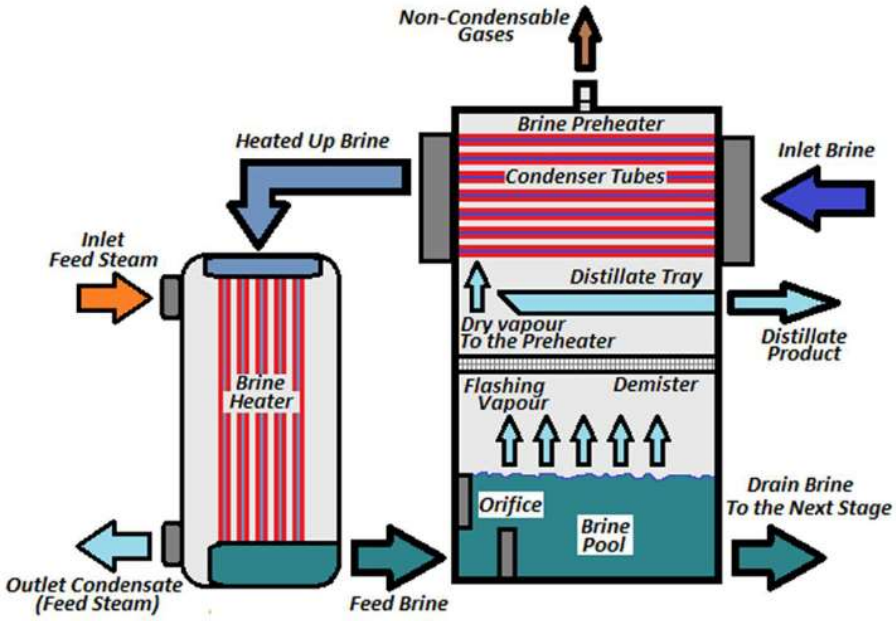

Figure 1.2 Scheme of a first MST stage and brine heater.

Zheng et al. [10] examined the flashing phenomenon of a LiBr-H2O solution in the generator of an absorption heat pump experimentally where the flashing phenomenon is used as an alternative to generators in these types of heat pumps. During evaporation, the solution does not transfer heat with the environment or the surroundings, only the enthalpy difference of the solution changes into the latent heat of the water vapor. In other words, the flashing evaporation is regarded as an adiabatic process.

Boile et al. [22] carried out an experimental study on the Crosby safety valve analyzing flows of flashing hot water at 150.7^oC and non-flashing cold water at 17.5^oC through the safety relief valve. In their experiments, the mass-flow rates, the inlet and outlet temperatures, and the pressure distributions inside the valve were measured. They conducted two series of experiments: testing in the first series a Crosby safety valve, and in the second series a model that enables the measurement of the pressure distribution inside the valve body. The experimental results were compared with the equilibrium and relaxation two-phase flow models, assuming adiabatic flow. The mass flow rate is given as a function of the square root of pressure difference between the inlet and the outlet of the valve. The results show that the mass flow rate for supercritical flow is an increasing function of the pressure difference between the inlet and the outlet of the valve. For hot water, the mass flow rate is limited by choking, while the discontinuity for the cold water is a result of cavitation. According to the homogeneous relaxation model, the flashing water flows were choked exactly at the moment they reached the saturation pressure [22, 23]. Boile et al. [22] found that the possible-impossible flow procedure is a suitable method for calculating the choked two-phase and that the frictionless Bernoulli equation for the nozzle cross-section area gives a good estimation for the non-flashing cold-water flow through the safety valve tested.

Boccardi et al. [24] presented a study on a commercial safety relief valve for the steam-water flashing system. This study was carried out with varying values of operating parameters such as vapor quality, inlet pressure, mass flow rate, and backpressure. The measured data was compared with the predictions of a commonly used homogeneous equilibrium model and the ω method. The homogeneous models assume the hypothesis of thermal equilibrium where the two phases travel at same velocity. For flashing systems, the physical properties of the mixture depend on the temperature and pressure conditions. For non-flashing systems, the two phases have the

same temperature, which means no mass transfer between the phases. If no heat transfer between the phases is assumed, then the flow is called frozen flow. The ω method is a further developed form of the Homogeneous Equilibrium Model (HEM) and one of the best methodologies for analyzing two-phase flow in relief devices. This method can be applied to both flashing (choked or not choked flows) and non-flashing systems.

1.2 Flashing

Flashing is a phenomenon that occurs often when liquid flows through nozzles working at either high temperatures or large pressure drops. Flashing starts when the temperature increases by a few degrees above the saturation temperature or an initially subcooled liquid may become saturated if the pressure drop is large enough to reduce the substance pressure below the saturation pressure corresponding to its temperature. Both results in the formation of a large number of bubbles, which may grow rapidly in both number and size [25]. In fact, the disintegration of a fully flashing jet is characterized by an abrupt phase transition (liquid to gas) through the process of a bubble nucleation and growth. Physical aspects involved in the flashing process include atomization, nucleation, phase change, internal two-phase flow, droplet size, and velocity.

1.2.1 Atomization

Atomization is the process of transforming a liquid bulk into small droplets, e.g. when a liquid jet flows through a nozzle into a low-pressure environment below its saturation pressure. Violent and explosive characteristics of the jet cause its break-up into smaller droplets. One of the key processes affecting spray behavior is atomization, as it is a key element in the successful combustion of liquid fuels and important in other applications of sprays, such as the coating and the painting. Atomization of a liquid jet is considered a two-stage process: an essential breakup

where the jet breaks up into large drops and a secondary breakup where the large drops break up further into smaller drops [25, 26, 27, 28].

1.2.2 Nucleation

The bubble nucleation process can be categorized into two combinations: homogeneous and heterogeneous nucleation. In homogeneous nucleation, bubbles form everywhere inside the liquid when a liquid is heated to the metastable state, or when the liquid droplets are formed in super-cooled metastable vapor. However, in heterogeneous nucleation, bubbles form on the interfacial regions between the liquid and another, normally solid [29, 25, 30]. In many cases, the nucleation in a superheated liquid at metastable state is more likely to occur adjacent to the solid surface of the container, depending on the condition of the fluid and solid surface. Experimental investigations of fully flashing jets proved that the nucleation rate increases with the superheat level [31].

1.2.3 Phase Change

When liquid is exposed to a sudden pressure drop, the liquid goes through a metastable state and then undergoes a fast phase transition process. The bubbles form inside the liquid consuming latent heat, which is provided by the surrounding fluid and cools down the fluid. This process continues until the temperature of the liquid equals the saturation temperature of the liquid at its pressure.

1.2.4 Bubble growth in a Superheated Liquid

For several years, considerable effort has been devoted to studying the growth of bubbles in a superheated liquid. It is part of the process of nucleate boiling and it is also related to depressurization (flashing) processes. Plesset et al. [32] presented discussion of the flow of a liquid (water) over a submerged body at rest. They divided the liquid flow over a body into three regimes,

namely: noncavitating flow, cavitating flow with a relatively small number of cavitation bubbles in the flow field, and cavitating flow with a single large cavity about the body. Aktershev and Ovchinnikov [33] presented a numerical simulation of the growth of a vapor bubble in a nonuniformly superheated liquid. They show that the bubble growth rate due to the nonuniform temperature of the liquid is faster than the case of the uniform superheating. Where the bubble growth rate decreases because of the nonuniform temperature. Numerical results were compared with experimental data for the growth of a vapor bubble near a cylindrical heater [34] and it was in good agreement at the initial stage of the vapor bubble growth under strong superheating.

A bubble can grow in two ways: the first is inertia-controlled growth and the second is heat transfer controlled growth [29, 35]. In the first process, the pressure inside the bubble is high enough that it can increase the bubble size by pushing the liquid aside. The second growth occurs when the heat from surrounding liquid is transferred to the liquid adjacent to the interfacial region of the liquid and vapor and changes the phase of liquid to vapor. By applying the pressure balance at the bubble interface, the equilibrium bubble size can be determined. Ashgriz [25] and Carey [36] presented the Gibbs–Duhem equation and the Young–Laplace equation for the bubble. They assumed the liquid is incompressible and inside the bubble the vapor temperature is uniform, and the vapor is an ideal gas. The bubble growth continues until evaporation at the interface stops and while the bubble grows the pressure difference between the inside and the outside of the bubble reduces [25].

1.2.5 Drop Size Distributions

The drops are described by their composition, velocity, temperature, and diameter, which are the most common quantities for different methods like discrete probability function (DPF), maximum entropy formalism (MEF), and others. The mean drop size and the drop size distributions are

important for spray applications. Some spray applications such as paint and respirable sprays require narrow size distributions, while some need wide ones such as gas turbine engines [25, 37]. The liquid properties such as viscosity, surface tension, and density are main factors influencing the mean drop size. With increasing liquid viscosity and surface tension, the mean drop size of the spray increases [38]. Van Der Geld and Vermeer [39] derived drop size distributions in sprays using MEF and investigated satellite formation. They were the first to point out that the Shannon entropy is not the proper measure if the drop volume is used instead of drop diameter. Christophe [40] suggested a new formulation of MEF by considering the disagreements of previous MEF to model and determine liquid spray drop size distribution. Kamoun et al. [31] investigated fully flashing superheated liquid ethanol jets injected into a vacuum chamber. They presented the axial and the radial distribution of the droplet size considering the limits of applicability of The Global Rainbow Thermometry (GRT) technique. They concluded that with increasing superheat level, the average droplet diameter decreases. Their findings are consistent with the experimental results of Cleary et al. [3]. Their findings also showed that the bubble nucleation controls the onset of the full flashing and the initial spreading of the jet. In addition, the experimental data for velocity and temperature showed that nucleate boiling mainly controls the properties of the two-phase flow and the atomization that takes place near the nozzle exit. The experimental data illustrated that the high velocity is due to bubble bursting or because of a choking condition at the nozzle outlet.

1.3 Research Objective

This research is a contribution to the ongoing discussions about flashing evaporation phenomena and generating shock waves from this phenomena by using water as a working fluid. This dissertation is dedicated to the investigation of the flash evaporation phenomenon that occurs when superheated water is injected into a vacuum chamber through a nozzle. The main aim is an

investigation of the generation of shock waves by spray flash evaporation process experimentally and numerically. The research presents shock waves as one of significant consequences that can be produced in flashing evaporation and utilization of those resulting shock waves in creating useful compression.

1.4 Dissertation Outline

This dissertation presents an experimental and numerical simulations conducted to understand more about flashing evaporation phenomenon and the induced shock waves.

- Chapter 2 presents an overview of the methods of generating flashing phenomena and resulting shock wave and presents the previous studies about it.
- Chapter 3 the dissertation provides the governing equations and 2D simulation methodology and the experiments boundary conditions.
- Chapter 4 presents the discussion of the 2D numerical simulation results and shows the flashing phenomenon, resulting shock wave, and reflected shock wave.
- Chapter 5 presents the experimental setup, experimental apparatus and procedure, and the discussion of the experimental results.
- Chapter 6 gives the conclusions from this work.

CHAPTER 2

Literatures Review

2. 1 Methods of generating flashing phenomena

Significant flashing can occur in different natural and technological circumstances. One of the flash evaporation methods is liquid pool flashing, where the bubbles rise in the liquid to break through the free surface of it. Another method is injecting a liquid jet through a nozzle into a vacuum chamber, so a spray forms with an unsteady turbulent motion of liquid droplets. In addition, the flow of air or gas over a liquid surface can also generate a flash spray when the relative velocity is high enough to reduce the static pressure sufficiently. In this review, several theories, experiments, and numerical methods are displayed to explain flash evaporation phenomena and their consequences.

2.2 Flash evaporation from a liquid pool

Over years, considerable efforts were invested in studying the flash evaporation phenomenon in a liquid pool. Saury et al. [41] studied experimentally the impact of the initial water level in the flash chamber and the depressurization rate on the flash evaporation. They carried out experiments with initial liquid temperature from 45 to 85 ^{o}C, superheats between 2 and 44 K, and an initial water height ranging from 25 to 250 mm. The study focused on the impact of initial water height on the characteristics of the flash evaporation such as the flashing time and the mass evaporated. The water mass evaporated is calculated based on an energy balance on the liquid in the flash chamber. The results show that a smaller flashing time is obtained when the rate of depressurization increases. The final mass evaporated through flashing was almost independent of the depressurization rate and was an increasing function of the initial water level and initial temperature.

In order to point out the effect of the initial height of liquid on the flash evaporation, Liao et al. [42] have proposed a quantitative method based on the temperature measurement of the water

and energy balance in the liquid. Experimentally and numerically, they investigated flash evaporation of water inside a vertical pipe under different pressure levels (10, 20, 40, and 65 bar). According to the experimental results and from comparison with simulated results, it was found that the evaporation rate was too small and flashing begins too late when the mean bubble diameter was larger than the critical value (critical bubble diameter that can succeed in initiating the flashing). In addition, the critical bubble size decreases with the increase of pressure, which means that bubble growth has a minor effect under high-pressure conditions. These results are in a good agreement with Guo et al. [43], Ghiaasiaan [29], and Liao and Lucas [44]. Furthermore, with the increase of absolute pressure, the total steam or vapor generation rate compared to the contribution of nucleation becomes significant [42, 45]. The experimental data showed a maximum steam volume fraction achieved at 10 bars. Whereas, the maximum superheat degree was the same in all the cases with the pressure varied from 10 to 65 bar [42]. Other research studied the functioning of a flash evaporator using flow rates and temperatures defined on real number intervals. The study focused on the thermodynamic aspects of the process using cascade evaporation. A constraint satisfaction problem solver (CSP) involving the global physical model of the two-stage flash evaporator was used in this study [46].

Cheng et al. [47] presented a mathematical model of vacuum flash evaporation cooling (VEFC) where pure water was the working fluid. This model considered both droplet flash and film flash to show the effect of droplet flash evaporation on vacuum flash evaporation, heat transfer ratio, and heat flux density. The mathematical model is validated by experimental results in this study. The results proved that one of the main factors affecting the VFEC heat transfer performance is the droplet flash, which has a great effect on the spray characteristics. When droplet flash is taken into consideration, the heat flux increases while the surface temperature decreases. By

comparing the results in this paper with the previous experimental results, it was found that the effective conductivity model of droplet flash coincides well [47]. Liu et al. [48] investigated experimentally flash evaporation of saltwater (NaCl) droplets released into a vacuum. The experiment's data showed that the shape variation of the droplet is related to the component and solution concentration. It proves that the evaporation rate decreases with increasing salt concentration in water. The experimental results also showed that the droplet temperature transition is affected by initial droplet diameter, environmental pressure, and initial droplet temperature. This is because the evaporation rate becomes faster and the molecular motion is more intensive with a higher initial droplet temperature and with a smaller initial droplet size [48, 49, 50]. Furthermore, Deb et al. [51] studied the effect of evaporation and condensation on droplet size distribution in turbulence. They reported that the temperature evolution of the droplet is influenced both by the local temperature difference to the gas and change in mass of the droplet due to phase change.

Saury et al. [52] carried out an experimental study of the flash evaporation phenomena of a water film with an initial water height of 15 mm, initial pressure between 50 and 200 mbar, and initial temperatures from 30 to 75oC. Figure (2.1) illustrates the experimental setup. The experiments specified the initial temperature of the liquid and superheat that influenced the flash evaporation. They concluded that increasing the superheat leads to an increase of the mass flow rate and the violence of the flashing phenomenon; also, the mass flow rate decreased with increasing initial pressure [52, 53, 54].

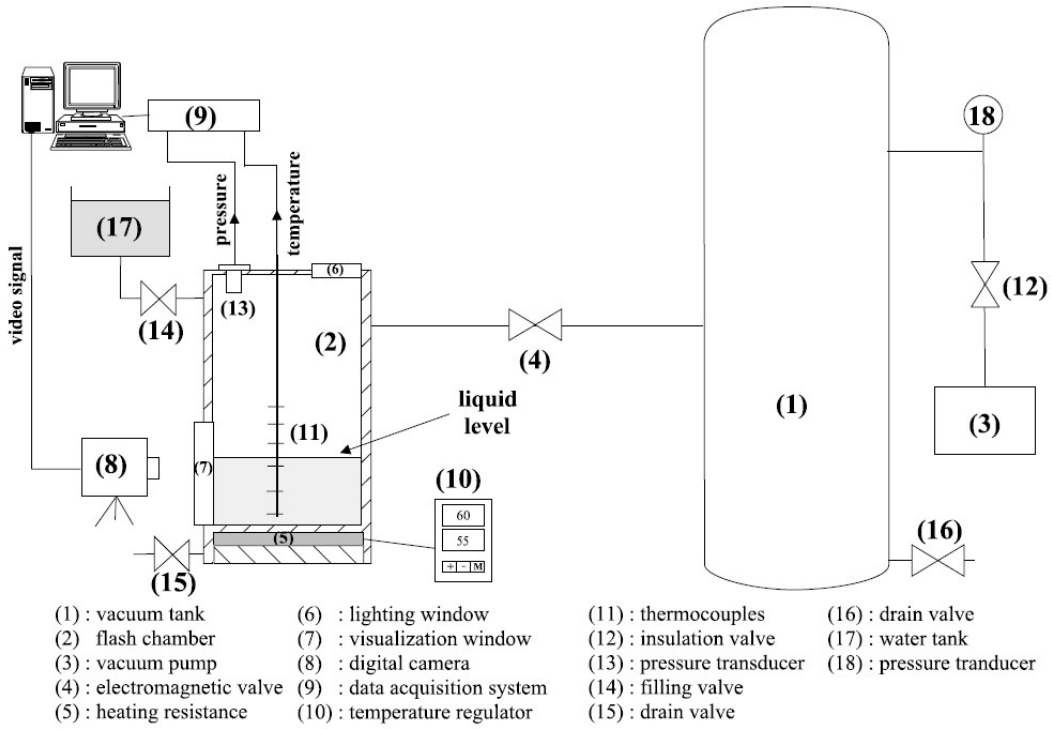

Figure 2.1 Experimental setup of flash evaporation.

Zhang et al. [55] studied experimentally the energy transformation and separation characteristic of circulatory flash evaporation. They introduced the steam-carrying ratio and the flash evaporation efficiency to estimate the energy transformation. The flash evaporation efficiency is defined by equation (2.1).

$$\eta = \frac{1}{1 - J_a.\,\mathrm{NE}F}(1 - \mathrm{NE}F) \tag{2.1}$$

$$\mathrm{NE}F = \frac{\mathrm{T}_{out} - \mathrm{T}_s}{\mathrm{T}_{in} - \mathrm{T}_s}, \qquad J_a = \frac{C_\mathrm{P}\Delta\mathrm{T}_{in}}{r} \tag{2.2}$$

where Ja is the Jacob number, NEF is the non-equilibrium fraction, and r is the latent heat. The steam-carrying ratio is a ratio of steam-carrying water mass to theoretical flash vapor mass. The experiments' data revealed that increasing flow rate and flash chamber pressure lead to an increase

in the flash evaporation efficiency while the steam-carrying ratio decreased. However, flash evaporation efficiency decreases with increasing initial water film height, while the steam-carrying ratio increases. In practice, the authors recommended a high chamber pressure and flow rate with suitable initial water film height [55].

On the other hand, particular attention has been given to the aqueous NaCl solution. Yang et al. [56] analyzed the evolution of the volumetric heat transfer coefficient and the non-equilibrium fraction NEF (the completeness of flash at any time). An experimental study of heat transfer characteristics in static flash evaporation of an aqueous NaCl solution was carried out with an initial concentration range from 0.0 to 0.26, initial height of 0.1m to 0.4m, and superheat between 1.8K and 49.5K. The results showed that the boiling or evaporation point of the NaCl solution increases with increasing concentration. In addition, bubble nucleation in aqueous NaCl grows smaller and appeared later than in pure water. The data also showed that the amount of crystals and the degree of completion of flash evaporation could improve and increase by increased superheat. The volumetric heat transfer coefficient, which represents the boiling heat transfer during the flash period, decreases with an increasing mass fraction of the aqueous NaCl solution when no crystallization occurs [56]. In other research, Zhang et al. [57] investigated experimentally the static flash evaporation of aqueous NaCl solution at different flash speed. Five different diameters of thin orifice plates (5, 10, 20, 40, 80 mm) were used to generate different flash speeds ranging between 4.8×10^{-4} and $2.18 s^{-1}$. The flash speed (FS) expressed in equation (2.3) is defined as the mean drop rate of NEF during flash duration time τ_{tp} (the duration of the fast evaporation stage).

$$FS = \frac{1 - NEF_{tp}}{\tau_{tp}} \tag{2.3}$$

The non-equilibrium fraction at a turning point NEF_{tp} represents the sufficient degree of flashing. The results showed that there is a negligible increase of flash speed with increasing superheat. However, NEF_{tp} decreases at higher superheat and smaller initial waterfilm height, which means sufficient flash evaporation. Moreover, shrinking the orifice diameter from 80 to 5mm might minimize flash speed (FS) because the diameter has nearly no effect on NEF_{tp} but can extend the flash duration time(τ_{tp}). A minimum value of the non-equilibrium fraction at the turning point (NEF_{tp}) exists with the increasing flash speed, while the volumetric heat transfer coefficient increased linearly [57].

Yang et al. [58] presented an experimental study on energy conversion efficiency (ECE) during the static flash evaporation of a NaCl solution. The results illustrated that increasing the initial height of the water film lead to a decrease in the ECE for both non-crystallization and crystallization zones. Other work presented a study on the steam-carrying effect in static flash evaporation based on an experimental system for both pure water and an aqueous NaCl solution [59]. The drop of the water film height, the equilibrium concentration of water film, and the steam-carrying ratio (K) were measured during the experiments. The results illustrated that the steam-carrying ratio (K) increases with rising initial water film concentration (f_{m0}) or with decreasing separating height (H_{sp}). In addition, increasing the mean pressure difference between flash and vacuum (D_{pm}) led to an increase in both the drop of the water film height (D_H) and the equilibrium concentration of water film (f_{me}) [59].

Petekson et al. [60] explained the flashing evaporation phenomena by obtaining data experimentally from liquid refrigerant R11 exposed to sudden depressurization. They examined the mass transfer rates during evaporation and flashing to find the differences between evaporation and flashing. The data proved that the flashing occurs when the change in pressure is large and

sudden pressurization takes place. It showed also that the mass transfer rates due to flashing were higher by about 10 to 12 times than the rate in evaporation [60]. By using a different facility, Mikuza et al. [61] studied experimentally and numerically the flash evaporation. A simulation of flashing in two different experiments was conducted with a TRACE code in the TOPFLOW facility as shown in Figure (2.2). Process A was performed with remaining water at the starting of the transient and process B with water circulation prior and through the transient. As a result, for the cases A with high initial pressure, the TRACE simulations were in a good agreement with measurements, while the difference was larger at lower initial pressure. In process B, from the pressure time curves, the discrepancy between measured final pressures and simulated was small and less than 0.3 bar, which implies that the pressure time curves were in a good agreement with the measurements.

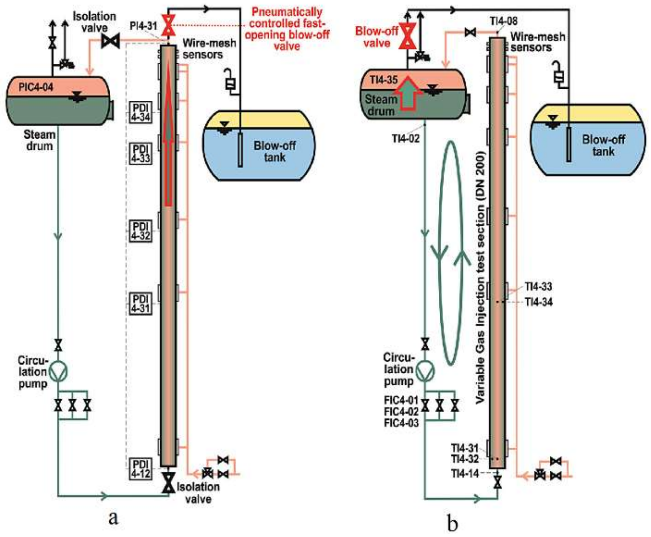

Figure 2.2 Schematics of the experimental: a) process A. b) process B on right.

In a particular study on the droplets behavior, Liu et al. [62] presented an experimental and theoretical study on rapid evaporation of ethanol droplets and kerosene droplets during depressurization. Through this study, the influence of parameters such as temperature, pressure, and droplet diameter on the droplet temperature were discussed, while a theoretical analysis was

conducted to examine the heat and mass transfer during the process. In addition, experiments were conducted to observe temperature transitions and the shape changes of ethanol and kerosene droplets during depressurized evaporation. The results illustrated that for both experiments and theoretical analysis when the ambient pressure inside the vessel decreases, the droplet temperature also decreases. Furthermore, the results showed that the droplet temperature decreases quickly, and the droplet evaporation rate becomes faster when the vacuum chamber pressure is low, or the droplet diameter is small. The evaporation rate of the ethanol droplet is much faster than that of the kerosene droplet, whereas the temperature of the kerosene droplet is much higher than that of the ethanol droplet. By comparing evaporation characteristics of water droplets with both the kerosene and ethanol droplets, the experimental and theoretical results proved that the ethanol droplet had the fastest evaporation rate followed by water [62].

Kim and Lior [63] studied critical transitions in pool evaporation in respect to initial temperature, critical time, and pool depth to understand the physics flash evaporation phenomena. The experimental results demonstrated that the non-equilibrium fraction (NEF) is inversely proportional with the initial temperature and the superheat, where NEF decreases with increasing initial temperature. In addition, the measurement results proved that the number of bubbles (N_b) is directly proportional with the initial temperature and the superheat; where the rise of N_b becomes steep as the initial temperature increases. Rapid rates of reduction of NEF were found during the critical time (t_c), which was three to four seconds of flashing: after that, the rate of decrease of the NEF became slower. The investigation of the non-equilibrium temperature difference (NETD) showed that NETD decreases with decreasing water depth and also increases with increasing initial temperature and superheat [63, 64].

2.3 The flashing jet and spray systems

Many experimental and numerical studies have appeared in recent years investigating the liquid jets and the spray flash evaporation phenomenon through circular nozzles. Kltamura et al. [65] carried out experiments to study the flashing of superheated liquid jests into a vacuum chamber. In this study, they used ethanol and differently treated water (city water, deionized water, degassed water, and aerated water) as working fluids. The results showed that complete flashing occurred at temperatures higher than the bubble point temperature corresponding to the vacuum pressure. For the flashing water jet, the critical superheat (the condition under which the complete flashing occurs) decreases with the increase of both the liquid velocities and the nozzle diameters. By comparing the critical superheat values for ethanol and water, the critical values for ethanol were lower than water. Adel et al. [66] discussed the effects of changing the pressure from 0.85, 0.87, to 0.9 bar inside the flash chamber within a range of an initial temperature between 40 to 70°C for water injected through circular nozzles. The measurements were taken under steady-state conditions. This study concluded that the degree of superheat increases with an increase of the depressurization. As a result, both the flashed vapor and the flashing efficiency increase. Miyatake et al. [67] studied the effect of changing inlet liquid temperature at 40 and 80°C in their experiments. They established general empirical equations appropriate for predicting the variance of liquid temperature in the center of the jet with residence time. In addition, they reported that the spray flash evaporation still has a higher evaporation performance and a faster evaporation rate compared with the flash evaporation occurring in other different systems.

Equation (2.4) illustrates the formula of the liquid temperature in the center of jet (θ).

$$\theta = F\frac{\theta_1}{[1 - exp\{-(\theta_1/\theta_2)\}]^{1/2}} \tag{2.4}$$

where the subscripts 1, 2 refer to the early and late evaporation periods, and i is the intermediate between the two evaporation periods.

$$\theta_1 = exp[-s_1(t - t_0)] \quad for \quad t_0 \leq t \leq t_0 \tag{2.5}$$

$$\theta_2 = \theta_i \, exp[-s_2(t - t_i)] \quad for \quad t_i \leq t \tag{2.6}$$

with t being the residence time in (sec)

The coefficient F expressed by

$$F = [1 - exp\{-exp(0.0243 \, g(\mathrm{T}_0)s_1 d)\}]^{1/2} \tag{2.7}$$

where T_0: temperature of liquid at the nozzle exit (^oC), and d: nozzle diameter (cm)

$$g(\mathrm{T}_0) = 1 - 0.60\left[\frac{\mathrm{T}_0}{60} - 1\right] \tag{2.8}$$

$$s = -\frac{d(ln\theta)}{dt} \tag{2.9}$$

In another paper, Miyatake et al. [68] discussed the effect of different circular glass nozzle diameters, flow rate, and degree of superheat on spray flash evaporation at 60°C jet inlet temperature. They compared their results with previous results from conventional multi-stage flash (MSF) evaporators and pool water exposed to an unexpected pressure drop. The comparison showed that the rate of spray flash evaporation is faster than that of a flowing superheated liquid in MSF evaporators and flash evaporation from pool water. It showed also that the intersection time and the time lag of flash initiation are related only to the nozzle diameter. In addition, the ratio of vertical distance from the nozzle exit to the diameter of nozzle is related mainly to the degree of superheat. Furthermore, increasing the degree of superheat leads to a rapid decrease of

the dimensionless temperature of liquid in the center of the jet. In another work, Miyatake and Tomimura [69] investigated the best methods of enhancing spray flash evaporation. They concluded that the injection of nucleated liquid through a specific nozzle arrangement into a low-pressure vapor domain was the best method for enhancing flashing.

Miyatake et al. [70] modeled the approach of a flashing horizontal flow to thermal equilibrium in a typical geometry to a flash chamber of a multi-stage flash (MSF) evaporator. The model combined the developed empirical correlation in this study with their results of a previous study of a numerical analysis of turbulent isothermal flow types in a flash chamber. The important parameter in this study is the non-equilibrium temperature difference (NETD), which is a good indicator of the approach to equilibrium in a flash chamber. The results showed that for any mass flow rate of the liquid and the baffle plate height, the NETD decreases with an increase of the mean outlet temperature of the liquid or the mean temperature of the emanating vapor. Moreover, the non-equilibrium temperature difference decreases when the higher baffle plate is installed near to the inlet orifice and when the mass flow rate increases [70].

Cai et al. [71] conducted experiments to study spray flash evaporation related to tube leakage problems in a high temperature and high-pressure steam-water test. These experiments investigated the effects of initial water temperature, injection pressure, injection rate, and injection direction in ten different experimental cases. The results showed that flash evaporation enhances with an increase in initial water temperature, the increase of the injection rate, and the increase of the injection pressure. The corresponding critical time is affected by the injection direction, where with the increase of the spray angle from 0^o to 180^o the corresponding critical time also increases. These results match well with the results studies of F. Du et al. [72], Xiao Jin et al. [73], and Abuaf, N et al. [74, 75], studying experimentally flashing liquid jets in a low-pressure environment by

injecting distilled water through a straight stainless steel capillary. They concluded that evaporation occurs if the initial temperature is high and the backpressure is low enough to cause a superheated exit conditions, which is consistent with the results of Kamoun et al. [31].

Zhou et al. [2] has carried out experiments to study the thermal characteristics of R134a two-phase flashing spray. In this work, a high-speed camera was employed to prove that fast expansion of the spray occurs at the exit of the nozzle that leads to a wide spray angle, which matches with the study by Xiao Jin et al. [73]. They found that the thermal field of the spray divided into three regions: a hot core region near the exit of the nozzle, a cold region in the downstream, and a warm periphery. The experimental results have shown that the non-dimensional velocities are self-similar and follow the Gaussian distribution.

The previous results also supported results of Mutair and Ikegami [76] investigated four parameters: the flow velocity, initial temperature, degree of superheat, and injection nozzle diameter to study their effects and influences on the flash evaporation. Their experiments displayed that an increase of the flow velocity increased the height of the inflection point. Moreover, an increase of the flow velocity at a short distance from the nozzle exit postpones the jet shattering and results in an increase of the overall distance required to complete evaporation. Furthermore, getting a strong level of jet shattering and more intense evaporation are related to increasing the degree of superheat [76, 54]. In addition, they found that an increase of the initial water temperature leads to acceleration and enhances the flash evaporation. On the other hand, the height of the inflection point is influenced by nozzle diameter, where increasing the nozzle diameter led to an increase in the height of the inflection point (the highest rate of the flash evaporation).

In other paper, Mutair and Ikegami [77] studied the desalination by flash evaporation of a superheated water jet experimentally. The results proved that increasing the flow velocity tends to

maintain the jet unshattered, increases the height of water column, and hence, delays evaporation. On the other hand, the evaporation increases with an increase of the initial water temperature. In order to prevent leakage, a mesh was used at different places as illustrated in Figure (2.3). When the mesh was installed at the nozzle exit, the evaporation rate became non-uniform; while when the mesh was installed above the nozzle exit with no resulting pressure drop, the evaporation accelerated [77].

Figure 2.3 Picture of top and side of the nozzle and mesh position.

To study the flow evaporation region of a multi-stage flash desalination and investigate the heat and mass transfer, a numerical model around a two-phase volume-of-fluid (VOF) formulation was developed by Nigim and Eaton [78]. Ansys fluent software was used in this simulation by applying the VOF model to simulate the multi-phase flow domain in the evaporation region of a horizontal flow-flashing chamber. The simulation results showed that increasing the brine level leads to an increase of the pressure with depth, which leads to a decrease in the mass transfer and phase change. The data can be used to estimate MSF design factors such as the non-equilibrium temperature difference and flashing efficiency. The increase of the brine level leads to an increase in the pressure with depth and leads to higher thermodynamic non-equilibrium losses in the

flashing chamber. In addition, the maximum values of vapor volume fraction occur in the bubble nucleation region.

Furthermore, Vu and Aguilar [79] presented a review of the state of flashing liquid sprays through glass tube nozzles and described the internal flashing phenomena. To get a flashing jet, the water was preheated and pressurized within a stainless-steel cylinder then injected into the atmosphere. The purpose of using glass nozzles was to allow the high-speed camera to take images of the internal two-phase flow. During the experiments, clear bubbles formation was observed near the nozzle wall. These bubbles merged into a vapor core surrounded by a liquid sheath at the tube nozzle exit. In similar work, Günther and Wirth [80] studied evaporation phenomena in the atomization of superheated liquids and their impact on spray characteristics, using glass and steel nozzles. Both nozzles have the same nozzle capillary diameter and same L/D (length/diameter) ratio, but a different inlet into the nozzle and different surface roughness. The possibility to monitor the bubble distribution inside the nozzle capillary was available when the glass nozzle was used. Whereas the actual shape and material applied in a technical process were represented by steel nozzles. By comparing the experimental results, the droplets generated in the glass nozzle were faster than those generated in the steel nozzle. Moreover, the mass flux for the glass nozzle was larger in comparison to the steel nozzle. However, the velocities measured on the spray axis were very similar for all temperatures and nozzles.

Ju et al. [81] studied the flash-boiling spray behaviors of R134a spray injected through a twin-orifice nozzle under atmospheric conditions. A high-speed digital camera was used to capture the images for internal and external flashing during the experiments. The results of these experiments were compared with previous numerical results from the work of Ju et al. [82] to clarify the flow through the twin-orifices. They carried out a multi-threshold image algorithm to

analyze the spray injected through twin orifice atomizers with different geometries and to compare the transient spray characteristics. The images showed that large bubbles were a bright area surrounded by a thin dark region; whereas the small bubbles were a dark region and difficult to recognize. The bubbles grow and easily nucleate inside and outside of the nozzle because of the pressure difference between the ambient pressure and the vapor pressure of R134a. These bubbles inside the mixing chamber increase with increasing of the ratio of gas and liquid in the expansion chamber [81, 83]. Due to quick vaporization and the flash-boiling effect inside the expansion chamber, and during the start of actuation, the external sprays were not stable [81].

In different research, Alghamdi et al. [6] presented an experimental study on the bubble expansion mechanism resulting from the explosive phase transition by injecting a liquid through a micro-metal and glass nozzles into a vacuum chamber. They used an ultra-high-speed video camera at up to 5 million frames per second to capture the temporal evolution of bubble expansion. They used PF_nH, M_eOH, $1-PB$, and $EtOH$ liquids as working fluid.

Furthermore, Günther and Wirth [84] analyzed occurring evaporation phenomena inside a nozzle capillary and their influence on the generated spray. To visually access the nozzle, a capillary glass nozzle was used during the experiments. The experimental results obtained with the glass nozzle were compared with steel nozzle results. The results showed that the ideal evaporation can not be achieved in glass nozzles, because of minimal nucleation sites. It also showed that the enhancement of the evaporation increases with increasing temperature. In addition, at higher temperatures, the velocity of droplets decreases while more vapor bubbles are contained in the fluid phase [84, 85]. Peter et al. [86] experimentally investigated the flashing and shattering phenomena of superheated liquid jets. By injecting a hot water through cylindrical nozzles in a low-pressure domain, they observed some physically categorized flashing liquid jets;

namely a non-shattering liquid jet, partially shattering, completely shattering, and flare flashing liquid jet. The results showed that for a cylindrical nozzle with a larger inner diameter and short length, it was easy to obtain shattering of the liquid water jet compared to the nozzle with a small inner diameter. In addition, increasing the superheated degree led to an increase in the number of smaller droplets released at the liquid jet breakup point, while the mean volumetric flow rate per unit area of the jet along the radial direction decreases.

With another different working fluid in their theoretical study, Vandroux et al. [87] examined and described the behavior of the liquid propane (C_3H_8) when it escapes from a tank and evaporates due to sudden depressurization. The mathematical model was based on Eulerian approach. The results were compared with the computational results that were obtained with the MC_3D Eulerian code, and the Eulerian-Lagrangian code of the study of Pereira and Chen [88] and they were in a good agreement. The results showed that the initial velocities are important and due to their high momentum, the propane droplets were very small and remained in the center of the jet [87]. Bharathan and Penney [89] carried out modeling of evaporation from turbulent water sheets and experimental studies of flash evaporation from water jets for three different initial thicknesses. The results showed that residence time, jet thickness, and shattered jets were not relevant correlating parameters. The experimental and analytical results proved that resulting surface renewals on the liquid side in destroying growing thermal boundary layers enhances evaporation phenomenon. Analytical results yielded a similar independence of evaporation effectiveness on the initial jet thickness for shattered jets, which leads to a vertical spout with minimal liquid side pressure losses [89]. Similarly, Mutair and Ikegami [90] presented an experimental study on flashing of superheated water jets and modeling the liquid-side heat transfer process accompanying the surface evaporation of superheated water drops. The results showed

that near the nozzle exit, a potential core zone appeared where there was no change in water temperature, which means that there is no flash evaporation yet. The data also showed that the actual evaporation rate obtained by the analytical solution of the interface evaporation was found to be lower than that from the superheated water drops [90]. With a view to consider significant characteristics, Cheng et al. [91] analyzed the impact factors of spray features, heating surface characteristics, fluid properties, and external circumference characteristics to investigate the heat transfer mechanisms of spray cooling and better understanding of flash evaporation cooling. Therefore, the heat transfer of spray cooling divided into three stages: single-phase stage, two-phase stage, and critical heat flux (CHF) stage. The study was carried out theoretically and experimentally. The results showed that the spray characteristics such as droplet velocity, droplet flux, spray flow rate, and spray angle are influenced by inlet pressure, ambient temperature, and those conditions impacted on the heat transfer. These results are in a good agreement with the results of the Kuznetsov et al. [92], Xiao Jin et al. [73], Wang et al. [85], Cheng et al. [93], and Zhou et al. [94] . Furthermore, the flash evaporation of liquid film and droplet causes a high cooling capacity, which is confirmed by critical heat flux [91, 95].

Wang et al. [96] studied a water droplet flash evaporation in vacuum spray cooling in a one-dimensional model by introducing a heat balance correlation and a phase transition model. They proved that the equilibrium temperature becomes higher and the droplet evaporation rate increases with high temperature conditions. The ambient temperature and the droplet diameter mainly affect the droplet lifetime, where with the increase in the ambient temperature, the lifetime of the droplet decreases. Furthermore, the droplet lifetime increases with an increase of the vapor concentration fraction especially for the droplet with a larger diameter. On the other hand, the increase of the ambient pressure and temperature increase the droplet freezing time. In another

work, Wang et al. [97] studied water flash evaporation under reduced pressure and developed a one-dimensional mathematical model of flash evaporation as well as a numerical solution method. They carried out both a theoretical analysis and experimental research on water flash evaporation. In the mathematical model, they considered four primary physical processes: gas outflow from the flashing chamber, water mild evaporation, water flash evaporation, and an update of the gas composition in the flashing chamber. The model predictions results were in good agreement with the experimental results. The results indicated that the occurrence of flash evaporation was delayed at higher initial pressure. Whereas the higher the initial water temperature, the earlier the flash evaporation occurred and longer the duration of the flash evaporation. The thermal follow-up coefficient (TFC), which expresses the superheat is increasing with increasing depressurization rate and had a linear random function distribution with it. As the outlet diameter increases, the flash duration would be shorter and the rate of water evaporation increase. In a different study, Jin et al. [98] experimentally examined the spray characteristics of liquid hydrocarbon fuel undergoing sudden depressurization and flashing injection. The results confirmed that the Mie scattering images of the superheated fuel spray showed some of the features of flashing. While the resultant liquid core becomes wider and shorter with increasing fuel injection temperature above the boiling point. In addition, the spray angle converged to a specific value with increasing fuel injection temperature, and in contrast with pressure drop across the injector. Four modes presented themselves: turbulent primary breakup mode; an aerodynamic bag and shear breakup mode; a transitional flashing mode; and a fully flashing mode, which comes from break down of the high temperature hydrocarbon liquid jets.

Experimental and mathematical studies were carried out to investigate the spray flash evaporation process of hot water injected trough a circular nozzle into a vacuum chamber. The

experiments were performed at velocities from $0.25\,m/s$ to $0.8\,m/s$ where the diameter of the circular nozzle was $9\,mm$. A mathematical model based on droplet analysis was used to capture the shattering phenomenon. Based on a mathematical model, the temperature profiles are translated into the mean droplet diameters of the spray. A commercial pressure swirl nozzle that produces spherical droplets was applied to collect the experimental data for validating the mathematical model. The results presented the effect of variables like initial temperature and flow velocities on the flash evaporation phenomenon. The mean droplet diameter was small at a high initial temperature difference (the difference between feed water temperature and saturation temperature) and starts increasing when the temperature exceeds 35°C. The results also showed that a smaller droplet diameter was produced at higher spray velocities. In addition, increasing the flow velocities lead to an increase in feed flow rate, which enhanced proportionally the evaporation rate [99].

Cai et al. [100] developed a model based on droplet analysis to study the upward water flash evaporation. They used Matlab programming to realize the function of the model and calculate the droplet motion, droplet size variation, droplet temperature, and also investigate the influences of the injection pressure, evaporation chamber pressure, and flow velocity on the gained output ratio (GOR) and spray flash speed (SFS). The GOR represents the energy utilization efficiency. The model was validated with previous experimental data and the calculated results by Wu et al. [101] and Mutair and Ikegami [77], where the results were in a good agreement. The results showed that the increase of the injection pressure leads to higher spray flash speed and increase in the evaporated mass rate, while the droplet size decreases. The results also showed that the decrease of the evaporation chamber pressure enhances the GOR as well as the intensity of the flash evaporation and leads to an increase of the evaporated mass rate. While the increase of the

flow velocity results in the decrease of GOR for a certain distance. In contrast, the increase of the flow velocity leads to an increase of the spray flash speed and the evaporated mass rate.

Miyatake [102] presented the comparative study of flash evaporation rates of different flashing methods. The comparative study included a flash evaporation from a water pool, those from a superheated liquid jet ejected into a low-pressure and flashing from superheated flowing liquid in multistage flash (MSF) evaporator. He considered the empirical coefficient of the flash evaporation rate (k) for the comparison. The comparison results showed that the empirical coefficient of the flash evaporation rate (k) obtained from a superheated liquid jet ejected from a circular orifice into a low-pressure vapor area is higher by about ten times than the counterparts obtained from other methods. This proves that flashing from a superheated liquid jet ejected into a low-pressure vapor area is the best method to enhance flash evaporation [102, 103].

2.4 Shock waves induced by flash evaporation

Shock wave is a very thin wave that propagates faster than the local speed of sound where the flow properties like pressure, velocity, density, and temperature are discontinuous. For several years, considerable effort has been devoted to investigating the resultant shockwave for different fluids during the flash evaporation. Many experimental, numerical, and mathematical methods have been developed to understand this phenomenon. When the Mach number is equal one, which means the flow velocity reaches the velocity of sound in the fluid, the flow becomes choked and the mass flow through the nozzle can not be raised further by decreasing the backpressure. Ashgriz [25] presented the sonic speed in a two-phase flow that depends on the volume fraction of the flow; therefore, a flashing nozzle may choke at much lower flow velocities as compared to the non-flashing nozzles.

$$\frac{1}{c^2} = \frac{\alpha}{\mathrm{KP}}[\rho_l(1-\alpha) + \rho_v\alpha] \tag{2.10}$$

where c: sonic speed, α: volume void fraction, K: polytropic coefficient.

Flashing can induce a shockwave when the fluid is exposed to a sudden pressure drop. This generated shockwave can transfer the energy of a high-pressure fluid directly to another low-pressure fluid. A wave rotor is a dynamic pressure exchanger that utilizes this mechanism, which exchanges energy from a high pressure to a low-pressure fluid via moving shock waves that are generated [104, 105, 106, 107]. Kurschat et al. [108] studied a complete adiabatic evaporation from a jet expansion by developing an appropriate model to describe the basic physical effects. For the experiments, Perfluorohexane (C_6F_{14}) was used as test substance, and a nozzle expansion into a vacuum chamber was used to examine the evaporation of extremely superheated liquid jets. The initial pressure (P_0) was taken between atmospheric and 20 bar, the final pressure (P_e) between atmospheric and $10^{-2}mbar$, and an initial temperature (T_0) was taken between room temperature and 180^oC. The degree of superheat (H) is defined as ($P_s(\mathrm{T}_0)/P_e$), where $P_s(\mathrm{T}_0)$ indicates the vapor pressure with respect to the initial temperature. The authors found that the experimental results are in good qualitative agreement with the developed model. The experimental results showed that increasing the stagnation pressure led to increase in the velocity at the nozzle exit. In fact, increasing the velocity at the nozzle exit helps to reach large values of the liquid jet core (s/d). The evaporation rate at the jet surface increases by decreasing final pressure and increasing initial temperature. Furthermore, as shown in Figure (2.4), with increasing degree of superheat, sonic conditions are reached [108, 109]. The jet frame is composed of a liquid core surrounded by a supersonic two-phase flow zone terminated by a barrel shock, a quasi-cylindrical lateral shock, and a Mach disc [108].

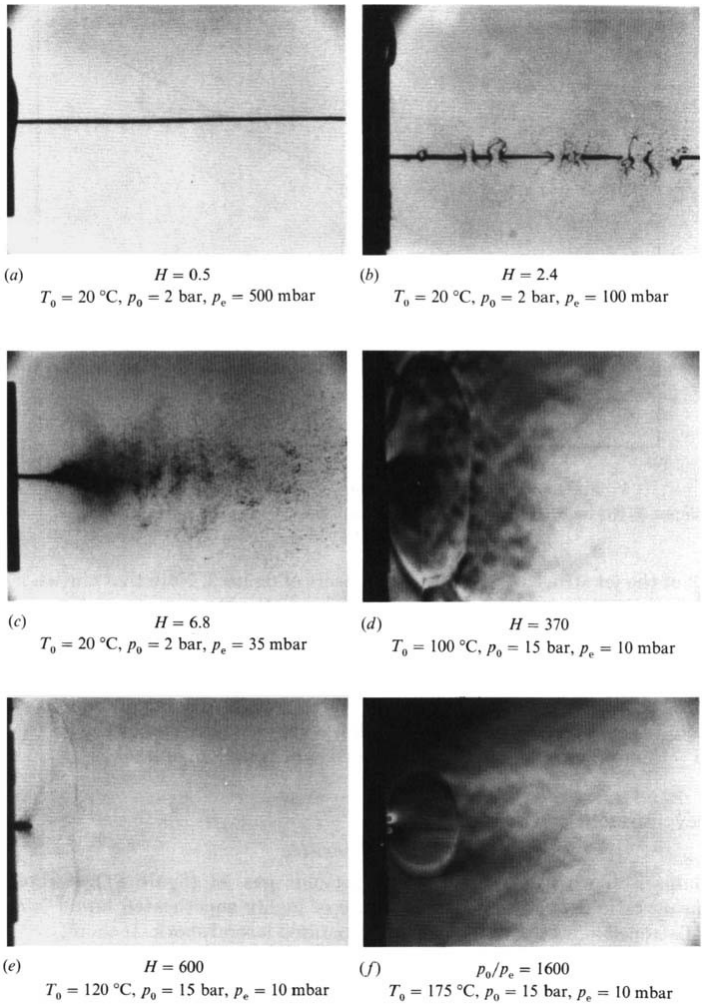

Figure 2.4 The shock structure on the nozzle exit.

Simões-Moreira and Shepherd [110] carried out experiments for saturated dodecane at temperatures ranging from 180ºC to 300ºC. They observed the propagating adiabatic evaporation waves in superheated liquid dodecane ($C_{12}H_{26}$). The experiments' results showed three regions downstream of the flow: a faster moving vapor phase, entrained liquid droplets are both in the core region, and a slowly moving liquid phase attached to the wall. They found that complete evaporation experimentally is possible with increased initial liquid temperature, but it was not actually obtained. However, the obtained relation between initial temperature and pressure from the experiments predicted that complete evaporation would occur in temperature range of 310ºC to 320ºC. In different study, Simões-Moreira [111] revised and extended the one-dimensional

theory (the theory of normal evaporation waves) to contain the oblique evaporation wave geometry in order to obtain relation between the wave and the turning angles of the flashing jet flow. In addition, he compared and discussed the results with previous experimental results obtained for the cases operating at the C-J condition. For examples, the previous experimental results of oblique flame fronts [112], the results studies of short tubes [113], Kim and O'Neal experiments [114], the experiments with flashing jets [108, 115], and others. Simões-Moreira analyzed and presented the relationship between the wave and turning angles. The conclusion showed that there is similarity between the theory of oblique evaporation waves and the one for oblique deflagration waves (oblique flame). He also found that the experimental results agree well with calculated C-J points [116].

Simões-Moreira et al. [117] carried out the experiments and one-dimensional numerical analysis to issue a flashing jet of liquid iso-octane in a short converging nozzle. They used a Showphast 1D code to solve the problem numerically. To capture the images of the expanding flashing jet, the Schlieren method technique using a charge-coupled device camera was used. The shock wave was observed during the experiments where the photographs were mathematically filtered using a subtraction type filter to get photographs with better quality. Calculations of the 1D code introduced the radial position of the shock wave location, whereas analysis of the images showed shock wave structure that was consistent with the numerical results. The liquid core was observed during the experiments, which implies that no internal nucleation has been observed and the phase transition occurs outside the nozzle [117, 43]. The experimental data also showed that the shock wave is coupled with a flashing jet, and the expansion regime is very different by increasing the ratio of the vapor pressure at the initial temperature to the backpressure value [117].

Angelo and Simões-Moreira [118] presented a numerical solution of an expanded flashing liquid jet into a low-pressure medium using a mathematical model for both one-and two-dimensional axisymmetric models. The conservation equations were solved by using the McCormack's integration technique (an explicit finite difference technique of second-order accuracy) along with a real equation-of-state. For solving the jump equations of the quick evaporation, they applied the theory of oblique evaporation waves with analyzing the problem of the expansion region. The results of the numerical solution were compared with previous experiments of a flashing jet in previous work [108] with the iso-octane as a working fluid. The comparison shows a good agreement between the previous experiments' pictures for the dimension of the shock wave with the corresponding numerical model as shown in Figure (2.5). The mathematical model results showed that the shock wave size increases by decreasing the backpressure especially in the radial direction and increases with increasing both the injection temperature and pressure where the backpressure is constant. In contrast, the maximum shock wave dimension in the axial direction decreases by increasing the injection temperature and is affected by the length of the metastable liquid core more than any other variable [118].

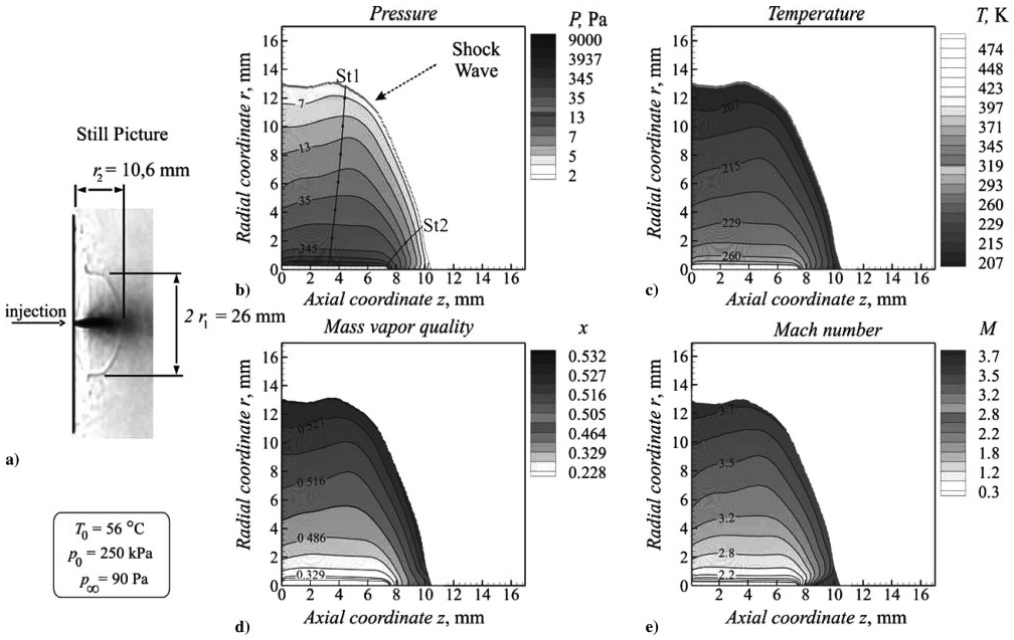

Figure 2.5 Iso octane flashing liquid jet: (a) picture of the test case, (b) pressure contour, (c) temperature contour, (d) mass vapor quality contour, and (e) Mach number distribution field.

In other research, Simões-Moreira and Bullard [7] investigated flashing mechanisms during a novel pressure drop and flow choking condition. The flow choking issues are examined and three refrigerants R-134a, R-22, and R-600a were presented numerically, assuming an ideal situation. The presented model in this work was based on previous experimental observations in short nozzles. The conclusions presented that a choking flow mechanism exists nearly downstream of the exit section, whereas no choking can occur within the nozzle as the speed of sound in liquids is very high. In addition, the evaporation wave and its associated shock structure were present between the metastable exit and the downstream evaporating pressure [7].

A two-dimensional numerical model was developed by Liu et al. [119] to examine the critical flashing flow of initially sub-cooled water through convergent-divergent nozzles. The oblique evaporation wave theory of Simões-Moreira [111] was utilized. The results demonstrated that the initial sub-cooled degree and inlet stagnation pressure (which is inversely proportional with the pressure difference) affect the flashing flow and the resultant shock wave. When the inlet

stagnation pressure increases, the velocity upstream of the evaporation wave also increases, while velocity downstream of the evaporation wave is fluctuated; so, it first decreased, then it increased. On the other hand, the pressures upstream and downstream of the oblique evaporation wave, the velocity downstream of the oblique evaporation wave, and the evaporation wave angle decrease with increasing initial inlet sub-cooled degree. In contrast, the velocity upstream of the oblique evaporation wave, the length of the non-homogeneous equilibrium region in the divergent section, and the velocity-turning angle are increased by increasing the initial inlet sub-cooled degree [119, 120].

In another work, Avila et al. [121] presented a numerical solution of the flashing phenomenon into a two-dimensional axisymmetric domain when liquid jets of a high-pressure and temperature are exposed to a sudden pressure drop. The dispersion-controlled dissipative (DCD) scheme was applied to solve the flashing of superheated jets numerically with iso-octane (C_8H_{18}) as the working fluid. The DCD is a hybrid between the Lax-Wendroff and Beam-Warming scheme with a flux function. The advantages of this method are that it gives transient solutions and immediately captures the shock wave. Figures (2.6) and (2.7) show the formation of a shock wave in the point 2.15m for both the pressure and Mach number contours and distributions, respectively, for the convergent–divergent nozzle problem (De Laval) in steady-state regime.

Furthermore, Niu and Wang [122] provided numerical simulation during two and three dimensions in order to solve the compressible two-fluid-six equation model, where a hybrid type Riemann solver was proposed. Both two-dimensional and three-dimensional numerical results confirm that the cavitation bubbles and the interaction of shock and rarefaction waves were captured.

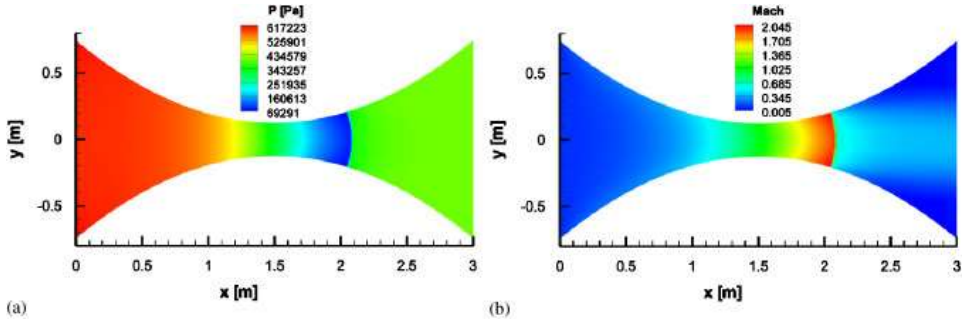

Figure 2.6 (a) Pressure contours and (b) Mach number contours.

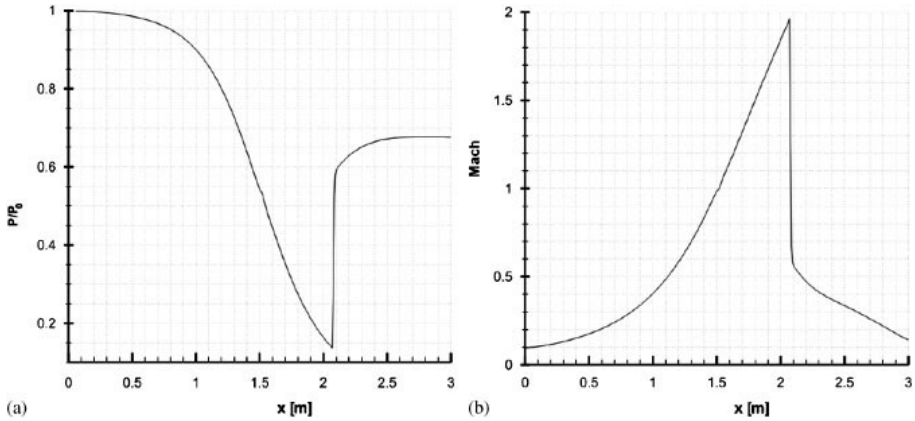

Figure 2.7 (a) Pressure profile and (b) Mach number profile.

In addition, the results demonstrate that the magnitude of the velocity impacts the growth rate of cavitation zone and impacts the pressure maximum which showed in the 2D case bigger than the 3D case. Furthermore, the rarefaction and the propagation or expansion of the shock wave is found to slow down when the inhomogeneous medium of the water droplet is shown.

Paudel et al. [123] presented 3D simulations of a shock-driven multiphase instability (SDMI) for two cases: the first case for a gas particle only (dusty gas case) and the second case for a gas particle with an evaporating particle cloud. For the implementation, they used the open-source hydrodynamics code FLASH (multi-physics hydrodynamic simulation code), which uses the Euler equations. The authors discussed the variations between the interface evolution of a SDMI and RMI (caused by a troubled interface between high- and low-density fluids). The discussion specified six different regions of the evolving interface named as primary vortex cores,

inner roll-up tip, outer roll-up tip, tail, upstream bubble, and downstream bubble as shown in Figure (2.8).

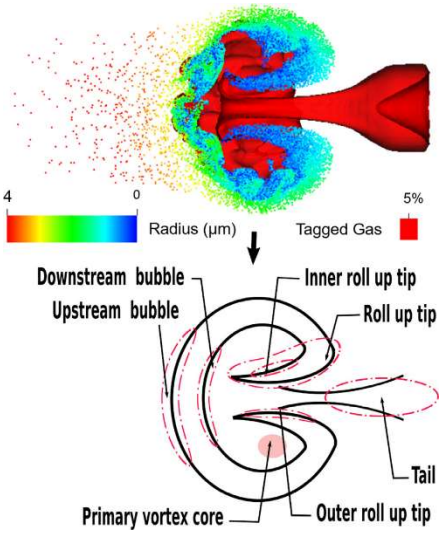

Figure 2.8 schematic of an evolving interface for SDMI.

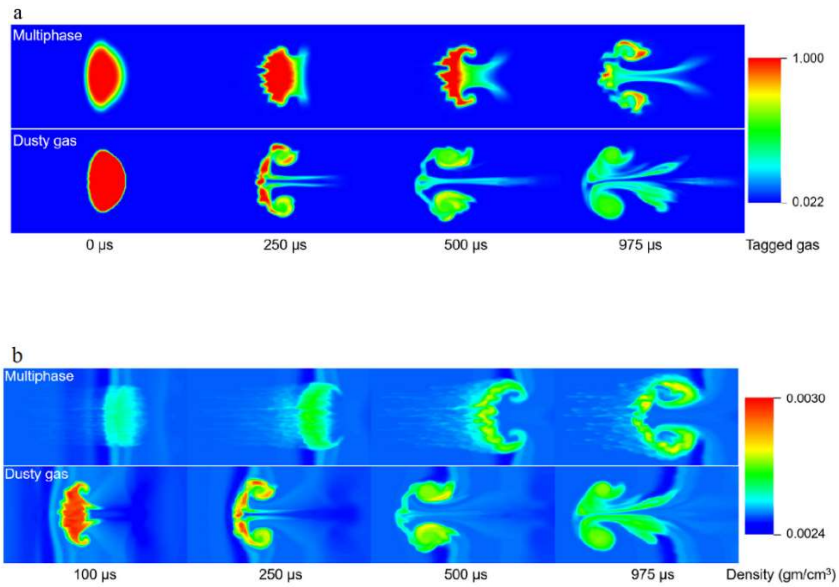

Figure 2.9 (a) The growth of the gas interface over time for the dusty gas and multiphase, (b) density variation in dusty gas and multiphase interface with time.

The initial simulation results show that the dusty gas interface has a higher density and grows much faster than the multiphase interface as shown in the Figure (2.9), which also shows that the large-scale shock bubble interaction controlled a typical MRI evolution. They also concluded that the initial spatial distribution and particle initial size have a strong influence on particle evaporation time in a SDMI.

In another paper, Dahal and McFarland [124] presented a numerical method for shock driven multiphase flow by using the FLASH code. The authors studied a 2D shock driven instability of a circular disturbance for two cases: the single and multiple particles size group. They combined the piecewise parabolic method with the Particle-in-Cell technique to get a solution of Lagrangian particles in a gas modeled on a Eulerian grid. The results showed that the gas interfaces cooled by evaporation created a gas density gradient (which means additional shock waves) lead to an increase in circulation and instability. In addition, the vorticity deposition was reduced with larger particles, while particle evaporation increases it. They also found that the particle temperature rises suddenly when the shock wave reaches the particle place: in turn, there is an abrupt decrease in droplet diameter rate occurred as illustrated in Figures (2.10) and (2.11) [124].

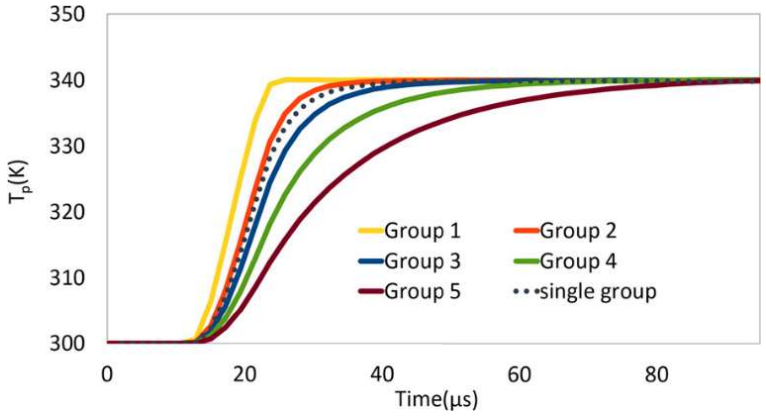

Figure 2.10 Changing droplet temperature with time history.

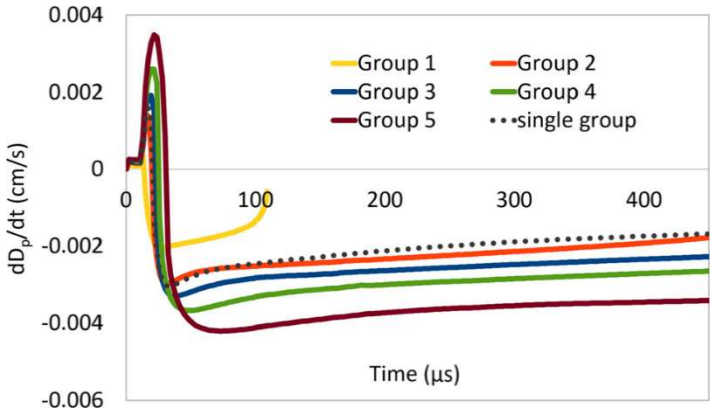

Figure 2.11 Time history of droplet diameter change rate.

Rodio et al. [125] presented a numerical simulation of compressible multiphase flow based on a discrete equation method (DEM) formulation. In this work, to obtain the mixture of a liquid and gas they used Fluorinert (FC-70 fluid) as the working fluid coupled with water as a liquid phase. The results obtained with the Discrete Equations Method (DEM) coincide with the numerical results obtained from the NZDG code, which solves the quasi-single-phase shock-tube flow. To obtain good predictions at the saturation curve conditions, it is significant to consider a more complex equation of state such as Peng-Robinson (PRSV) EOS. The results confirmed that the gas volume fraction has a significant impact on the velocity of the flow, especially at the compression shock, contact discontinuity, and the rarefaction shock wave (RSW). Moreover, the velocity of the rarefaction shock wave and gas volume fraction are inversely proportional; when gas volume fraction decreases, the velocity of the rarefaction shock wave increases [125].

Dai et al. [126] established a shock- tube model to study numerically the superposition behaviors like rarefaction shock waves, for three unsteady discontinuities in water vapor flows near the liquid equilibrium region. The compressible Navier–Stokes equations were used to model the water (R718) vapor flow with the Eulerian–Eulerian approach. The numerical results guarantee that there are one rarefaction, one contact face, and one shockwave at the initial disconnected

boundary condition. Consequently, there is only one couple of shocks encountered within the superposition shock tube [126, 127]

Several experiments were performed in recent years to enhance and prove the numerical results. To observe choking behavior and investigate the existence of shock waves, Vieira and Simões-Moreira [128] examined a flash evaporation phenomenon in an iso-octane liquid jet. This work was done experimentally by injecting iso-octane through a short nozzle into a chamber at low-pressure less than the liquid saturation pressure. The images of a shockwave were captured by using the Schlieren method technique, while the back-lighting method was used to observe the central liquid core. The experimental data displayed that two-phase flow reaches very high velocities indicating that the maximum mass flow rate occurs during flashing. In addition, a choking behavior was observed at low backpressure; where this choking increased and becomes clearer as the backpressure decreased. For higher injection pressure, injection temperature, and lower backpressure, an axial dimension of a shock wave structure was larger as shown in Figure (2.12). The experiments also illustrated that the choking or limiting mass flow rate depend on the initial injection temperature and initial pressure and backpressure. These results are in a good agreement with Kuznetsov et al. [120] and Attou et al. [129].

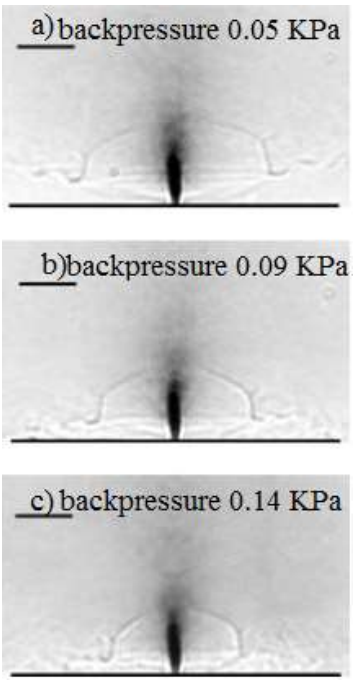

Figure 2.12 Schlieren picture for shock wave structure at 1 s apart from each other. At initial pressure 249 KPa and Initial temperature 56.9 ^{o}C.

For confirmation, the authors used a shaving blade in front of the jet to confirm that there is a shock wave. They concluded that the existence of supersonic flow around the shaving blade and a complex shock wave reflection are proof that the phenomena is a shock wave as shown in Figure (2.13) [128].

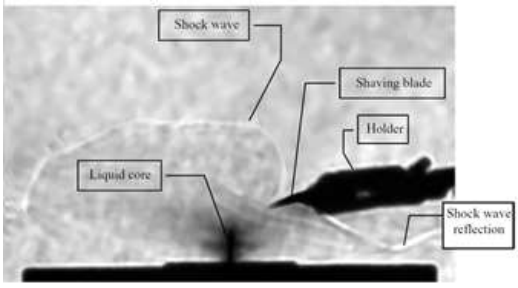

Figure 2.13 Shock waves around shaving blade.

Lamanna et al. [130] presented a study on flashing atomization, which was valid for standard and retrograde fluids. In this study, acetone, ethanol, and iso-octane are selected as test fluids where three aspects namely spray morphology, lateral spreading, and transition threshold are considered for the analysis. They proved that standard and retrograde fluids terminated by a

complex shock structure were observed at high initial superheat. At highly superheated conditions, the evolution of fully flashing iso-octane and acetone sprays showed that for both fluids the morphology of the formed shock structures is very similar, as shown in Figures (2.14) and (2.15). The parameter R_P is defined as the ratio between the saturation pressure and the backpressure(P_∞). The model in this article, provided a correlation between the bubble population and the jet lateral spreading, where the results showed that at the wide spray angle, the larger population of bubbles were found.

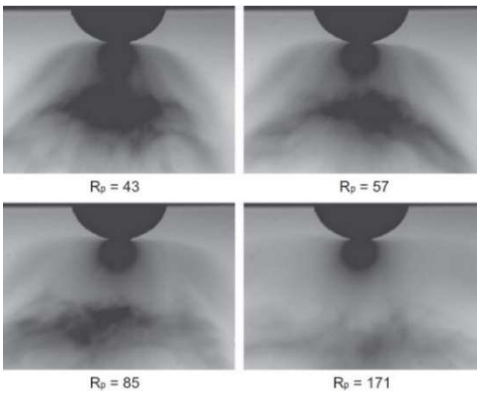

Figure 2.14 Shock structures for fully flashing iso-octane spray with increasing R_P.

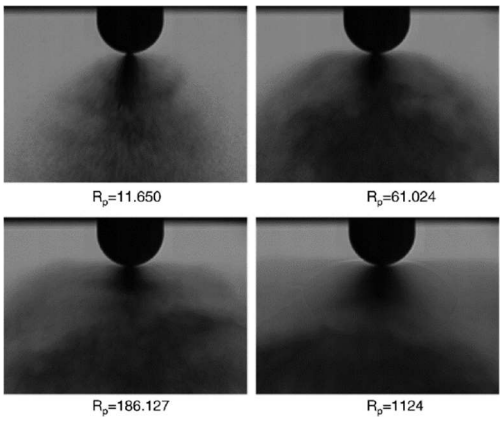

Figure 2.15 Shock structures for fully flashing acetone spray with increasing R_P.

Avdeev [131] investigated the geometry of shock waves in different regions of superheated liquid jets. The study focused on the gas dynamic mechanisms of the formations of wave structures that occur during flashing jets. He found that the flow separates into two regions flow moves in an

axial direction (the central core region) and radial direction (the peripheral region). A good agreement has found by comparing the studied geometry of shock wave fronts for high temperature liquid in different flashing systems with pervious experimental data obtained from references [128, 132, 133].

CHAPTER 3

Modeling and Governing Equations

3.1 Two-Dimensional Numerical Analysis

These days, Computational Fluid Dynamics (CFD) is an engineering tool which is used to predict fluid flow behavior by numerical simulations. CFD simulations consider a significant way for solving the multiphase flow and heat transfer problems. There are two approaches for multiphase flow modelling: Euler-Euler and Euler-Lagrange. The Euler-Euler approach has three sub-models as shown in the Figure (3.1).

Many theoretical, experimental, and computational research have been carried out to predict and better understand the fluid behavior undergoes a sudden phase change from liquid to vapor. A numerical model was developed nearly a two-phase volume-of-fluid formulation to better understand the flow evaporation region of a multistage flash and investigate the heat and mass transfer for the brine. Ansys Fluent software was used in this simulation by applying the volume-of-fluid (VOF) model to predict the multiphase flow domain in the evaporation area of a horizontal flow-flashing chamber [78]. Furthermore, Angelo and Simões-Moreira [118] presented a numerical solution of an expanded flashing liquid jet into a low-pressure medium using a mathematical model for both one- and two-dimensional axisymmetric models.

In this dissertation, 2D simulation carried out using Ansys Fluent, which is commercial computational fluid dynamics software to predict choking behavior and investigate the existence of shock waves by using water as working fluid. Ansys Fluent is used in this simulation by applying the Mixture model to simulate the multiphase flow zone in the evaporation area.

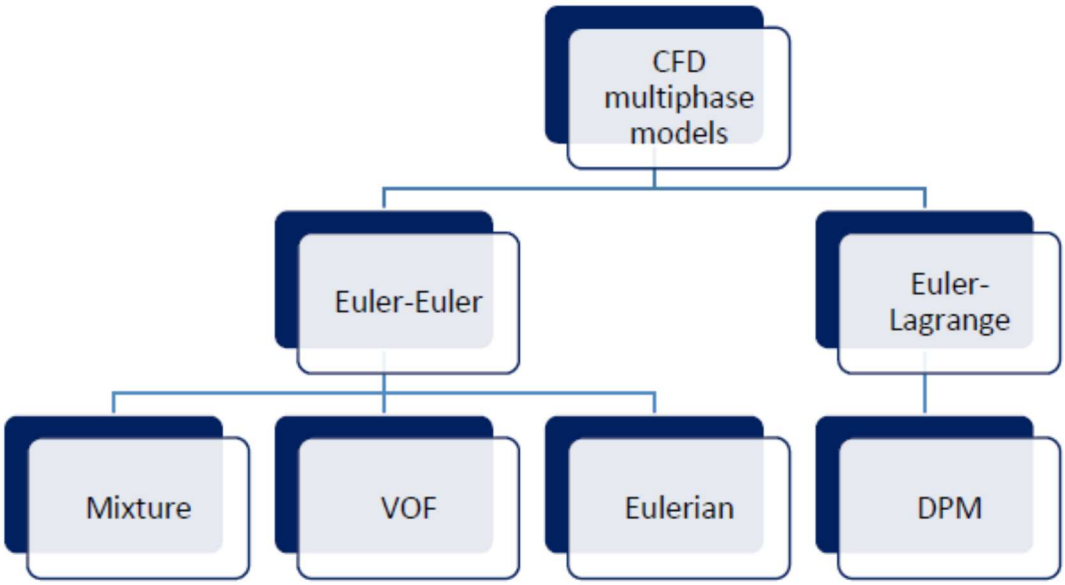

Figure 3.1 Multiphase modelling approaches in ANSYS Fluent.

The mixture model has many advantages than other models like Eulerian and VOF. One of these advantages that by using the concept of slip velocities, mixture model can be used to model multiphase flows as a homogeneous where the phases move at the same velocity or with different velocities as non-homogeneous multiphase model. The other advantage that using mixture model allow to model many phases by solving the continuity equation, the energy equation, and the momentum equation for the mixture. In addition, solving the relative velocities to describe the dispersed phases, or using the model without relative velocities for the dispersed phases to model a homogeneous multiphase flow. The mixture model also solves the volume fraction equations for the secondary phases where the phases can be interpenetrating; therefore, the volume fractions (α) for any phase can be equal to any value between 0 and 1 depending on the area occupied by the phase. Thus, if the cell has a value of the volume fraction ($\alpha_1 = 0$), implies that the cell is totally occupied by second phase α_2, and vice versa. Furthermore, if any cell has a value between zero and unity, it means that an interface exists in that region. The interface is a very thin layer, which disconnects the two phases and has distinguish properties.

3.2 Governing Equations.

The basic of computational fluid dynamics is the fundamental governing equations of fluid dynamics (continuity, momentum, and energy equations). These equations and others were solved using Ansys Fluent and presented for the following equations [134, 135, 136, 137, 138, 139].

3.2.1 Continuity Equation for the Mixture.

The continuity equation for the mixture is

$$\frac{\partial}{\partial t}(\rho_m) + \nabla.(\rho_m \vec{v}_m) = \dot{m} \tag{3.1}$$

$\dot{m}$: represents mass transfer due to user-defined mass sources using the equation below.

$$\mathrm{T} = (-24.57 * \ln(\mathrm{P})) + \left(6.2152^{\ln(\mathrm{P}^2)}\right) - \left(0.47549^{\ln(\mathrm{P}^3)}\right) + \left(0.016186^{\ln(\mathrm{P}^4)}\right) + 273.15 \tag{3.2}$$

$\vec{v}_m$: The mass-averaged velocity:

$$\vec{v}_m = \frac{\sum_{k=1}^{n} \alpha_k \rho_k \vec{v}_k}{\rho_m} \tag{3.3}$$

$\vec{v}_k$, α_k, and ρ_k are the velocity, volume fraction, and density of phase k, and ρ_m is the mixture density which can be calculated in present study from the following formula:

$$\rho_{m=}\ \alpha_v \rho_v + \alpha_l \rho_l \tag{3.4}$$

Or in general formula

$$\rho_m = \sum_{k=1}^{n} \alpha_k \rho_k \tag{3.5}$$

3.2.2 Momentum Equation for the Mixture.

The momentum equation for the mixture can be obtained by summing the individual momentum equations for all phases. It can be expressed

$$\frac{\partial}{\partial t}(\rho_m \vec{v}_m) + \nabla.(\rho_m \vec{v}_m \vec{v}_m) = -\nabla \mathrm{p} + \nabla.[\mu_\mathrm{m}(\nabla \vec{v}_m + \nabla \vec{v}_\mathrm{m}^\mathrm{T})] + \rho_m \vec{g} + \vec{F} + \nabla.\left(\sum_{\mathrm{k}=1}^{\mathrm{n}} \alpha_k \rho_k \vec{v}_{dr,k} \vec{v}_{dr,k}\right) \tag{3.6}$$

The term $[\mu_\mathrm{m}(\nabla \vec{v}_m + \nabla \vec{v}_\mathrm{m}^\mathrm{T})]$: is the stress tensor $\bar{\bar{\tau}}$

n : The number of phases, $\vec{F}$ is a body force, and μ_m is the viscosity of the mixture:

$$\mu_\mathrm{m} = \sum_{\mathrm{k}=1}^{\mathrm{n}} \alpha_k \mu_\mathrm{k} \tag{3.7}$$

Which means that the viscosity in this study is

$$\mu_\mathrm{m} = \alpha_\mathrm{v} \mu_\mathrm{v} + \alpha_l \mu_l \tag{3.8}$$

$\vec{v}_{dr,k}$: The drift velocity for secondary phase k:

$$\vec{v}_{dr,k} = \vec{v}_k + \vec{v}_m \tag{3.9}$$

3.2.3 Energy Equation for the Mixture.

The energy equation for the mixture takes the following form:

$$\frac{\partial}{\partial t}\sum_{k=1}^{n}(\alpha_k\rho_k \mathrm{E_k}) + \nabla.\sum_{\mathrm{k=1}}^{\mathrm{n}}\left(\alpha_k\rho_k(\rho_k \mathrm{E_k} + \mathrm{p})\right) = \nabla.(\mathrm{k_{eff}}\nabla \mathrm{T}) + \mathrm{S_E} \quad (3.10)$$

The first term on the right-hand side of equation represents energy transfer due to conduction.

k_{eff}= k+k_t is the effective conductivity.

k_t : The turbulent thermal conductivity defined according to the turbulence model being used.

S_E : includes any other volumetric heat sources ($\rho\dot{q}dxdydz$).

For a compressible phase E_k expressed as:

$$\mathrm{E_k} = \mathrm{h_k} - \frac{\mathrm{p}}{\rho_k} + \frac{\mathrm{v_k^2}}{2} \quad (3.11)$$

For an incompressible phase E_k =h_k, where h_k is the sensible enthalpy for phase k.

3.2.4 Relative (Slip) Velocity and the Drift Velocity.

The relative velocity or the slip velocity is defined as the velocity of a secondary phase relative to the velocity of the primary phase. In this study the second phase is water vapor (V), and the primary phase is liquid water (L):

$$\vec{v}_{lv} = \vec{v}_v - \vec{v}_l \quad (3.12)$$

The drift velocity and the relative velocity $\vec{v}_{lv}$ are connected by the following expression:

$$\vec{v}_{dr,v} = \vec{v}_{lv} - \sum_{k=1}^{n}\frac{\alpha_k\rho_k}{\rho_m}\vec{v}_{lk} \quad (3.13)$$

The basic assumption of the algebraic slip mixture model is that, to prescribe an algebraic relation for the relative velocity, a local equilibrium between the phases should be reached over short spatial length scales [140]. Assuming the particles follow the mixture flow path, then, the slip velocity between the phases is

$$\vec{v}_{lv} = \tau_{lv}\vec{a} \tag{3.14}$$

τ_{lv} is the particulate relaxation time.

$$\tau_{lv} = \frac{(\rho_m - \rho_v)d_v^2}{18\mu_l f_{drag}} \tag{3.15}$$

Where d_v is the diameter of the particles (or droplets or bubbles) of secondary phase, and the drag function f_{drag} is taken from Schiller and Naumann 1935 [141, 142];

$$f_{drag} = \begin{cases} 1 + 0.15R_e^{0.687}, & R_e < 1000 \\ 0.0183R_e, & R_e \geq 1000 \end{cases} \tag{3.16}$$

$\vec{a}$ is the secondary-phase particle's acceleration

$$\vec{a} = \vec{g} - (\vec{v}_m.\nabla)\vec{v}_m - \frac{d\vec{v}_m}{dt} \tag{3.17}$$

The simplest algebraic slip formulation is the so-called drift flux model. If the slip velocity is not solved, the mixture model is reduced to a homogeneous multiphase model.

3.2.5 Volume Fraction Equation for the Secondary Phases.

The volume fraction equation for secondary phase can be obtained from the continuity equation for secondary phase:

$$\frac{\partial}{\partial t}(\alpha_v \rho_v) + \nabla.(\alpha_v \rho_v \vec{v}_m) = -\nabla.(\alpha_v \rho_v \vec{v}_{dr,v}) \quad (3.18)$$

3.3. Simulation Methodology and Boundary Conditions.

This study presents a 2D simulation carried out using Ansys Fluent to investigate the occurrence of a shock wave generated by a flashing water jet. The Mixture model was applied in conjunction with the concept of slip velocities to model interpenetrating multiphase flows as non-homogeneous, where the phases (liquid water and water vapor) move at different velocities. The model solves the compressible Navier-Stokes equations coupled with mass transfer between the phases using a user define function (UDF). The two-dimensional flow field is simulated as transient using the pressure-based solver method with gravitational acceleration. The standard k−ε model was adopted to consider turbulent effects. Water vapor was modeled as ideal gas using piecewise-polynomial specific heat and the liquid water was modeled as compressible fluid. Time steps of 10^{-5} s were used with a maximum of 20 iteration and maximum scaled residuals of 10^{-5} for all equation.

The 2D computational mesh was generated with Ansys ICEM-CFD with 137500 quadrilateral cells for the 5.5 mm high nozzle and the vacuum chamber. The vacuum chamber had one inlet and no outlet, where the 100 mm long nozzle was defined as pressure-inlet (Figure (3.2)).

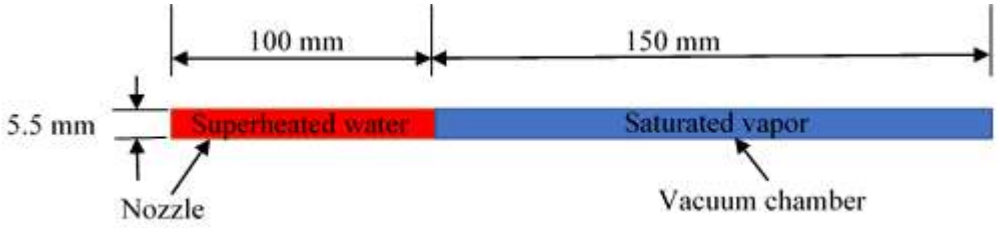

Figure 3.2 Schematic diagram of the nozzle and vacuum chamber.

The superheated liquid water was injected trough this nozzle with 101325 Pa initial pressure and 373.15 K initial temperature, while the water vapor in the 150 mm long vacuum chamber was initially at 1002 Pa vacuum pressure and corresponding saturation temperature of 280.12 K. A user-defined function (UDF), written in C and dynamically linked with the Fluent solver calculated the mass transfer between the liquid and vapor phases in the multiphase mixture, based on saturation temperature.

CHAPTER 4

Numerical Results

4.1 Simulation Results

When the superheated water is injected through the nozzle into the vacuum chamber, a flashing jet is created in conjunction with unsteady turbulent motion. The transient results of the evaporating water inside the flashing chamber at different time steps are presented below in terms of pressure, liquid water volume fraction, Mach number, velocity, and density. All calculations were taken at the center line of the flashing chamber. The results show that once the superheated water injected, it flashes immediately and generates shock wave. The generated shock wave is not stationary, and it is traveling through the fluid as moving shock wave.

The shock is a compression front across which the flow properties jump. The shock may also be described as compression front in a supersonic flow field and the flow process across the front results in an abrupt change in fluid properties. When a structured wave becomes sufficiently rapid in its rise time that the thickness of the wave can be ignored or is not measurable, then the wave is viewed as a discontinuous jump in the principal mechanical and thermodynamic parameters (e.g. pressure, velocity, temperature) [143]. The changes in flow properties across the shock take place within a very short distance. Hence, the velocity and temperature gradients inside the shock structure are large. These large gradients result in increase of entropy across the shock [144].

4.2 Moving shock waves

A shock wave is characterized by an abrupt discontinuity in fluid properties across very small region in the fluid, where static pressure and density increase almost instantaneously. When a wave becomes sufficiently rapid in its rise time that the thickness of the wave can be ignored or is not measurable, then the wave is viewed as a discontinuous jump in the principal mechanical and thermodynamic parameters (e.g. pressure, velocity, temperature) [145]. Moving shock waves

are known e.g. from industrial application when a valve is suddenly closed and a shock propagates upstream (water hammer), and from shock tube experiments where a high-pressure fluid is suddenly exposed to low pressure chamber. A moving shock wave transports energy while propagating through the medium.

4.2.1 First time step 0.01 ms - shock induction by flash evaporation

Once the superheated water is injected into the vacuum chamber, the sensible heat of the liquid converts into the latent heat of vaporization and the liquid undergoes a rapid phase transition process due to the sudden pressure drop. The onset of the phase change is triggered at the nozzle exit - the inlet of the vacuum chamber. At first time step 0.01 ms, the velocity increased from zero to about 10.61 m/s at location x=0.1004 m indicated by the vertical green line in below figures. Even though the velocity may not seem to be high, it exceeds the speed of sound of the two-phase fluid, which is around 4.25 m/s at this point.

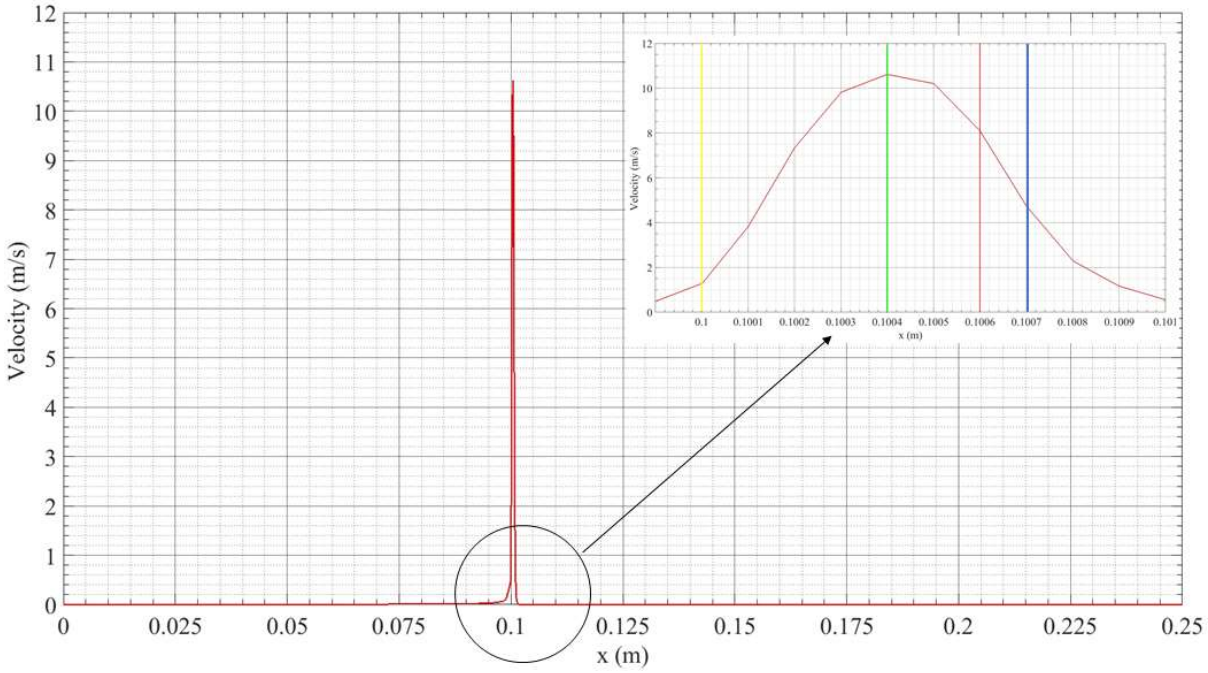

Figure 4.1 Velocity distribution along the center line at time 0.01 ms.

The speed of sound of the mixture can be much smaller than that of either of its constituents [146, 147]. Figure (4.2) illustrated the variations of the speed of sound with the liquid water volume fraction.

Due to the sudden phase change, speed of sound varies from speed of sound of the liquid water of around 1484 m/s to the speed of sound of the mixture of about 4.25 m/s at location x= 0.1004 m where the liquid water volume fraction is 0.07. The variation of the speed of sound during the flashing process along the flashing chamber at first time step 0.01 ms is illustrated in Figure (4.2). As a result of the superheated water injection, a supersonic flow downstream of the nozzle is induced and the Mach number increases from 0.0 to about 2.21 at the point $x = 0.1004$ m. Figure (4.3) shows the Mach number distribution along the center line of the flashing chamber at first time step 0.01 ms. While the pressure drops in the nozzle from 101325 Pa to around 1000 Pa at location x = 0.1 m, it increases from 1000 Pa at location x > 0.101 m to 1442 Pa at location 0.1007 m. Figures (4.4) shows the static pressure distribution along the center line at the first time step 0.01 ms.

The sudden pressure drop at the nozzle exit results in a strong flash evaporation with the highest gradient of the liquid water volume fraction at x = 0.1 m (Figure (4.5)), signified by the yellow vertical line. The magnification in Figure (4.5) shows that evaporation zone extends into the vacuum chamber to location x= 0.1006 m. Figure (4.6) shows that the front of the evaporation zone coincides with the highest temperature gradient signified by the vertical red line. All the new vapor created in evaporation zone accumulatively acts like a fast moving piston generating a shock wave that moves even faster ahead of the evaporation front, signified by the vertical blue line for the highest pressure gradient in front of the evaporation zone. It is noted that the gradients at location x_i are calculated for the difference of the quantity between the locations x_i and x_{i+1}, so that

the steepest pressure line in the magnification of Figure (4.4) is seen between locations (nodes) x_i = 0.1007 m and x_{i+1} = 0.1008 m.

The increase in Mach number behind the shock reflects the induced speed of the vapor in the vacuum chamber that was at rest before the moving shock moved through, compressed, and accelerated it [148, 149, 150], whereas the increase of the Mach number in front of the nozzle reflects the accumulative increase of the speed of the new vapor created by the flash evaporation of the incoming fluid. The density distribution in Figure (4.7) is primarily determined by the liquid water volume fraction distribution in Figure (4.5).

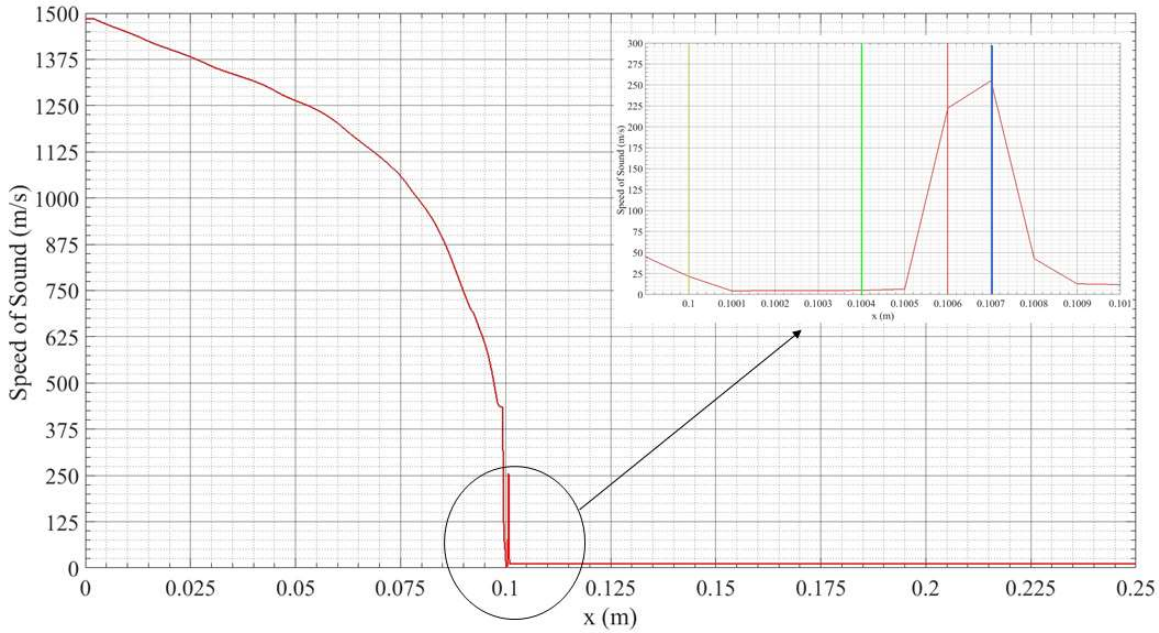

Figure 4.2 Speed of sound distribution along the center line at time 0.01 ms.

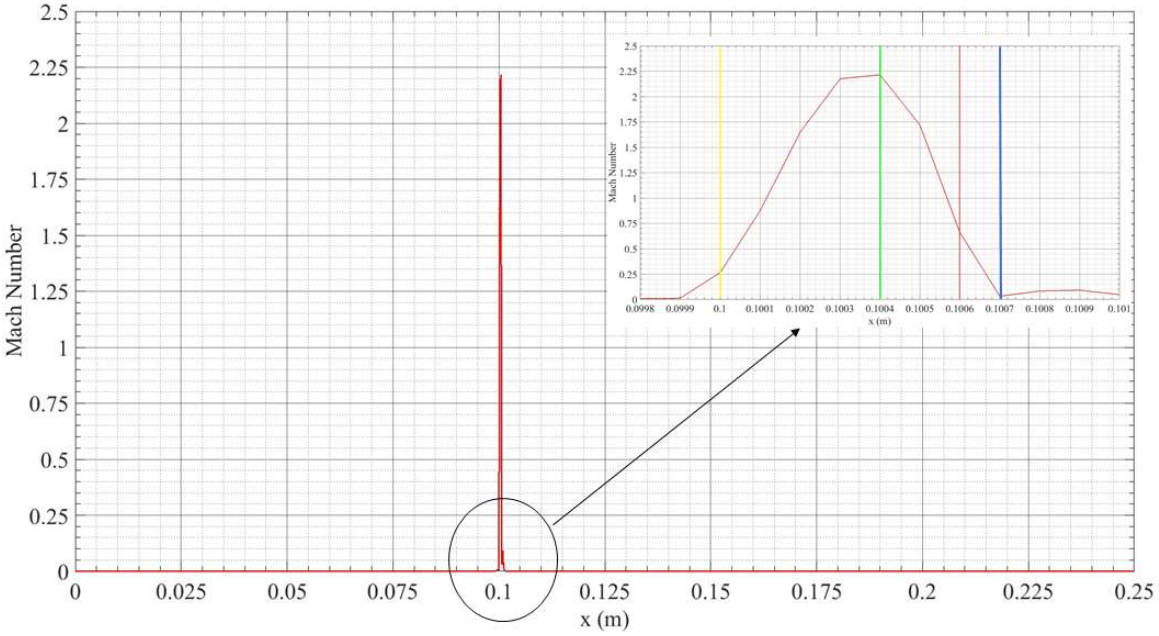

Figure 4.3 Mach number distribution along the center line at time 0.01 ms.

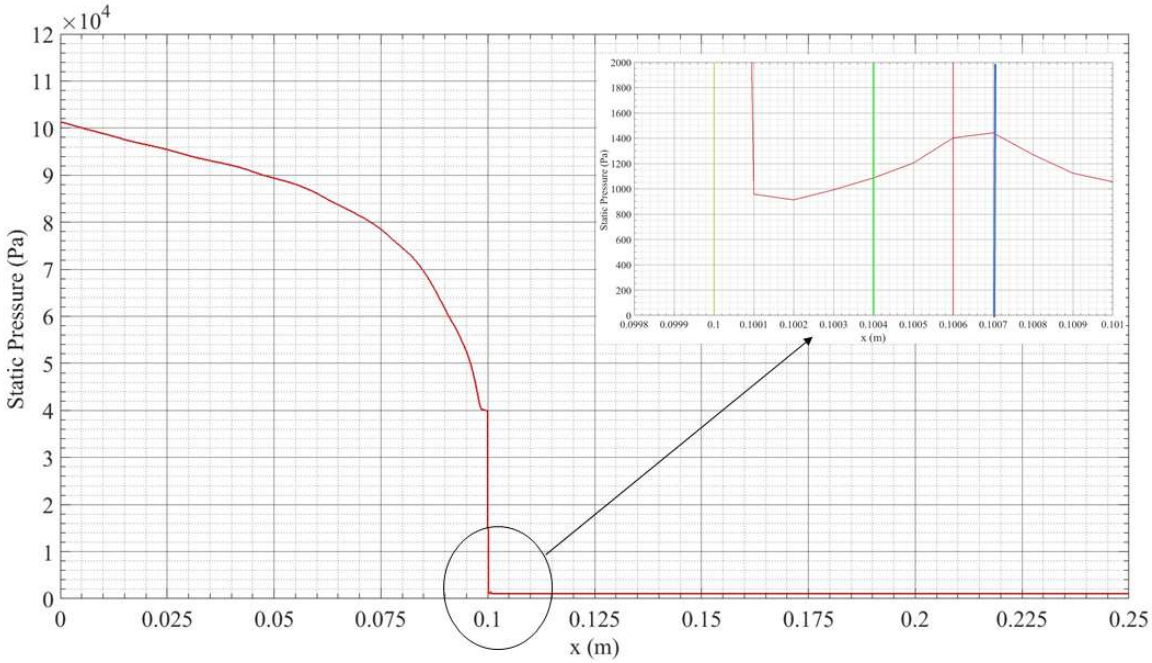

Figure 4.4 Static pressure distribution along the center line at time 0.01ms .

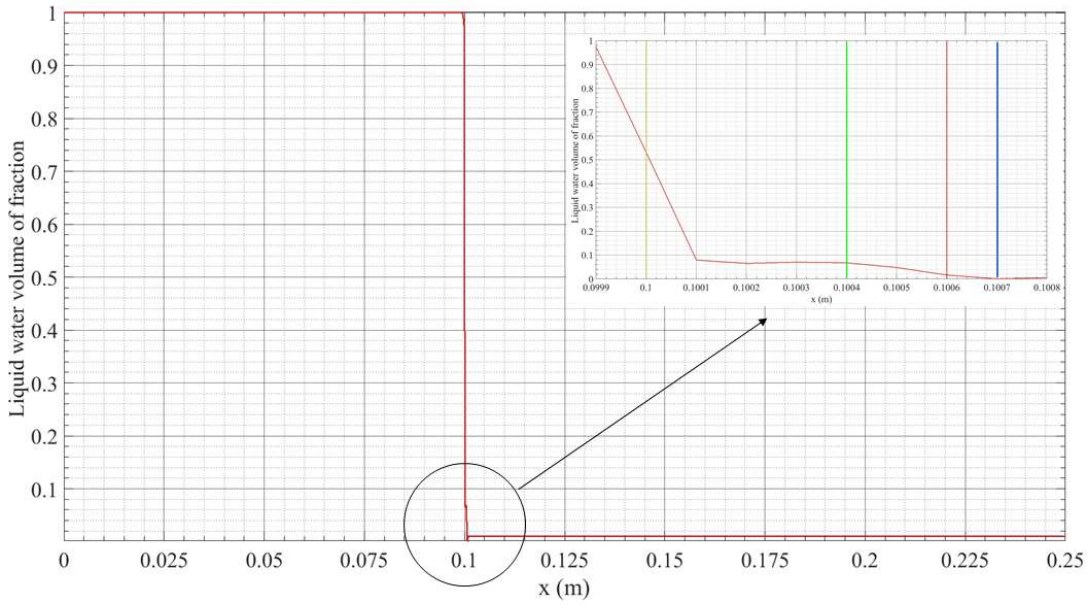

Figure 4.5 Liquid volume fraction distribution along the center line at time 0.01 ms.

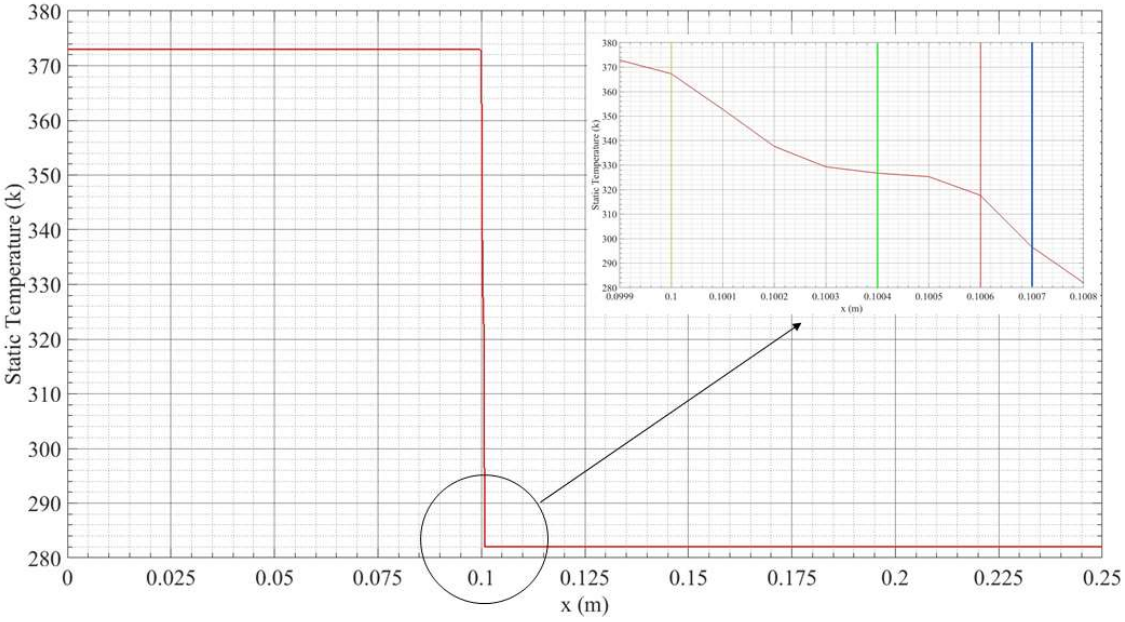

Figure 4.6 Static temperature distribution along the center line at time 0.01 ms.

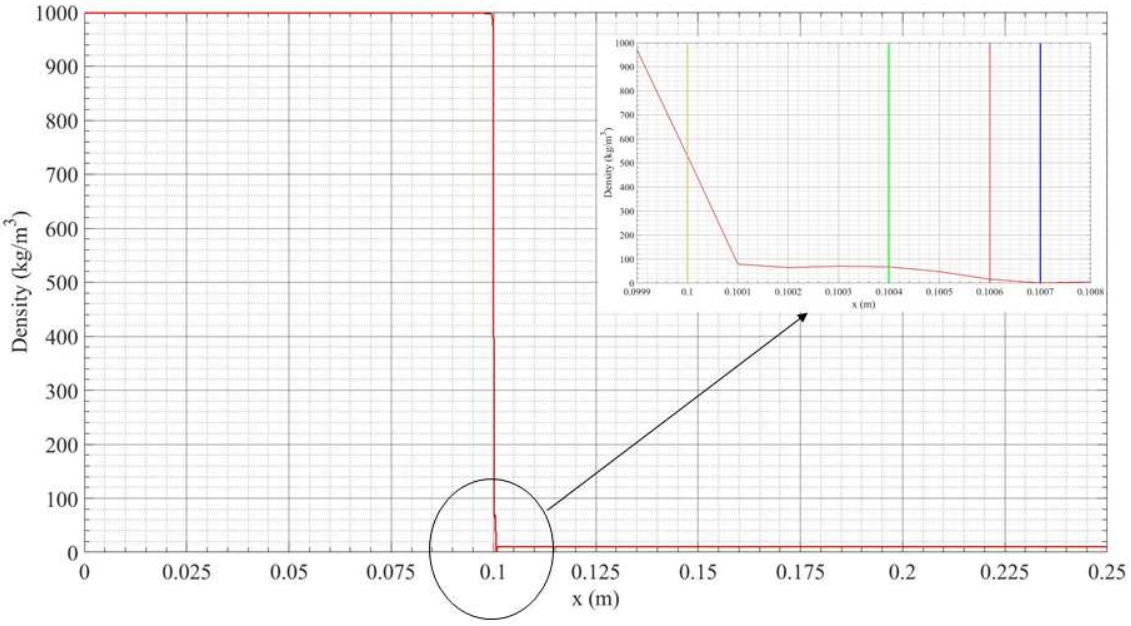

Figure 4.7 Density distribution along the center line at 0.01 ms.

4.2.2 Time step 7 ms – moving shock wave

After the sudden evaporation began at the first time step 0.1 ms, through evaporation the newly created two-phase mixture (evaporation zone) continued to expand further behind the moving shock wave that traveled even faster into the previously stagnant vapor. At time step 7 ms, Figures (4.8) shows the moving shock wave reached location x = 0.2059 m indicated by the maximum pressure gradient (blue vertical line), while Figures (4.9) shows the evaporation front reached location x = 0.1724 m indicated by the maximum temperature gradient (red vertical line). Hence, the distance between the moving shock wave and the evaporation front increased from 0.1 mm at the first time step 0.01 ms to 33.5 mm at time step 7 ms.

Figures (4.10) shows how the highest temperature gradient coincide with front of the evaporation zone (end of change in liquid water volume fraction). Furthermore, Figure (4.10) shows an increase of the liquid water fraction across the moving shock wave, rendering it a condensing shock. Figures (4.12) shows how the velocity of the formerly stagnant vapor increases behind the shock to the induced velocity of the now compressed vapor. Also, Figures (4.12) shows

how due to the newly generated vapor the velocity of the two-phase mixture in the evaporation zone accumulatively increases from left to right to its maximum behind the evaporation front signified by the maximum temperature gradient (red vertical line).

The Mach number in Figure (4.13) increases in front of the nozzle from left to right to its maximum at location x = 0.1500 m after which it decreases despite the velocity continues to rise to its maximum close behind the evaporation front. This is because starting at x > 0.1500 m the speed of sound (Figure (4.14)) starts to increase significantly faster than the velocity of the tow-phase mixture. The speed of sound increases at this point because of the continued decrease of the liquid water volume fraction below 0.2 (Figure 4.15).

The 2-D color contour plots of the complete flashing chamber are added to all Figures showing the predominantly 1-D behavior of the phenomena supporting the use of the center line presentation.

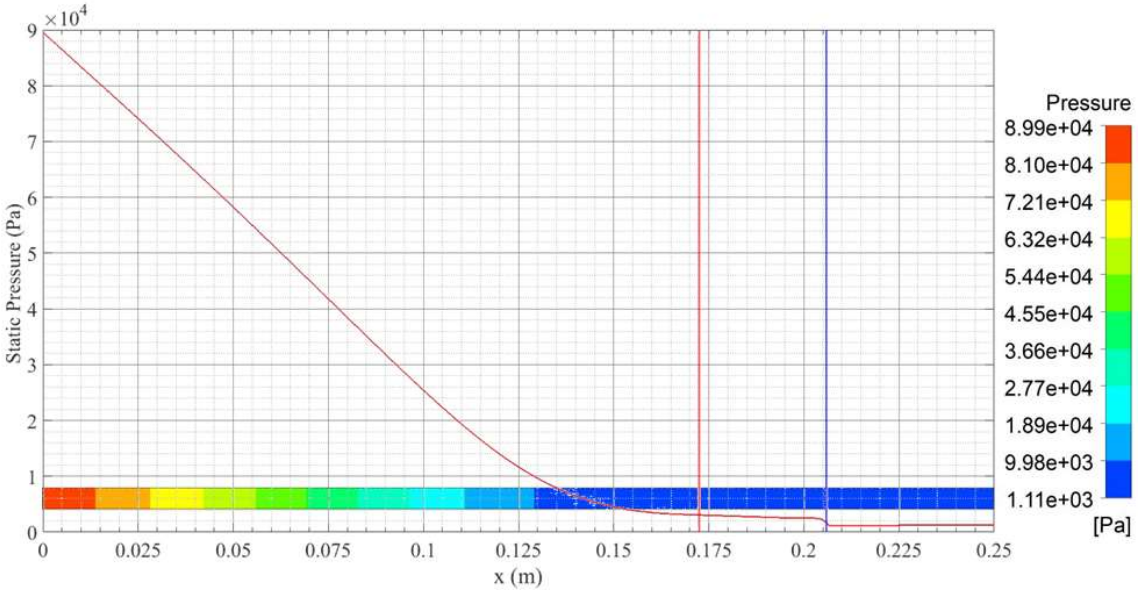

Figure 4.8 Static pressure distribution along the center line and 2-D contour at time 7 ms.

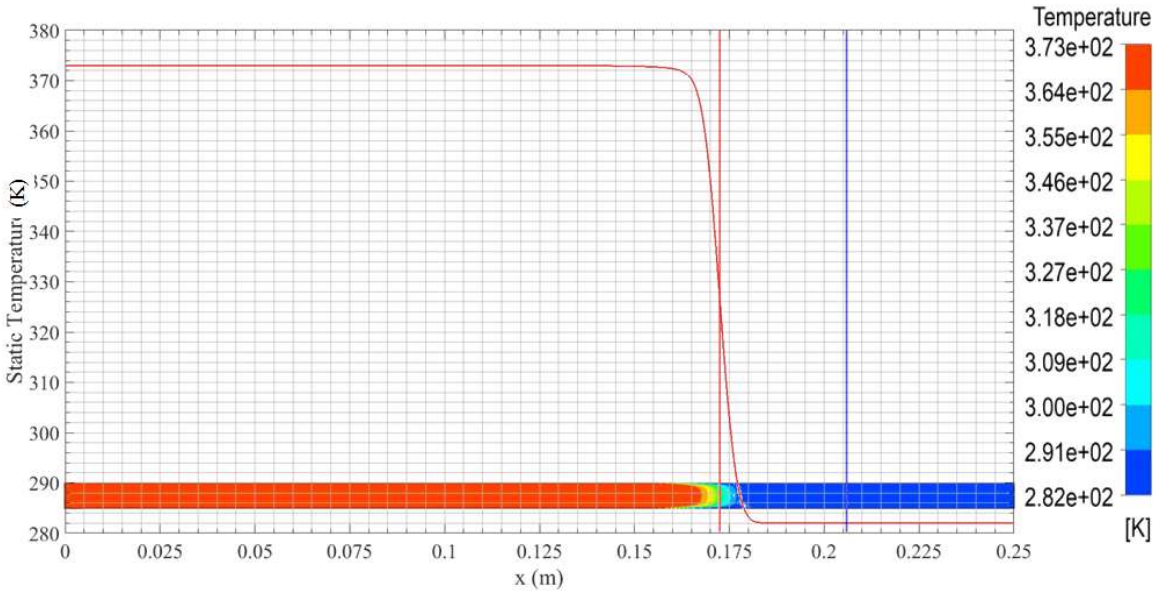

Figure 4.9. Static temperature distribution along the center line and 2-D contour at time 7 ms

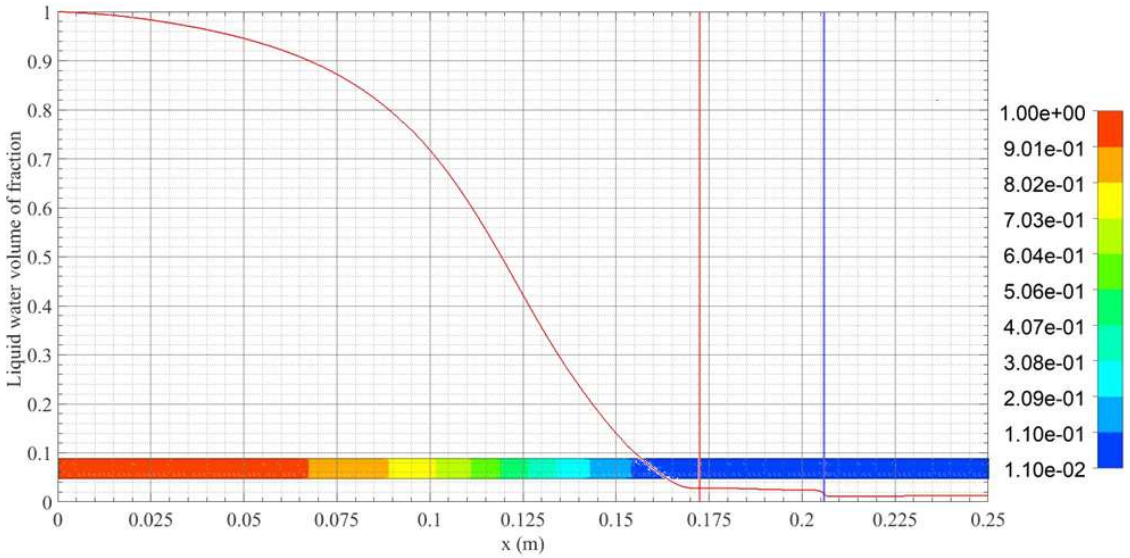

Figure 4.10 Liquid water volume fraction distribution along the center line and 2-D contour at time 7 ms.

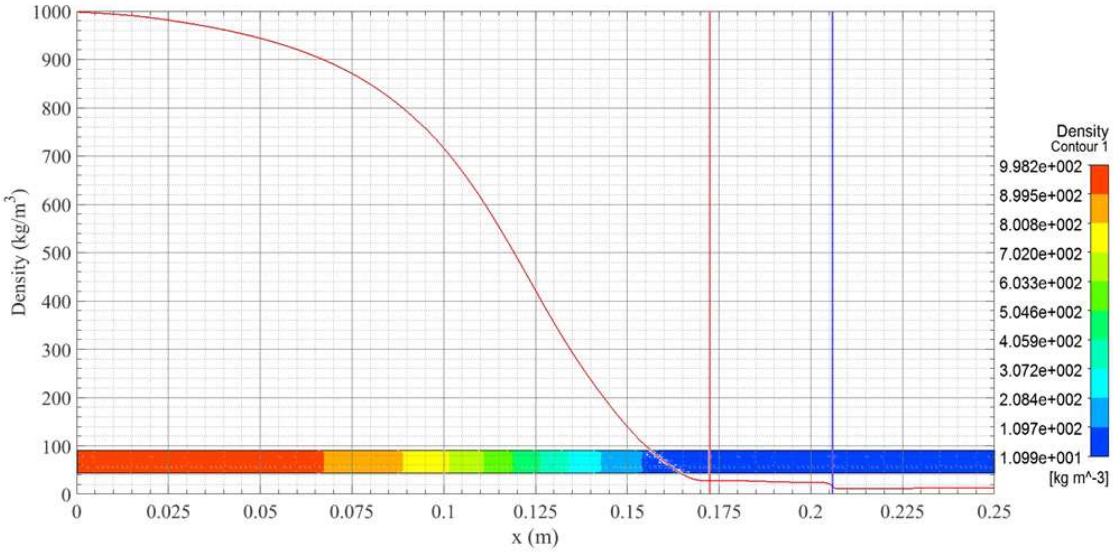

Figure 4.11 Density distribution along the center line and 2-D contour at time 7 ms.

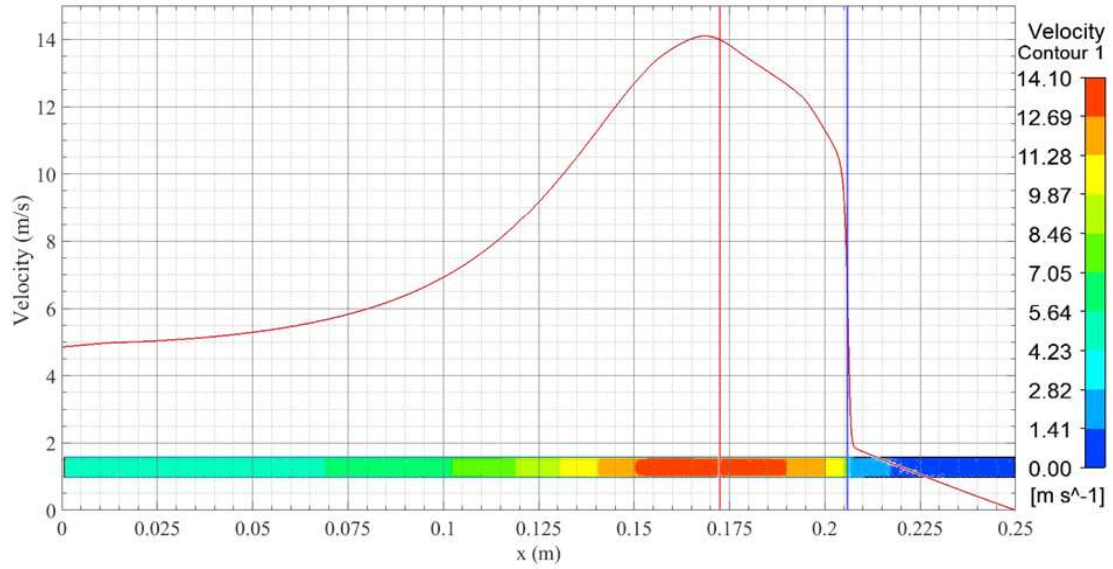

Figure 4.12 Velocity distribution along the center line and 2-D contour at time 7 ms.

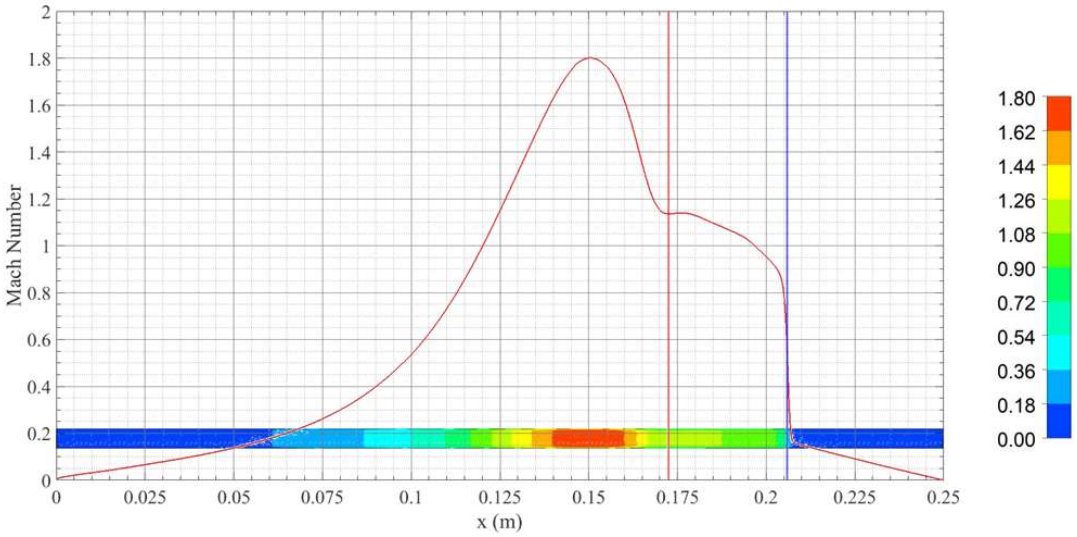

Figure 4.13 Mach number distribution along the center line and 2-D contour at time 7 ms.

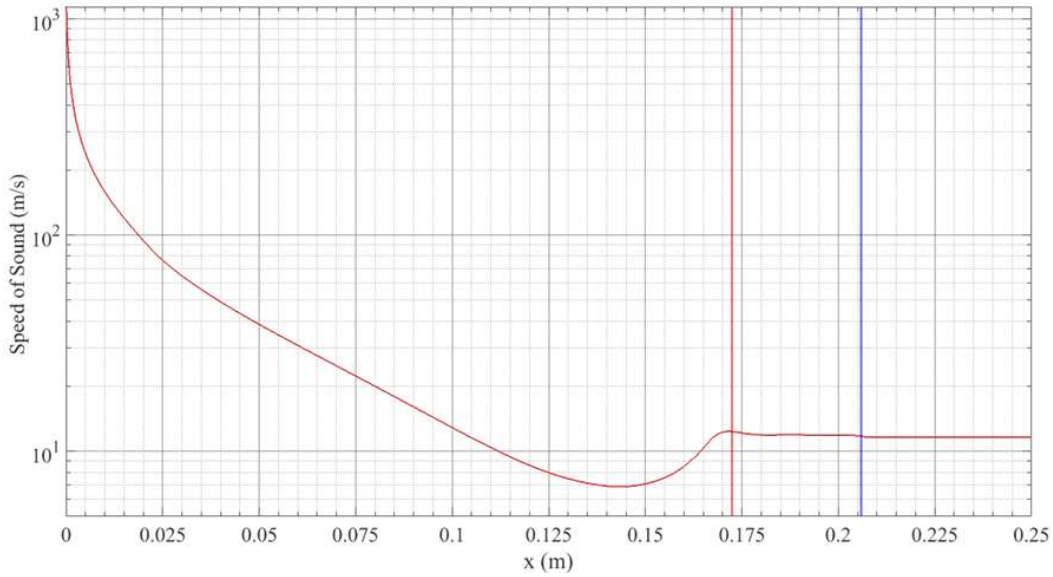

Figure 4.14 Speed of sound vs. location at time 7 ms.

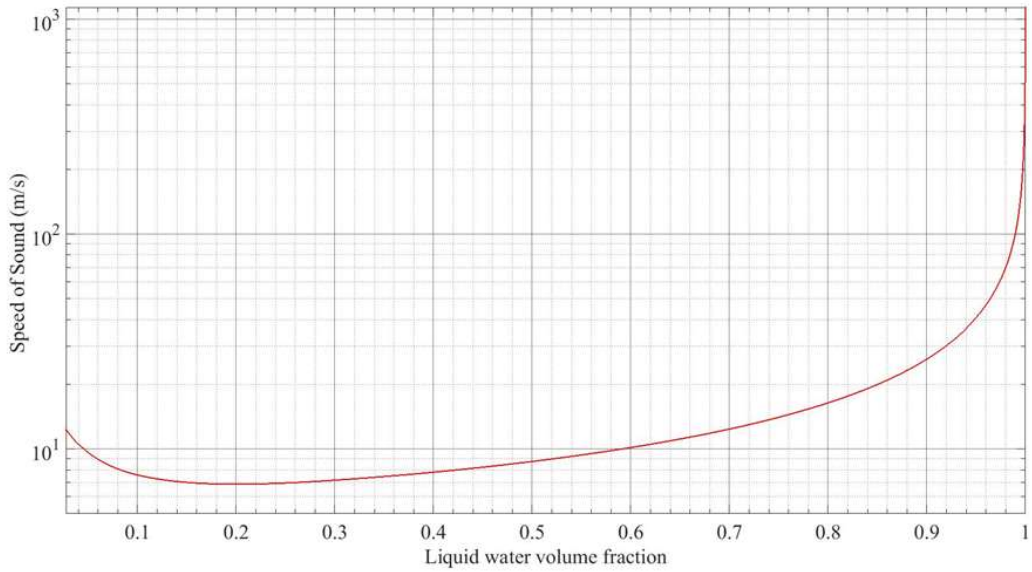

Figure 4.15 Speed of sound vs. liquid water volume fraction at time step 7 ms.

4.2.3 Time step 16.30 ms – reflected shock wave

The moving shock wave continued to travel through the vacuum chamber until it struck the right end of the vacuum chamber (x = 0.25 m) at 9.70 ms. It then reflected from the wall as reflected shock wave and propagated back into the chamber, where it met the evaporation front at 11.40 ms and x = 0.2400 m and then penetrated further into it reaching location x = 0.2270 m at 16.30 ms. Figure (4.16) shows t-x wave diagram that illustrates the moving shock wave and its location at different time throughout the flashing chamber.

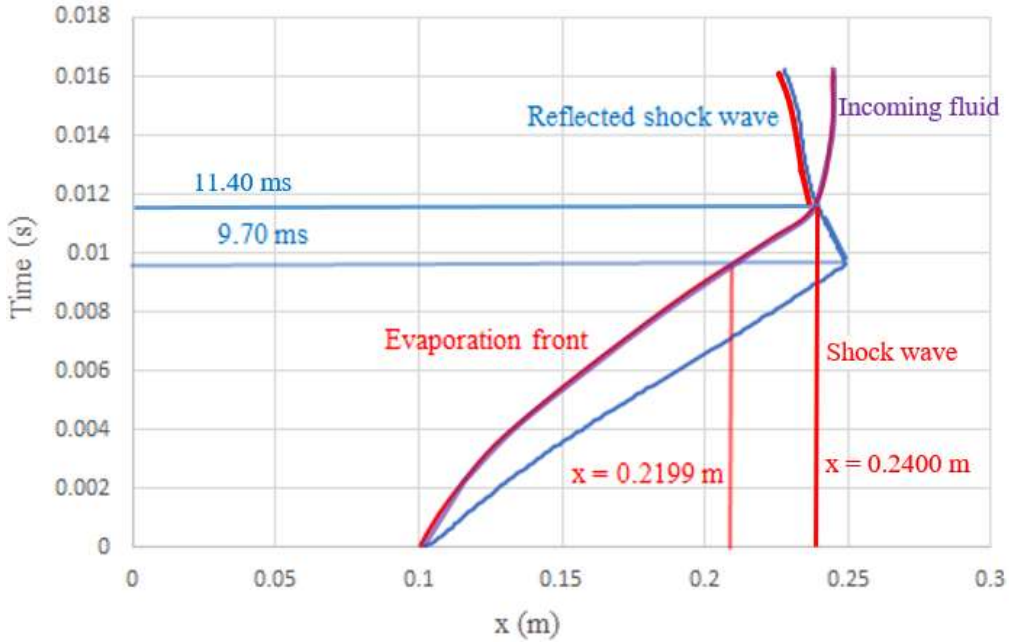

Figure 4.16 t-x diagram shows tracks of primary and reflected shock wave (blue), evaporation front (red), and interface of incoming fluid (purple) along the center line of the flashing chamber through time step 16.30 ms.

Figure (4.16) also illustrates the location of the evaporation front at all-time steps through time step 16.30 ms. It shows that the two-phase mixture continued to expand further behind the moving shock wave. At 9.70 ms when the shock wave struck the wall the evaporation front arrived at point x = 0.2199 m, 30.1 mm behind the shock. Figure (4.17) shows the distribution of the static temperature along the flashing chamber through 16.30 ms. Represented by the high temperature plateau, it shows how the incoming two-phase fluid moved into the vacuum chamber and compressed the low temperature vapor in the vacuum chamber against the wall at the right end. It slowed significantly down when the reflected shock wave met and penetrated it.

Figure (4.18) shows the distribution of the velocity along the flashing chamber through 16.30 ms. The highest velocity is always found at the evaporation front, which is at the highest temperature gradient behind the shock; and once the reflected shock penetrated the incoming two-phase fluid, it is found in front of the reflected shock (see also Figure (4.16)).

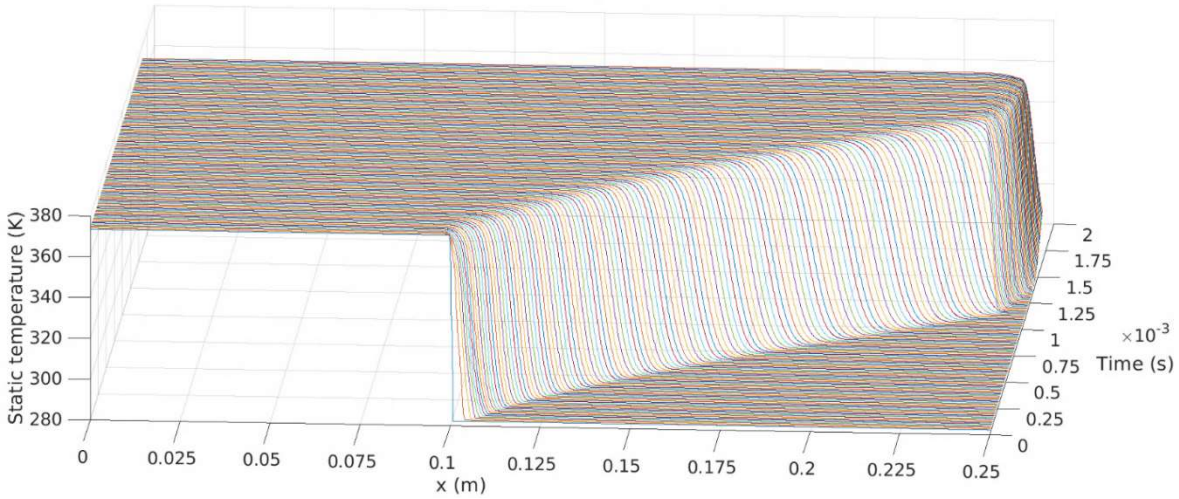

Figure 4.17 The distribution of the static temperature along the center line of the flashing chamber through 16.30 ms.

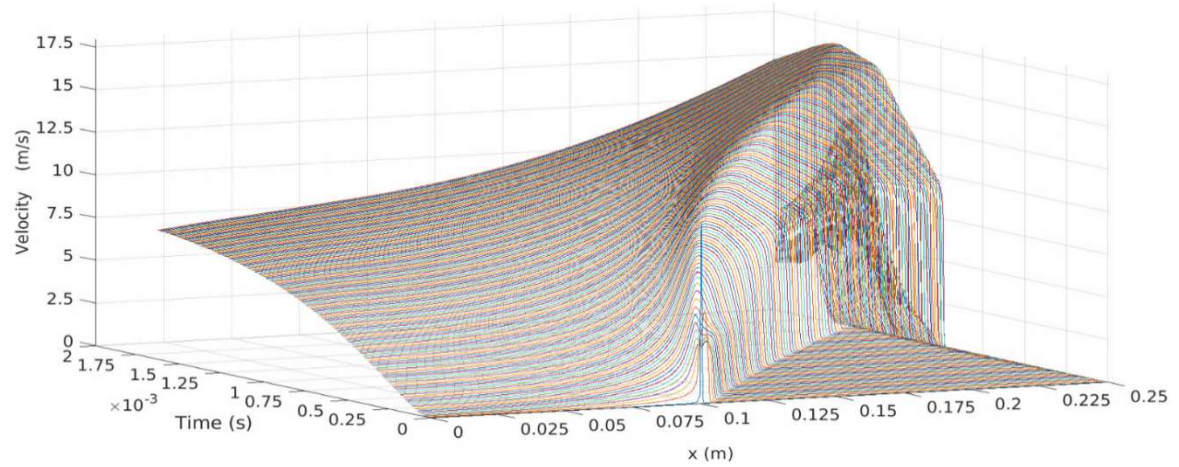

Figure 4.18 The distribution of the velocity along the center line of the flashing chamber through 16.30 ms.

Figure (4.19) visualizes the distribution of the liquid water volume fraction along the flashing chamber through 16.30 ms, indicating the increase of the liquid water volume fraction after the primary shock and even more after the reflected shock, rendering these as condensing shocks.

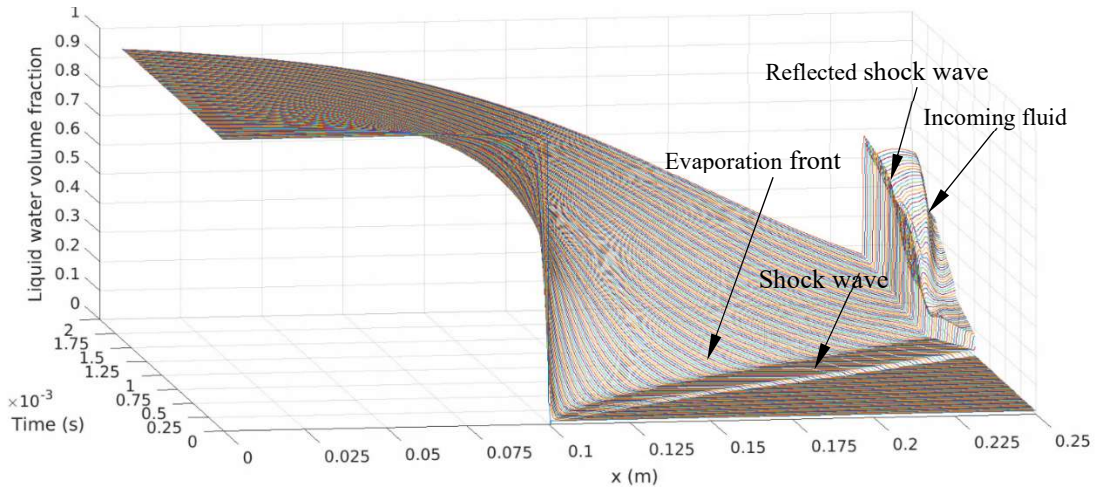

Figure 4.19 The distribution of the liquid water volume fraction along the center line of the flashing chamber through 16.30 ms.

Figures (4.20) shows the pressure distribution at 16.30 ms where the reflected shock reached the location x = 0.2498 m indicated by the maximum pressure gradient (blue vertical line). At this location, the static pressure increases from 12157 Pa to 71549 Pa indicating strong reflected shock wave with pressure ratio 5.88. Representing a temperature - location plane of Figure (4.17), Figures (4.21) shows the static temperature distribution at 16.30 ms, indicating that incoming two-phase fluid has moved past the reflected shock. Figure (4.22) shows how the liquid water volume fraction decreases in the evaporation zone from 1 to the lowest value of 0.2484 at the evaporation front (x= 0.2271 m) and jumps to 0.6544 after the reflected shock at x = 0.2278 m, indicating the condensing character of the shock. The density distribution in Figure (4.23) follows the liquid water volume fraction distribution in Figure (4.22), showing that like in all previous time steps the liquid water volume fraction predominantly determines the density.

Figure (4.24) shows how the velocity of the incoming two-phase fluid increases due to the generated vapor in the evaporation zone accumulatively to its highest value 15.57 m/s at x = 0.2270 m in front of the reflected shock. Due to the velocity induced by the reflected shock, the velocity

of the incoming fluid reverses across the reflected shock to 6.83 m/s (at x = 0.2305 m) following the reflected shock back in the direction to the nozzle, while the velocity at the wall remains zero.

The Mach number in Figure (4.25) follows the pattern of the velocity in Figure (4.24). It increases in the evaporation zone to supersonic speed with its maximum value of Mach 1.68 at x = 0.2270 m in front of the reflected shock. Across the reflected shock the Mach number reduces significantly to subsonic Mach 0.18 at x = 0.2278 m. The change from supersonic to subsonic condition across the reflected shock is amplified by the increase of speed of sound from 9.28 m/s to 20.46 m/s (Figure (4.26)) due to the increase of the liquid water volume fraction accompanying the condensation.

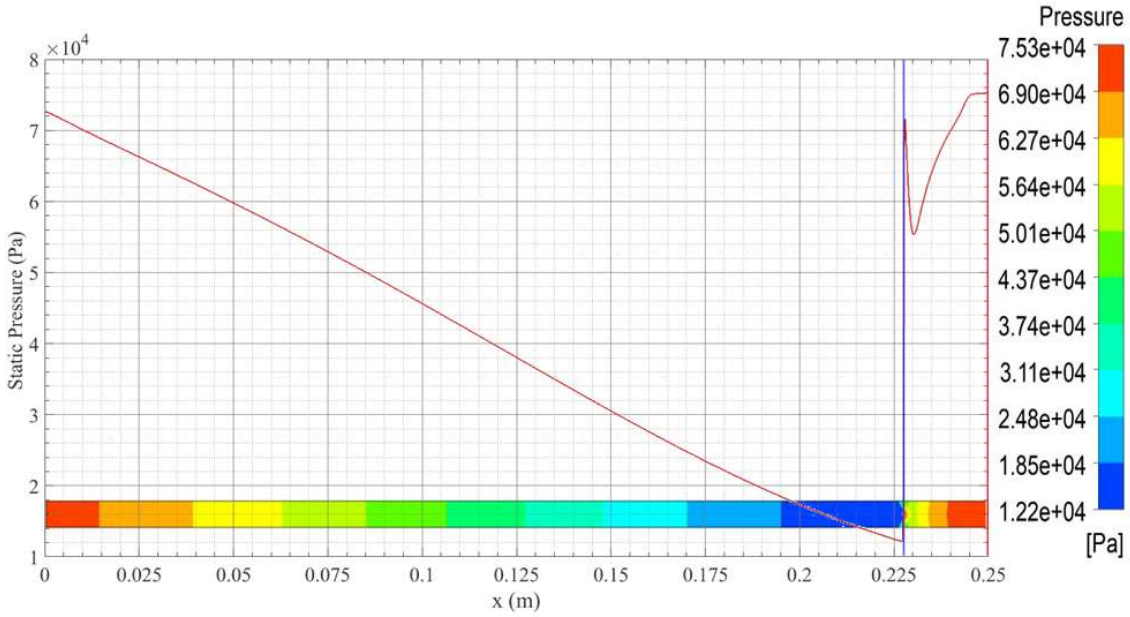

Figure 4.20 Static pressure distribution along the center line and 2D contour at 16.30 ms.

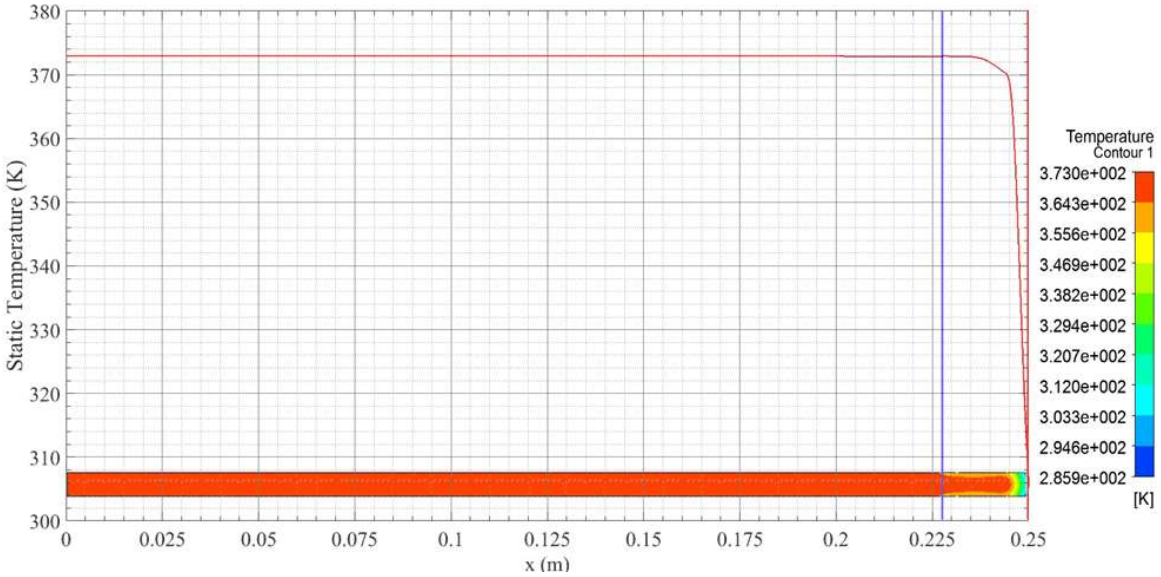

Figure 4.21 Static temperature distribution along the center line and 2D contour at 16.30 ms.

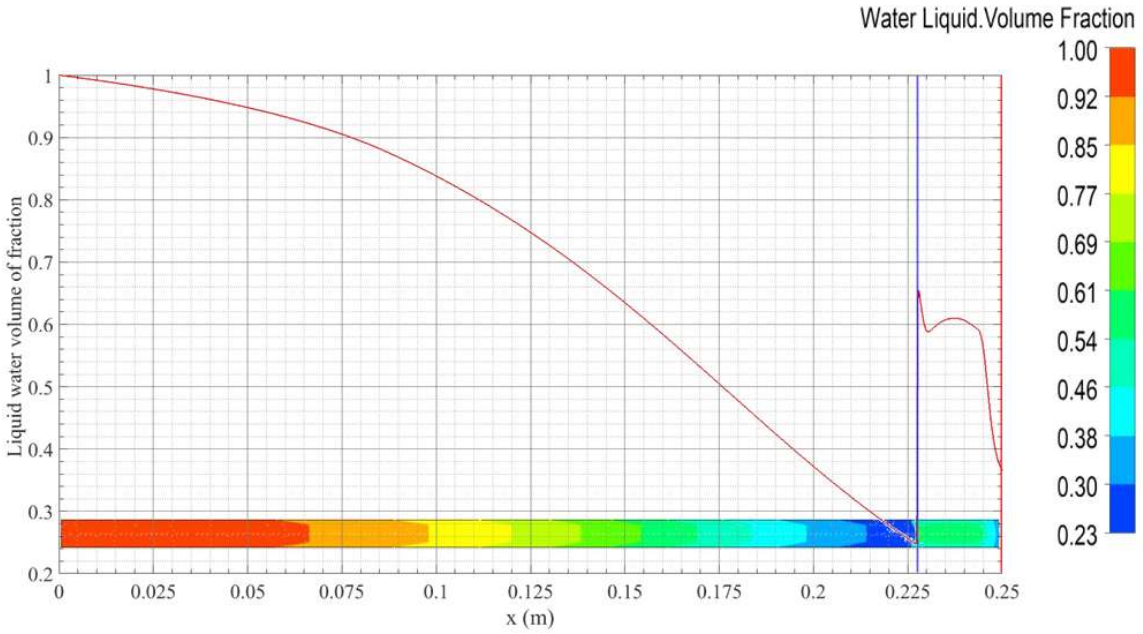

Figure 4.22 Liquid water volume fraction distribution along the center line and 2D contour at 16.30 ms.

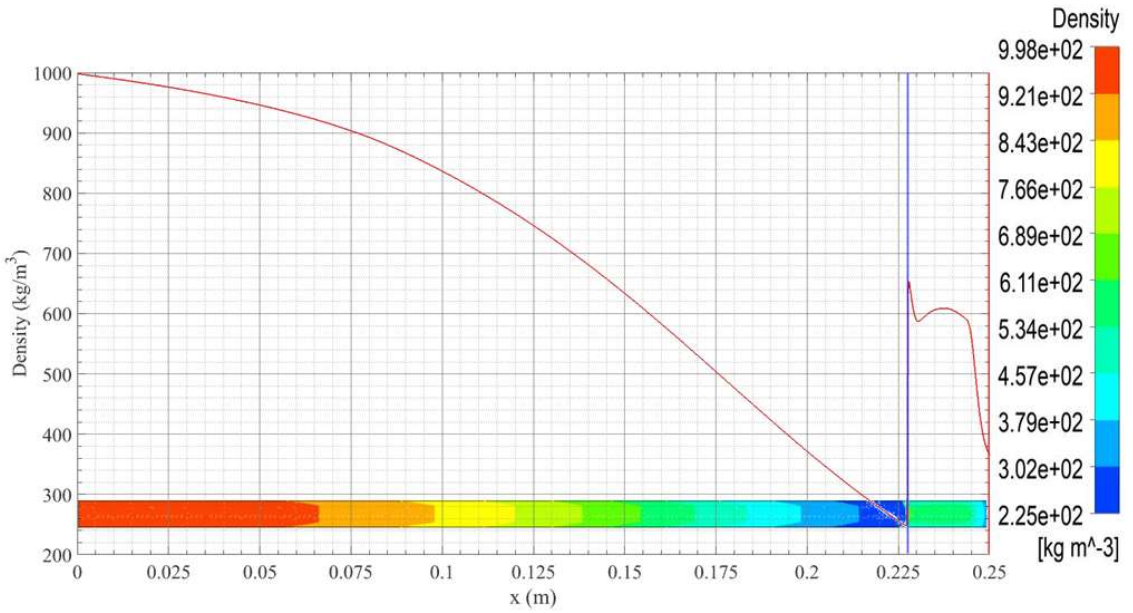

Figure 4.23 Density distribution along the center line and 2D contour at 16.30 ms.

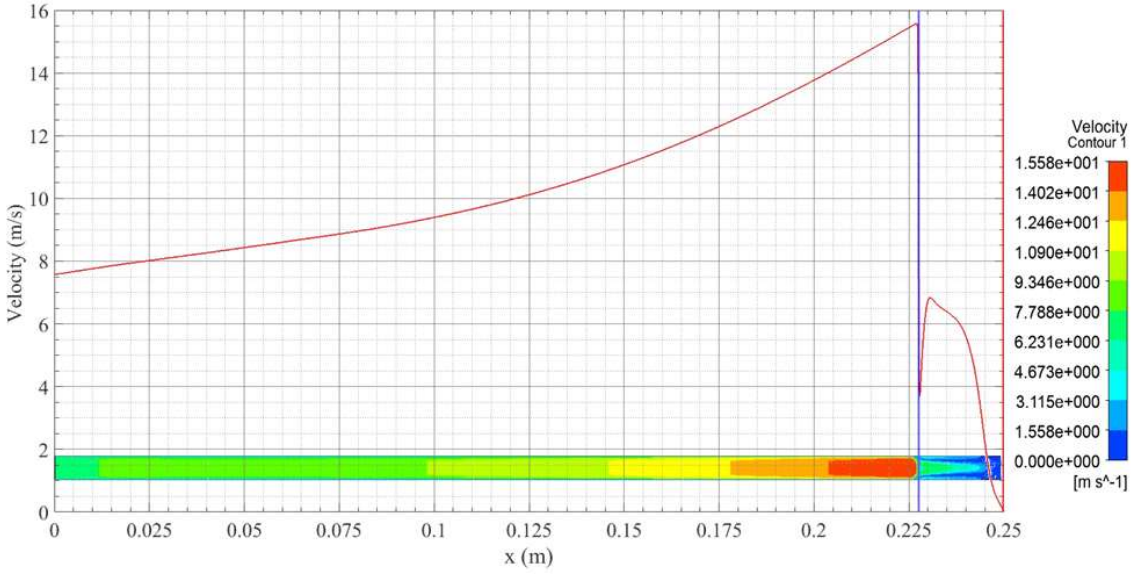

Figure 4.24 Velocity distribution along the center line and 2D contour at 16.30 ms.

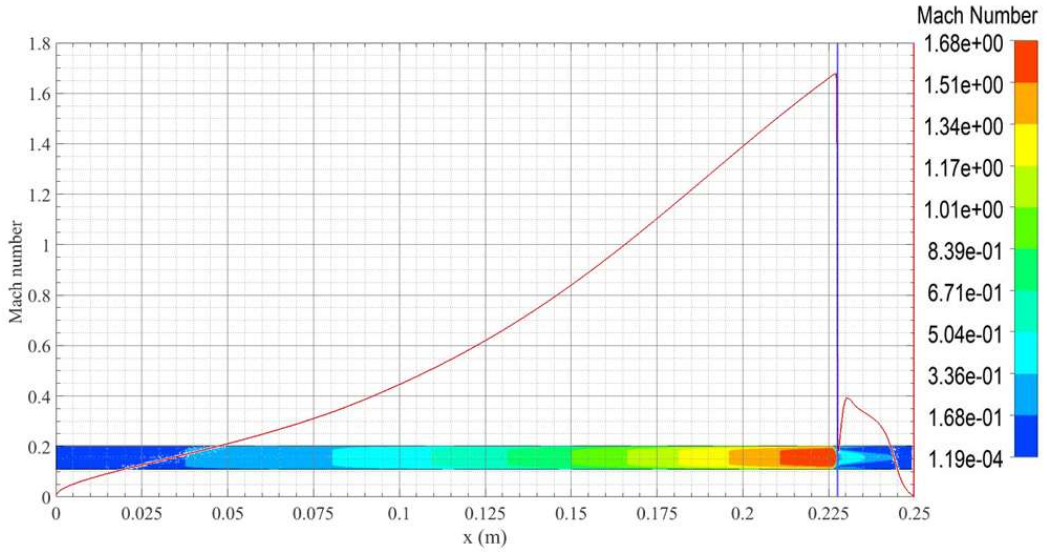

Figure 4.25 Mach number distribution along the center line and 2D contour at 16.30 ms.

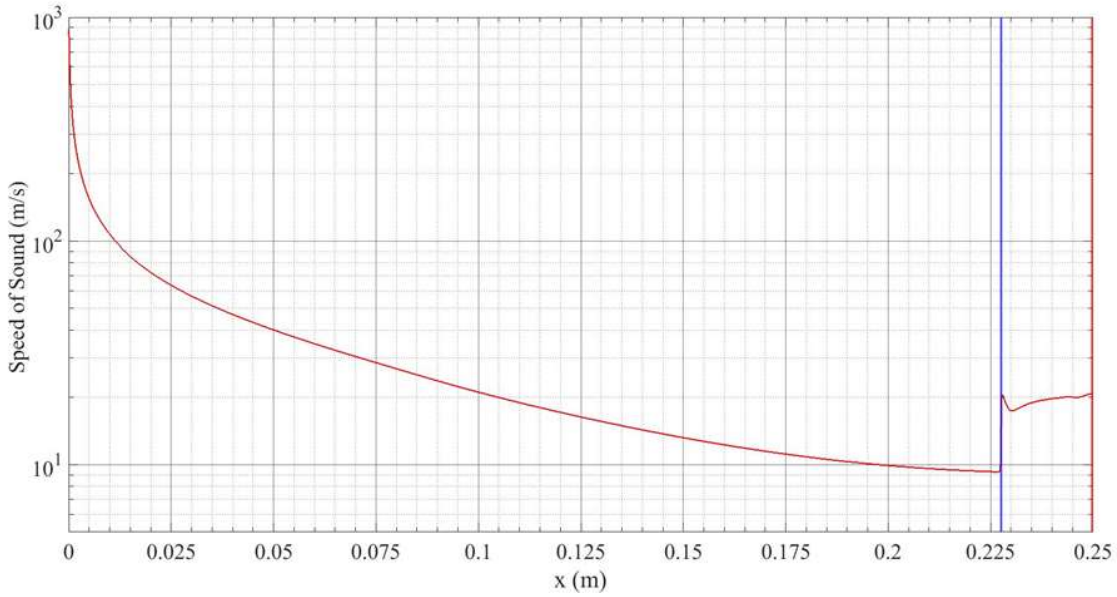

Figure 4.26 Speed of sound distribution along the center line and 2D contour at 16.30 ms.

The t-x diagrams that shown below present the flow characteristics through time step 16.30 ms. The distributions of pressure, temperature, density, Mach number, Velocity, and liquid water volume fraction influenced by moving and reflected shock waves present on the contours of t-x diagrams in Figure (4.27). The t-x diagrams show that all the flow characteristics are discontinuous

across the shock wave. Figure (4.27) shows t-x diagrams as contours plots of density, velocity, pressure, liquid water mass fraction, Mach number, and temperature through 16.30 ms with the tracks like in Figure (4.16) of the shock waves indicated by a blue line and the front of the incoming fluid indicated by a red line.

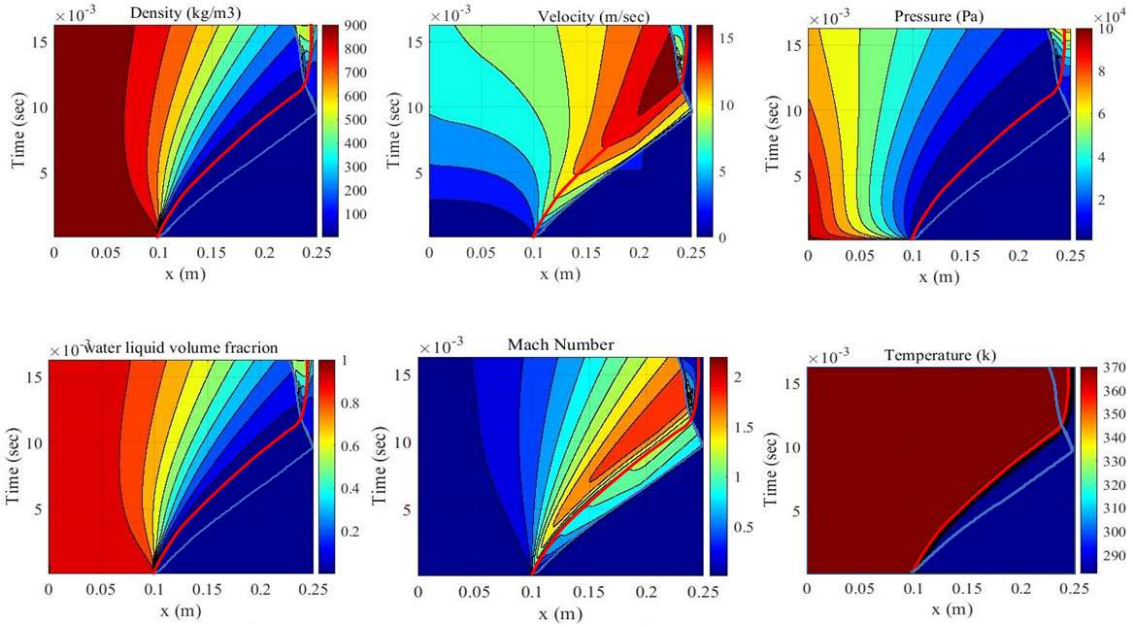

Figure 4.27 Fill contours of density, velocity, pressure, liquid water mass fraction, Mach number, and temperature at 16.30 ms.

Like in Dai et al. [29, 48] the steep gradients and discontinuities in the x–t diagrams indicate the propagation of the shock waves, reflected shock wave, and fluid interface, where Dai et al. investigated a single shock generated by one rupturing diaphragm [48] and two shocks generated by two simultaneously rapturing diaphragm [29]. In difference to Dai et al. [29, 48] who used superheated water vapor to generate the shocks, in the present work the shocks were generated by the flashing of incoming superheated liquid water, proving that a shock wave can be generated in water vapor under vacuum by flashing liquid water entering the vacuum.

4.3 Second 2D Simulation Results

Another simulation was conducted with different geometries of the flashing chamber. The mesh was generated by using ICEM-CFD and the cell size were 440500 quadrilateral cells for the nozzle and the rectangular channel. The flashing chamber (nozzle and vacuum chamber) shown in Figure (4.28) has inlet and without outlet, where the nozzle 0.1 m long with 5.5 mm orifice diameter is defined as pressure-inlet. The superheated liquid water was injected trough the nozzle at initial pressure 101325 Pa and initial temperature 373.15 k while a water vapor in a 0.15 m long and 0.025 m width vacuum chamber at pressure 1002 Pa and saturation temperature 280.12 k.

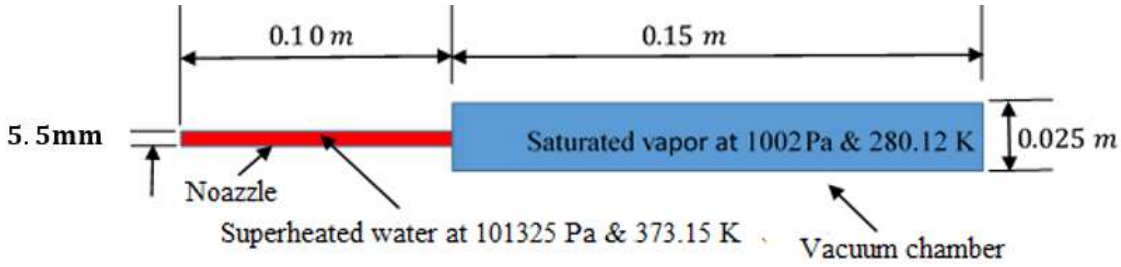

Figure 4.28 Schematic diagram of the second flashing chamber

The obtained results were in a good agreement with the previous simulation. The results show that once the superheated water is injected, it flashes immediately and generates a shock wave. The generated shock wave is not stationary, and it is traveling through the fluid as moving shock wave. The transient results of the evaporating water inside the flashing chamber at different time steps are presented below in terms of pressure, temperature, velocity, speed of sound, liquid volume fraction, and Mach number.

4.3.1 First time step, 0.01ms

During the sudden drop in pressure, the sensible heat of the liquid converts into the latent heat of vaporization and the liquid undergoes a rapid phase transition process at first time step

(0.01ms). As a result, a supersonic flow downstream of the nozzle is induced behind the generated shock wave progressing into the channel. The velocity increased from zero to about 10.5 m/s at location x= 0.1004 m where the speed of sound of the two-phase fluid about 4.42 m/s at this point. Figure (4.29) shows the velocity magnitude distribution along the center line of the flashing chamber at first time step 0.01 ms.

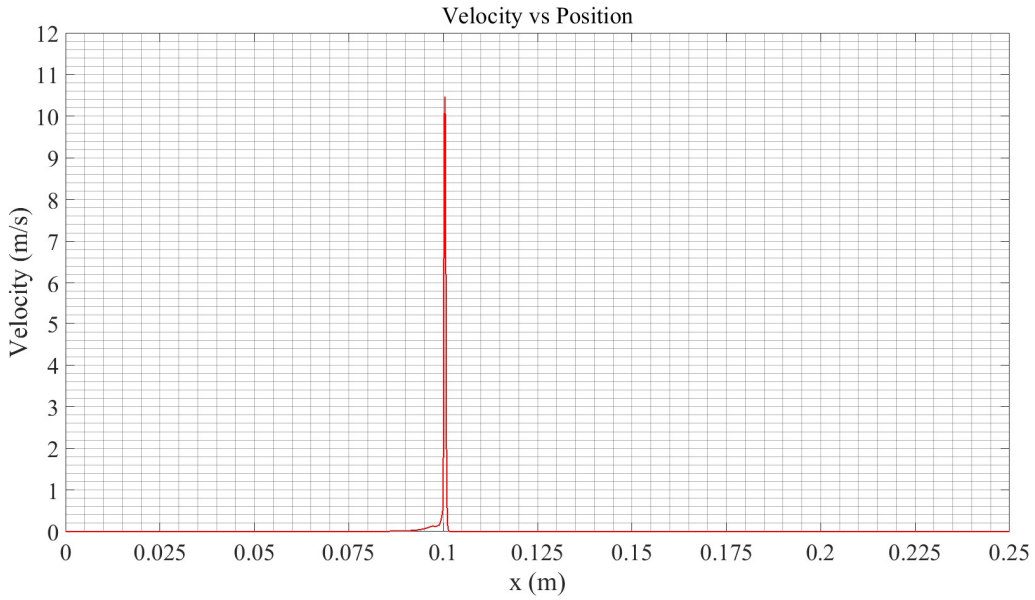

Figure 4.29 Velocity distribution along the center line of the flashing chamber at time 0.01 ms.

Due to the abrupt phase change, speed of sound changes from speed of sound of the liquid water around 1484 m/s to the speed of sound of water vapor or mixture for about 5 m/s. Figure (4.30) shows the variation of the speed of sound during the flashing process along the flashing chamber at first time step 0.01 ms. The Mach number increased from 0.0 to about 2.36 at the point $x = 0.1004$ m , while it remains less than one ahead of the point $x = 0.1007$ m where the fluid is still undisturbed. Figure (4.31) shows the Mach number distribution along the center line of the flashing chamber at first time step 0.01 ms.

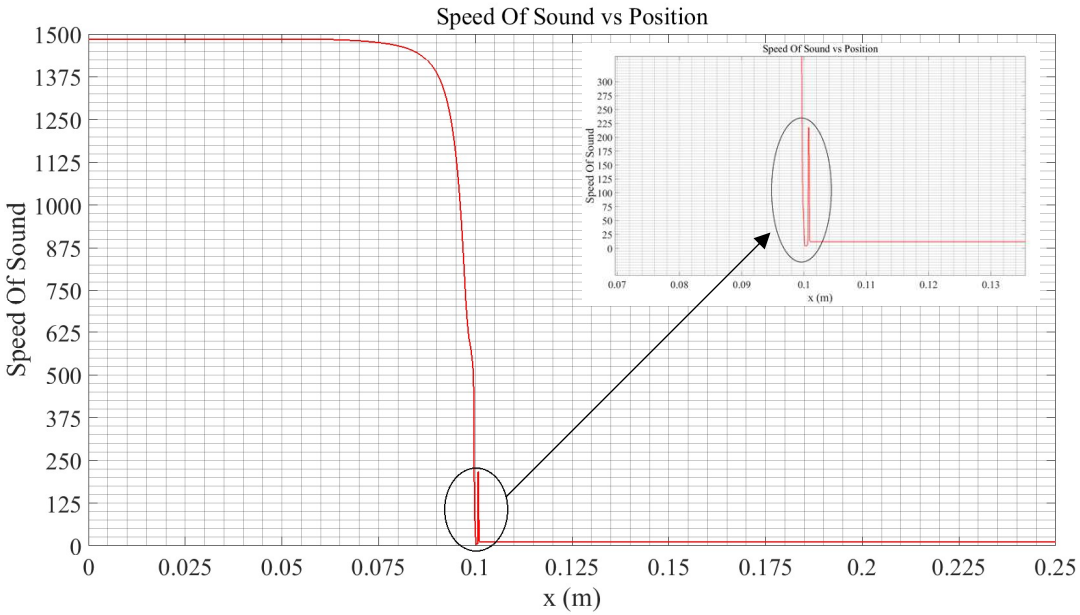

Figure 4.30 Speed of sound distribution along the center line at time 0.01 ms.

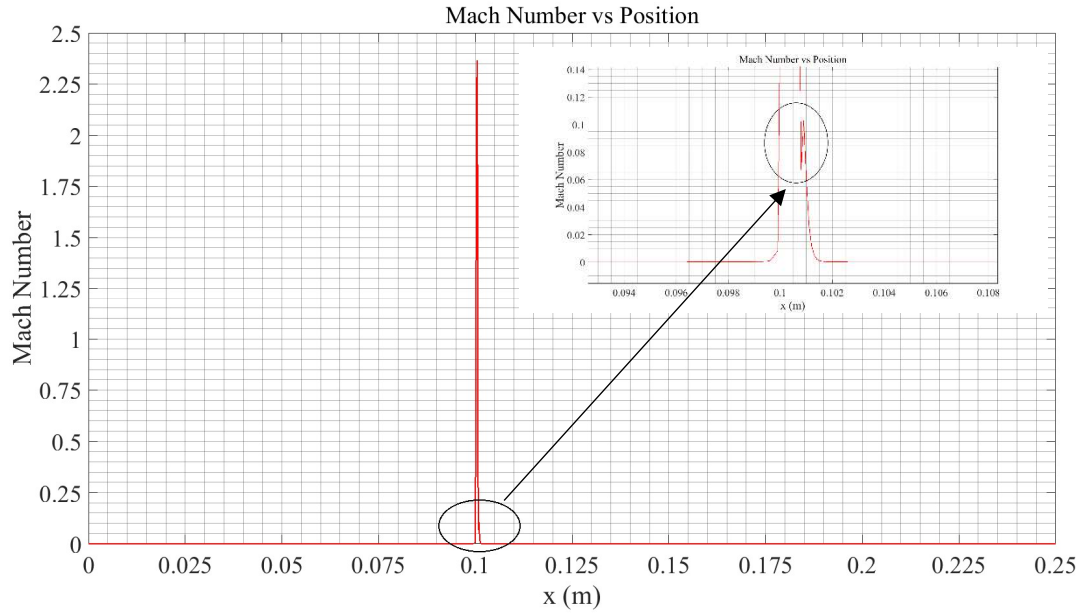

Figure 4.31 Mach number distribution along the center line of the flashing chamber at time 0.01 ms.

Due to the pressure difference between the nozzle and vacuum chamber, the static pressure dropped from 101325Pa to 879 Pa at location x = 0.1002 m, then increases suddenly to 1418 Pa

at location 0.1007 m. Figures (4.32) shows the static pressure distribution along the center line at the first time step 0.01 ms.

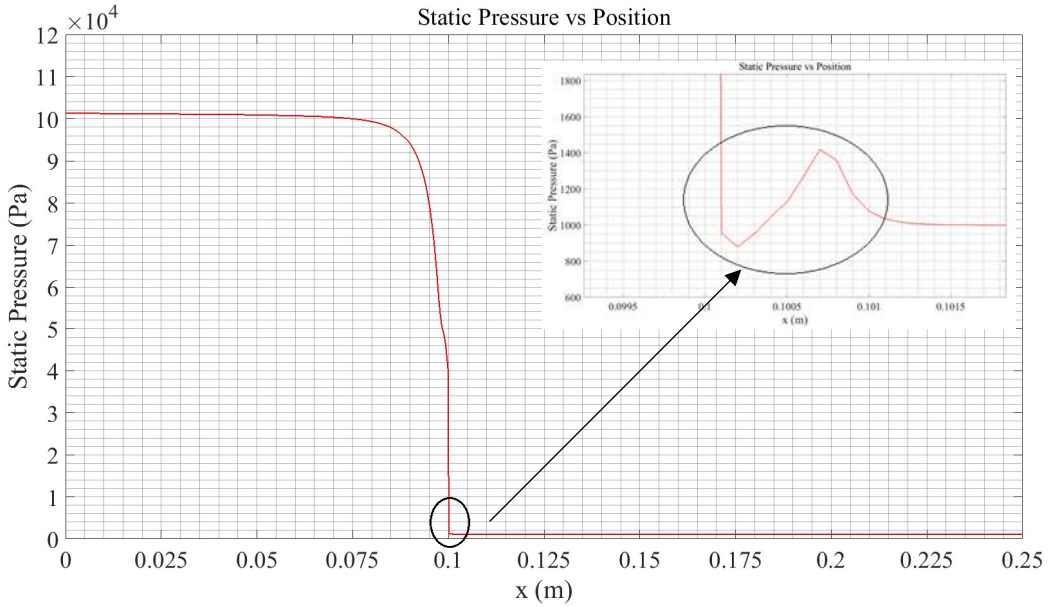

Figure 4.32 Static pressure distribution along the center line of the flashing chamber at time 0.01ms .

Using the Mixture model allows solving the volume fraction equations for the phases where the phases can be interpenetrating; therefore, the volume fractions for any phase can be equal to any value between 0 and 1 depending on the area occupied by the phase. Figure (4.33) shows the liquid volume fraction distribution along the flashing chamber at time 0.01 ms. The distribution shows that the quick phase change happens directly from liquid water to water vapor due to the sudden pressure drop.

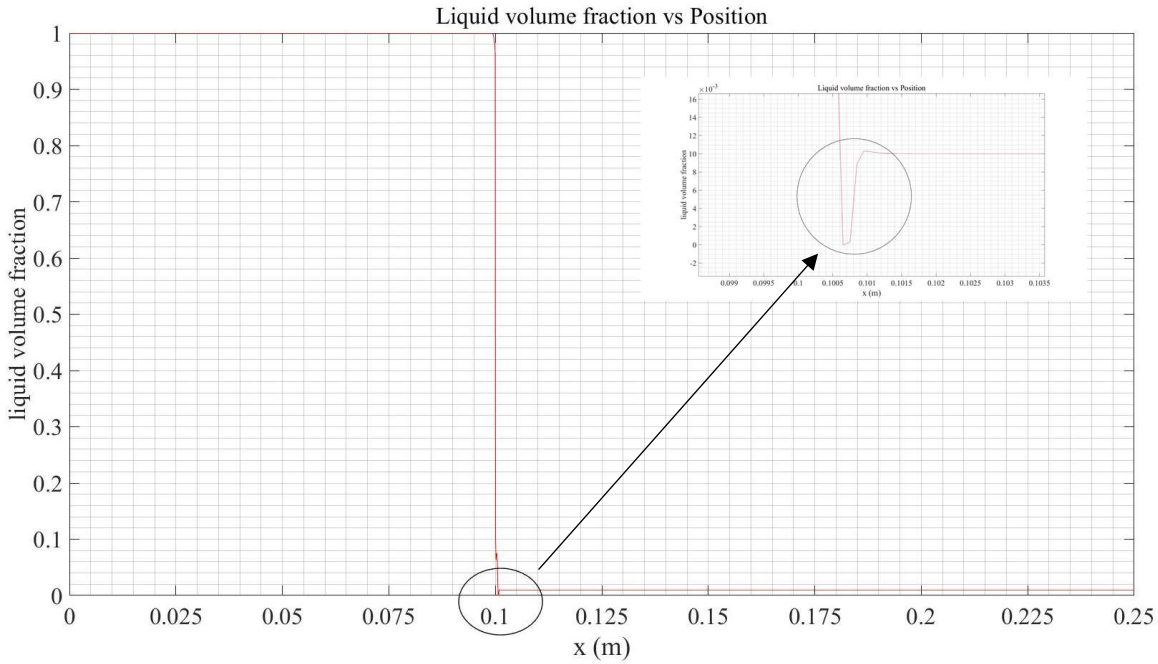

Figure 4.33 Liquid volume fraction distribution along the center line of the flashing chamber at time 0.01 ms.

4.3.2 Time step 7.74 ms

After the sudden pressure dropped and flash evaporation occurred at first time step, the two-phase mixture continues to expand further behind a moving shock wave that travels towards vapor region. Reaching to time step 7.74 ms, the pressure and density decrease while the velocity and the Mach number increase reaching supersonic values and giving rise to a strong moving shock wave formation located at point $x = 0.1312$ m. The Mach number reached value of 1.96 and dropped suddenly to 0.76 coincided with increasing in pressure from value of 1226 Pa to 5316 Pa with pressure ratio 4.33. Figures (4.34) to (4.37) present the flow characteristic distributions and contours for the Mach number, density, pressure, and the liquid volume fraction where the entire flow characteristic are discontinuous across the shockwave.

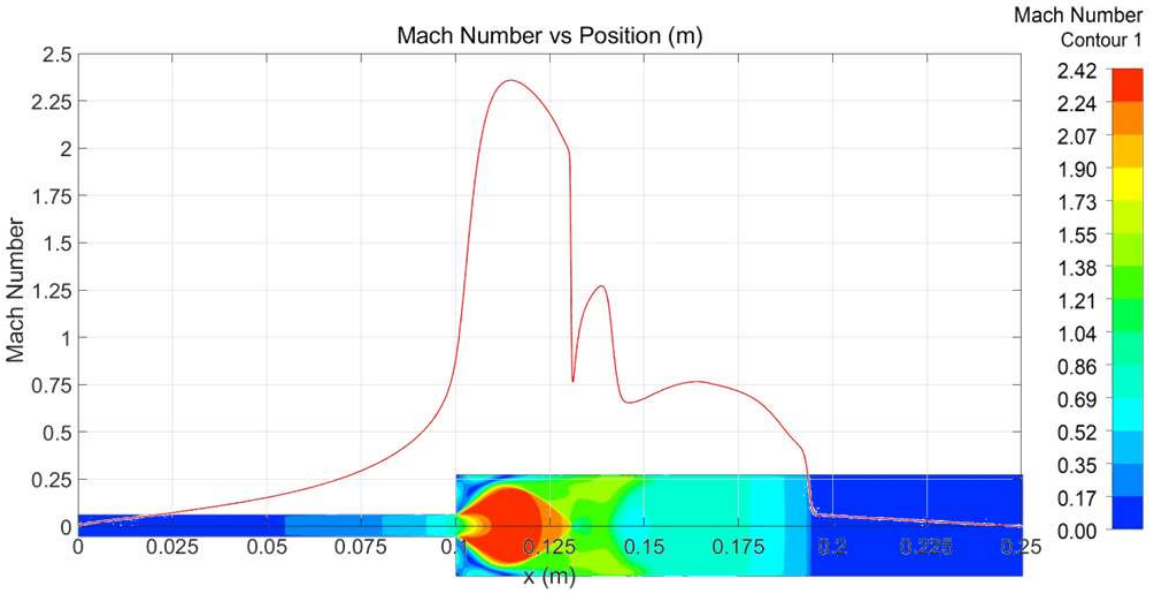

Figure 4.34 Mach number distribution along the center line and 2-D contour at time 7.74 ms.

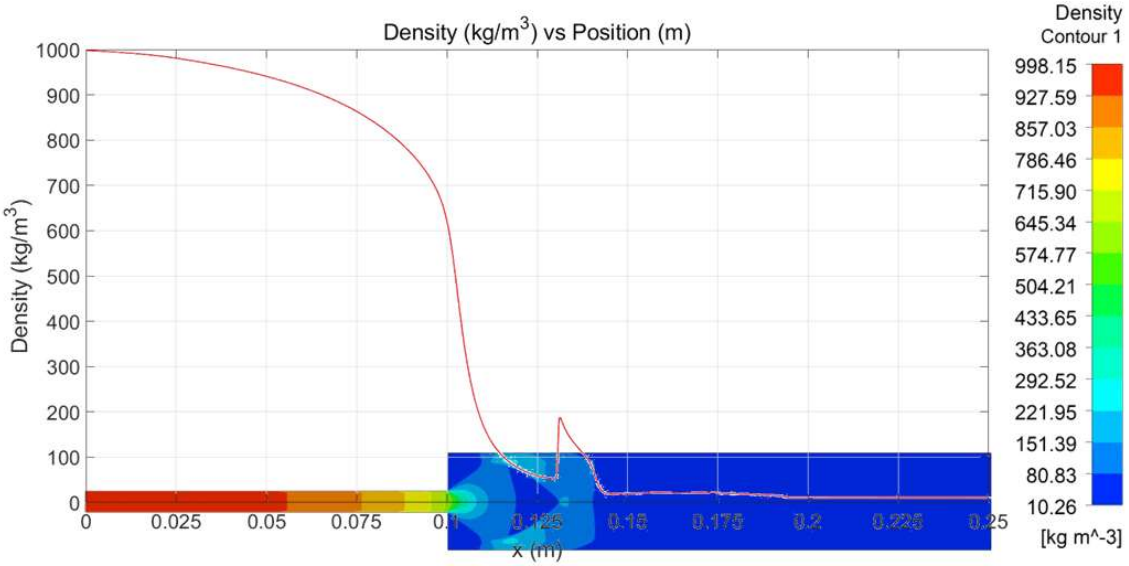

Figure 4.35 Density distribution along the center line and 2-D contour at time 7.74 ms.

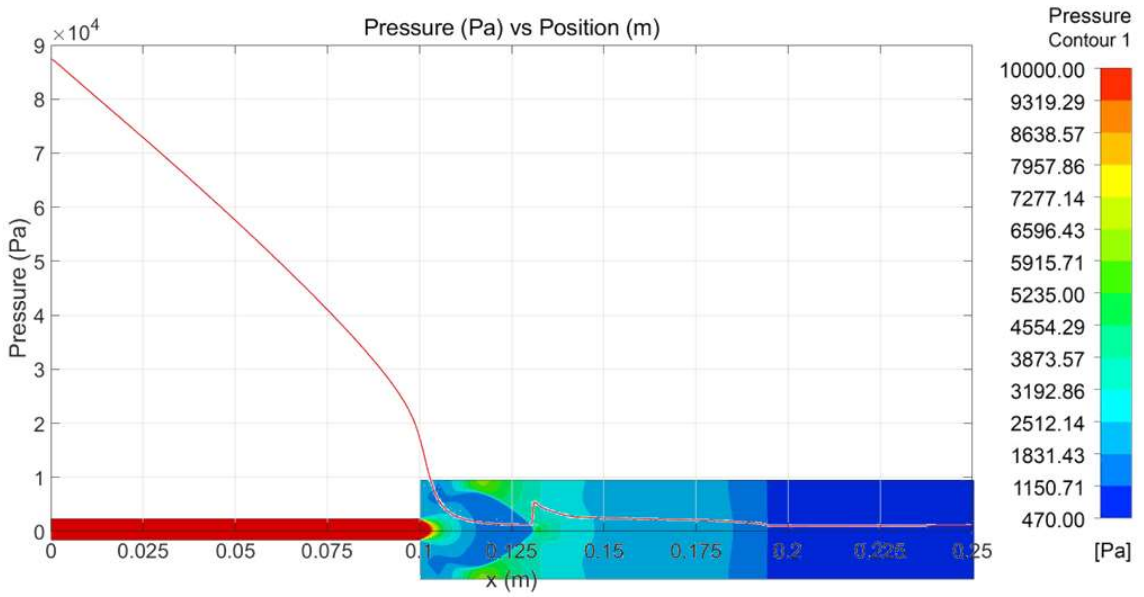

Figure 4.36 Static pressure distribution along the center line and 2-D contour at time 7.74 ms

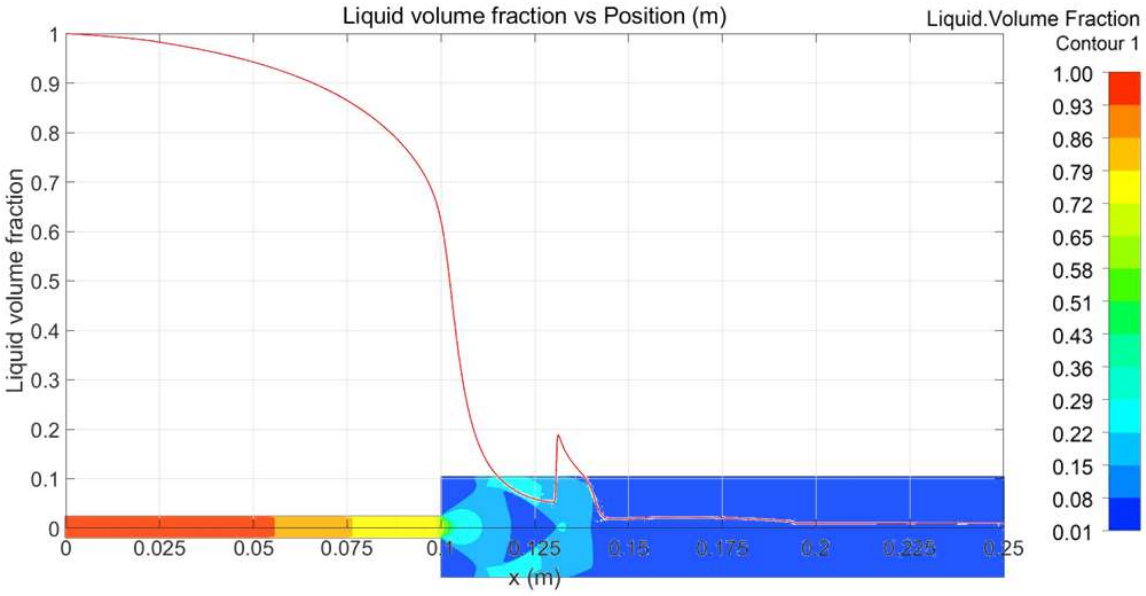

Figure 4.37 Liquid volume fraction distribution along the center line and 2-D contour at time 7.74 ms

4.3.3 Time step 35.99 ms

The two-phase mixture continues to expand further behind a moving shock wave that travels faster through flashing chamber. The paths of the shock wave and evaporation front are illustrated in Figure (4.38), which shows the distribution of the liquid water volume fraction with the time and

position along the flashing chamber at time 11.82 ms. The two-phase mixture continues to expand further until it meets with the reflected shock wave at point x = 0.230 m at time step 15.51 ms as shown in the Figure (4.39). It shows the distribution of the liquid water volume fraction with the time and position along the flashing chamber.

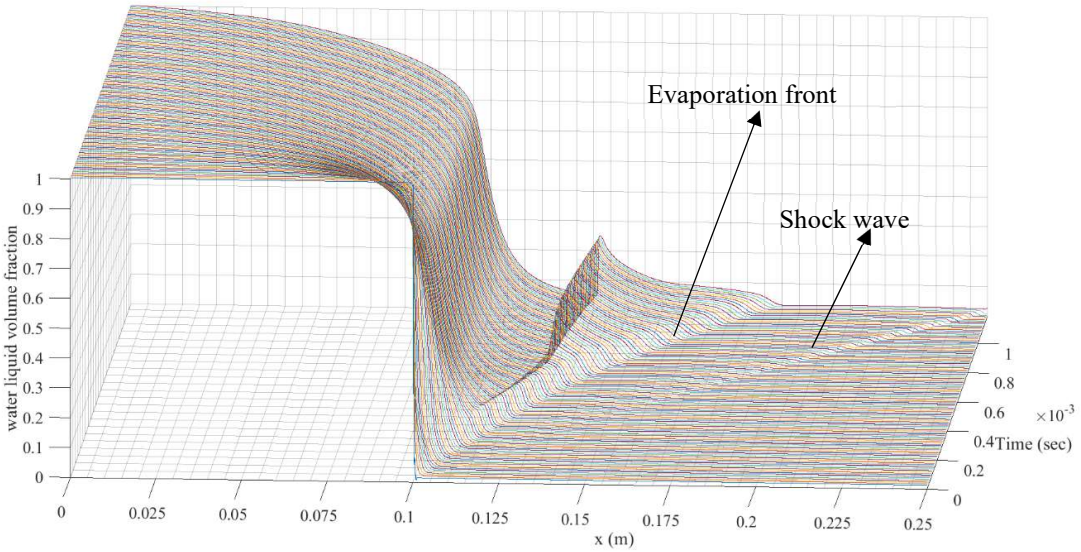

Figure 4.38 The liquid water volume fraction distribution along the center line of the flashing chamber through 11.82 ms.

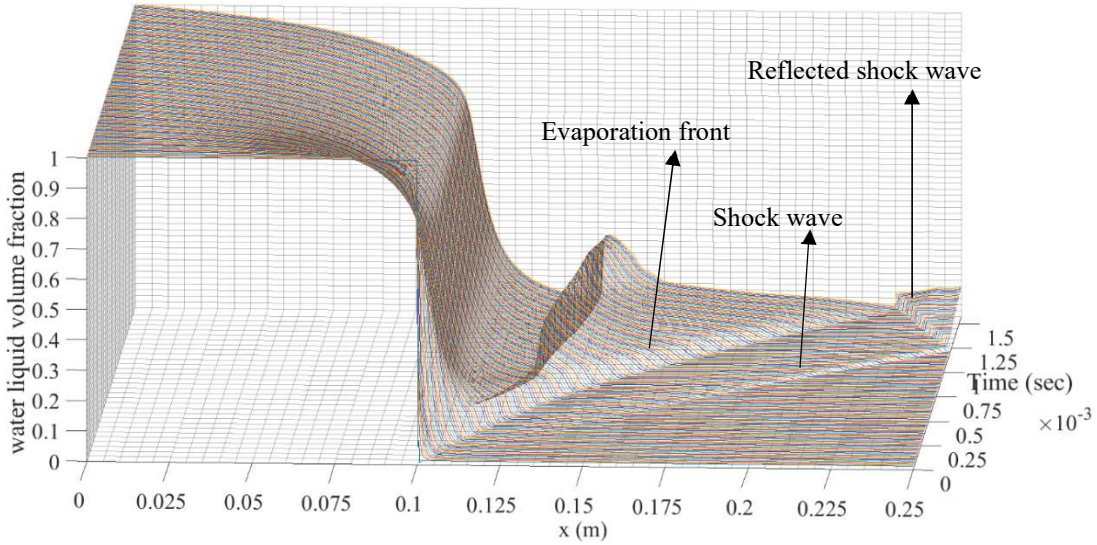

Figure 4.39 The liquid water volume fraction distribution along the center line of the flashing chamber through 11.82 ms.

Reaching to the time 35.99 ms, the pressure and density increase while the velocity and the Mach number suddenly decrease during the expansion reaching supersonic values and giving rise to a strong reflected shock wave. Figure (4.40) shows the Mach number distribution along the center line and 2D contour at time 35.99 ms. This figure shows a strong reflected shock wave at point $x = 0.1493$ m where Mach number dropped from about 2.65 to 0.23. Whereas the static pressure increased from 3026 Pa to 64984 Pa due to the reflected shock wave with pressure ratio 21.4 as shown in Figure (4.41), which shows the static pressure distribution along the center line and 2D contour at time 35.99 ms.

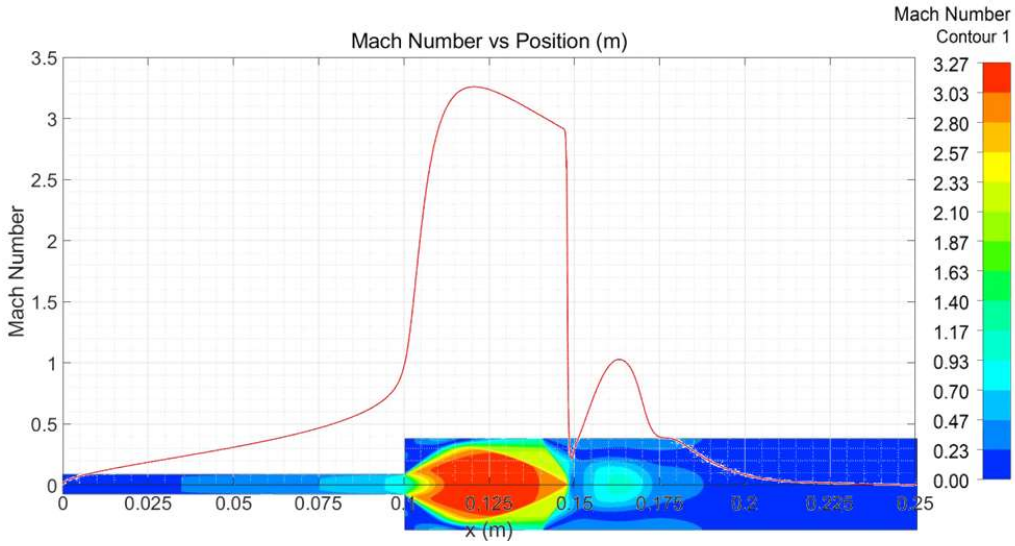

Figure 4.40 Mach number distribution along the center line and 2D contour at time 35.99 ms.

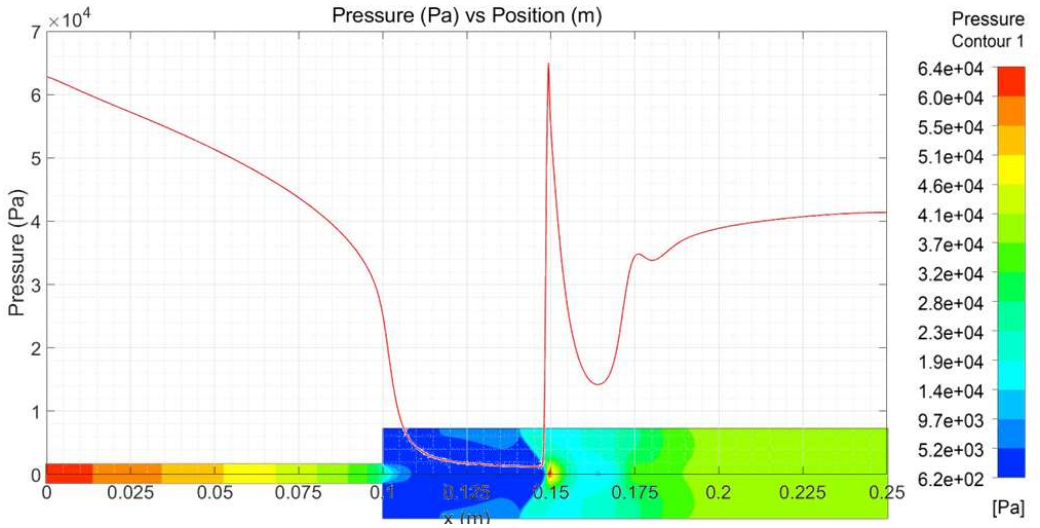

Figure 4.41. Static pressure distribution along the center line and 2D contour at time 35.99 ms.

The density and the liquid volume fraction are also discontinuous across the reflected shock wave as shown below in Figures (4.42) and (4.43). The figures show that the density and liquid volume fraction increased suddenly at the same time and location where Mach number decreased. Increasing liquid volume fraction and density across the reflected shock wave, rendering it a condensing shock. The effect of density gradients is significant especially experimentally during observing the picture of the shock waves. This was proven by using a convex or knife-edge to provide a calibration of the light deflection caused by density gradients and improve the pictures [128, 151].

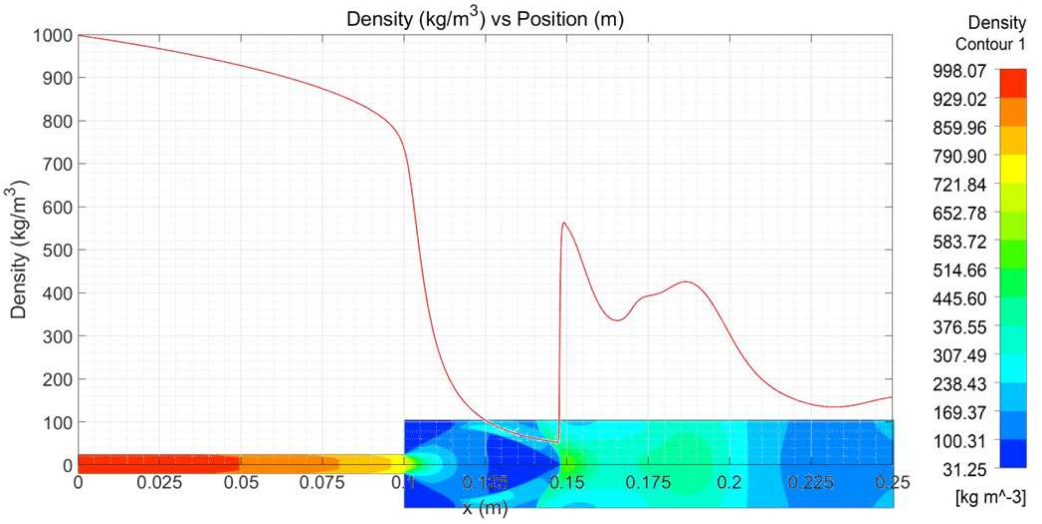

Figure 4.42 Density distribution along the center line and 2D contour at time 35.99 ms.

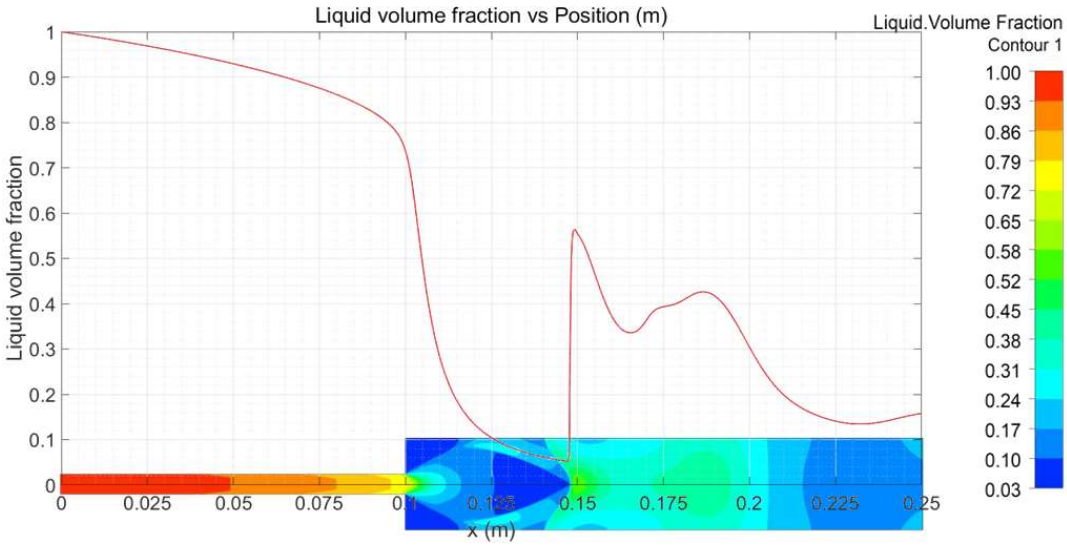

Figure 4.43 Liquid volume fraction distribution and 2D contour at time 35.99 ms.

By comparing the results of both simulations, it was found that the results were conformable; however, the values of the properties, the position of the shock wave and the evaporation front, were different. The moving shock wave generated in the first simulation propagates faster than the generated shock from the second simulation. At time step 9.70 ms, the shock wave hits the end of the vacuum chamber, while in the second simulation the shock wave hits the end of the vacuum chamber at time step 11.82 ms. The reason for that is that the geometry

of the flashing chamber is smaller than the second vacuum chamber. Where increasing the nozzle diameter led to an increase the highest rate of the flash evaporation, which coincided with Mutair and Ikegami results [76, 54].

CHAPTER 5

Experimental Setup and Results

5.1 The Experimental Apparatus and Procedure.

The experiments in the present work focus on spry flash evaporation occurring when a superheated water is injected through a nozzle into vacuum chamber. The vacuum chamber is the main part of the experimental setup. The total volume of this chamber is 93.75 cm^3 getting from 15cm in long with 2.5cm square cross-section area as shown in Figure (5.1). This vacuum chamber has two walls of specific glass each one is 20cm long and 4cm in width to allow watching the occurring of the flash evaporation. There are three taps inside of the vacuum chamber to connect with a pressure transducer (OMEGA PX309, Ranges -15 to 50 psig), a thermocouple, and a vacuum pump. In addition, another tap in the top accommodates a short 12.7 mm nozzle with 1.5 mm diameter.

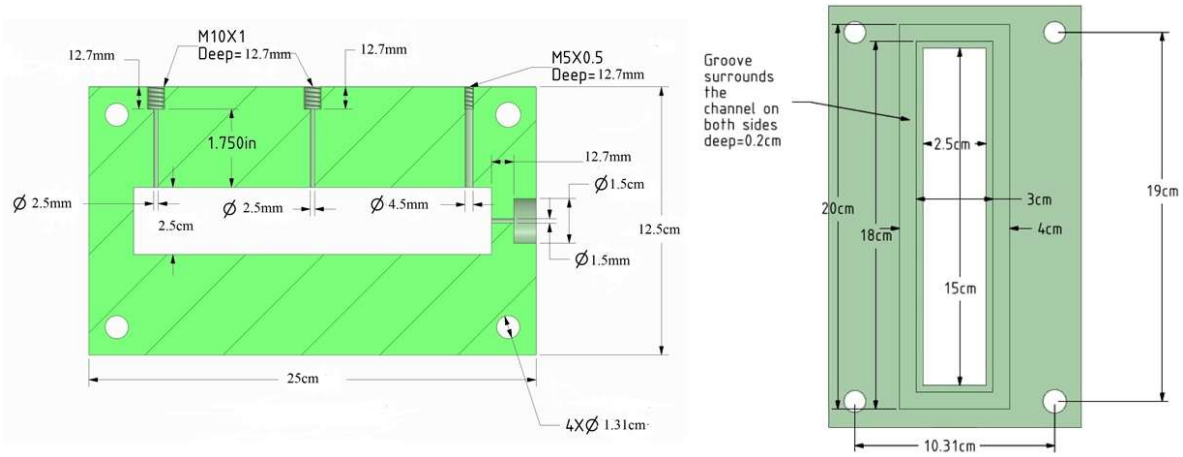

Figure 5.1 Schematic diagram of the vacuum chamber.

5.2 Experiment Setup.

A z-type Schlieren system illustrated in Figure (5.2) was used to capture pictures of the flashing and induced shock wave. Because flash evaporation phenomena occur too quickly, a high-speed camera Photron SA4 [152] with 768 x 640 mega pixel resolution at 10000 fps (frame per second) was employed to capture the images. Beside the high-speed camera, this system consisted of a point light source, and two similar concave mirrors of diameter D = 0.15 m and focal distance f =

1.54 m. Most previous studies presenting Schlieren technique have recommended using a convex lens or knife-edge to provide a calibration of the light deflection caused by density gradients and improve the pictures quality [128, 153, 151, 154]. In this study, both were used, and the better quality obtained with the convex lens.

It is difficult to capture the shock wave in the vapor phase by using the Schlieren technique alone. Therefore, prober mathematical filtering has enabled a qualitative visualization of the shock wave structure of the flashing jets leaving a nozzle [108, 117, 128, 118, 155]. The Image Processing and Analysis in Java (ImageJ) mathematical filter was used in this study. A data acquisition system was connected to the pressure transducer and thermocouple to record and measure the data using LabVIEW interface.

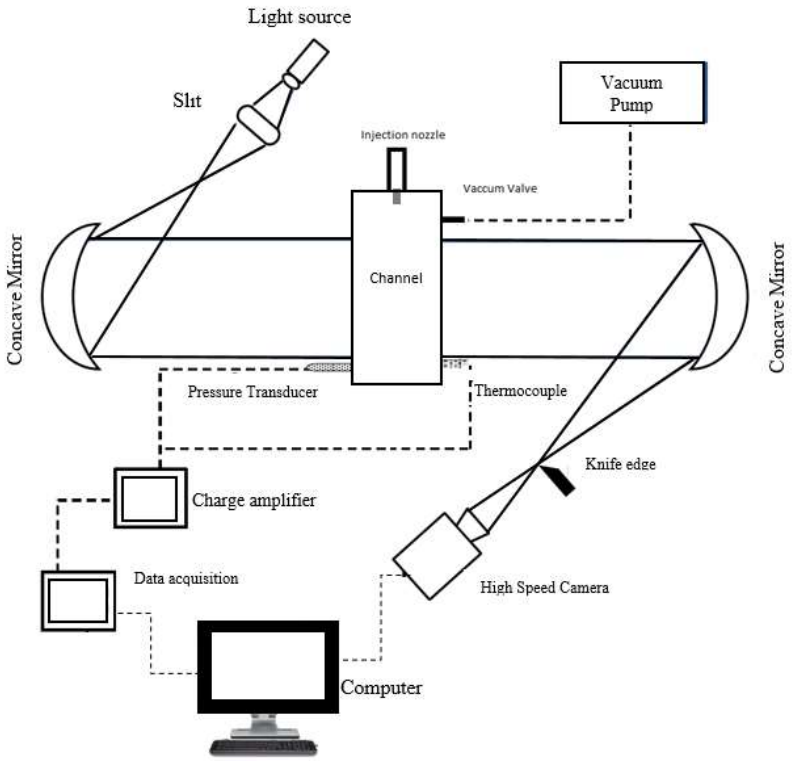

Figure 5.2 Schematic diagram of high-speed Schlieren optical arrangement.

5.3 Experimental Results

The experimental results discussed in this dissertation were carried out for superheated liquid water at initial pressure (P_i) 101325 Pa and initial temperature (T_i) ranging from 40 ºC to 100 ºC. The superheated water was injected into the vacuum chamber filled with saturated water vapor at backpressure (P_b) ranging from 4000 Pa to 10000 Pa. The Schlieren method with high speed camera was used to capture the picture of flashing and inducing shock wave. The experiments were carried out by using a high-speed Photron SA4 camera with frame rate of 8000 to 20000 fps (frame per second) to capture the images of flashing and the generated shock wave.

Groups of experimental runs have been performed. In the experiments, pure water is used as a test material. About 1 mL superheated water is filled inside the nozzle, while the nozzle is open to the ambient. Upon injecting the superheated liquid water through the nozzle into the vacuum chamber, a flashing jet formed inside the vacuum chamber. The outcome of the experiments reveals the change of the pattern or structure of liquid jets and the flashing phenomena in the vacuum chamber with decreasing backpressure and increasing superheat. The Schlieren photographs shown in Figure (5.3) were captured with initial conditions P_i = 101325 Pa, T_i = 40 ºC, and P_b = 6000 Pa. After the first frame, a partially flashing liquid jet occurred with an irregular evaporation front where the length of the non-shattering inner liquid fluctuated. The liquid core of the water jet appeared clearly at the exit of the nozzle and water droplets deposited and remained at the walls. This phenomenon of the partial flashing was found to prevail up to moderate superheated degree levels. That means, at low initial temperature and high backpressure, no complete flashing appeared.

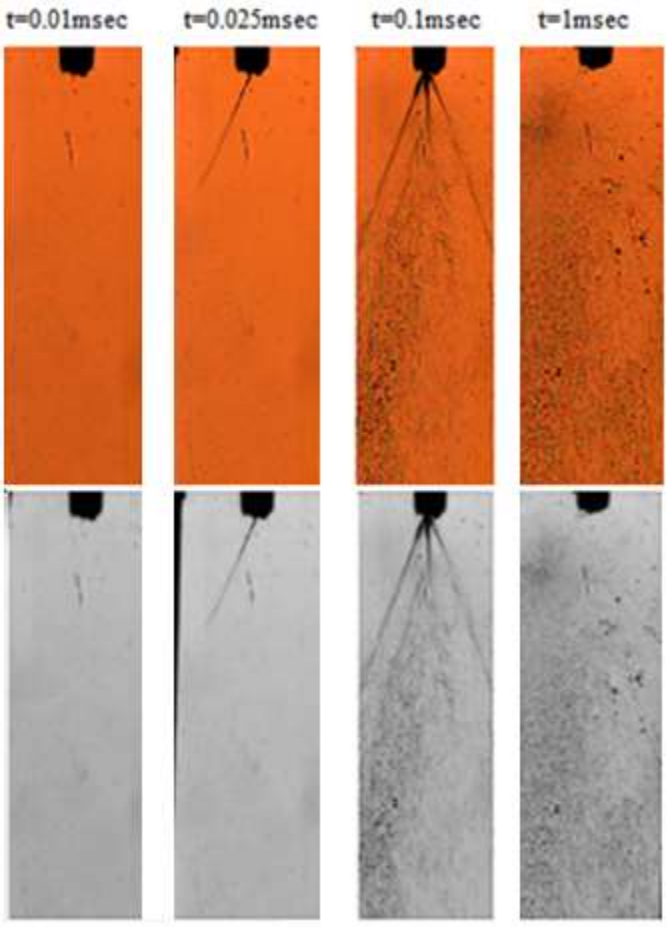

Figure 5.3 Images of partial flashing at P_i = 101325 Pa, T_i = 40 ºC, and P_b = 6000 Pa.

With increasing initial temperature, the evaporation rate at the flashing jet surface increases and the jet structure changes. The flashing images shown in Figure (5.4) were obtained in another experiment, with injected water at P_i = 101325 Pa, T_i = 80 ºC, and P_b = 6000 Pa. The images show complete flashing with no liquid droplet depositing at the glass wall, confirming that the intensity of flashing is affected by the initial temperature of the injected water. The images show a shattered jet, with clouds of very fine droplets that may be dispersed by many rapidly growing and then bursting bubbles near the nozzle exit. At first time step 0.01ms, the image illustrates the onset of the flashing phenomenon with complete flashing of the superheated liquid water into water vapor, due to the sudden pressure drop in the interfacial region surrounding the liquid core in the nozzle.

The subsequent images show the liquid core growing out of the nozzles and dispersing in a growing cloud of very fine completely flashing droplets.

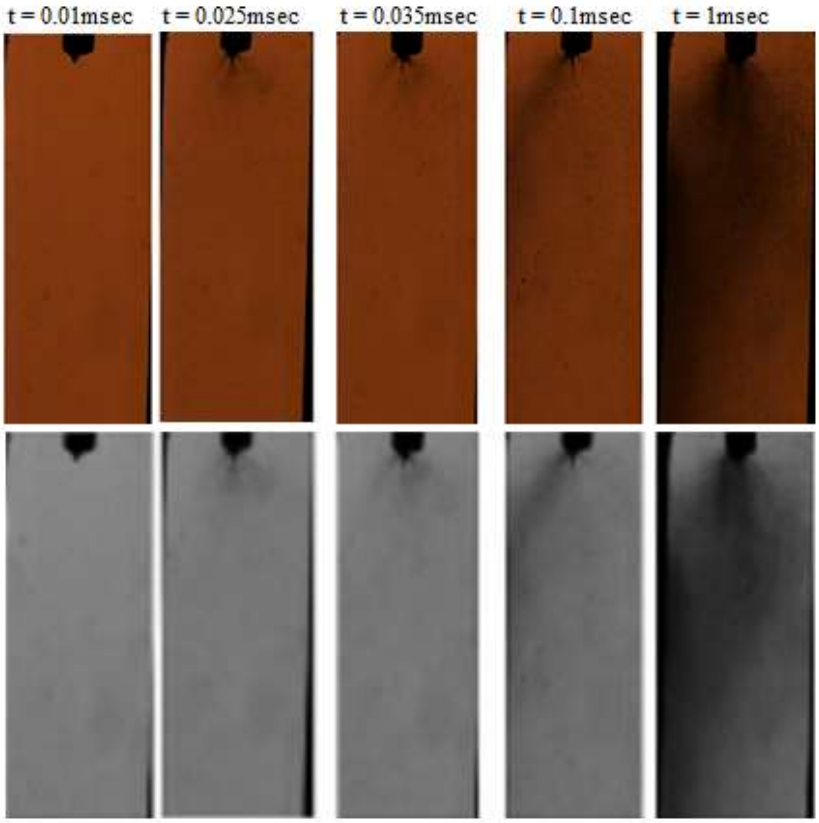

Figure 5.4 Images of the flashing at P_i = 101325 Pa, T_i = 80 ºC, and P_b = 6000 Pa.

Simões-Moreira et al. [117], observed a complete structure of a shock wave in Schlieren pictures that were mathematically filtered. According to them, the choking behavior is characterized by a flow rate remaining constant although the backpressure decreases further. This choking-type behavior is observed, as the backpressure is decreased, while keeping the liquid injection condition unchanged. A further characteristic of the choking-type behavior is the occurrence of a spheroidal or ellipsoidal shock wave in the two-phase mixture generated by the flashing jet. In addition, with decreasing backpressure, the shattering of the liquid jet generates a cloud of droplets, indicating a large number of nucleation sites and rapid bubble growth [117, 72].

On increasing the initial temperature and decreasing the backpressure further, it is possible to see the liquid jet (liquid core) emerging from the nozzle, with a cloud of droplets, and a shock-wave structure enveloping the liquid core.

Therefore, an experiment was performed with decreasing backpressure to 4000 Pa and increasing initial temperature to 90 ºC, where the injected initial pressure was 101325 Pa. In addition, the ImageJ filter was used to mathematically filter the Schlieren photographs to qualitatively visualize the shock wave structure generated by the flashing jet leaving the nozzle as shown in the Figures (5.5 b & d). The results show that once the superheated water is injected, it flashes immediately and generates a shock wave. The liquid is evaporating completely within a very small region at the surface of the liquid jet core.

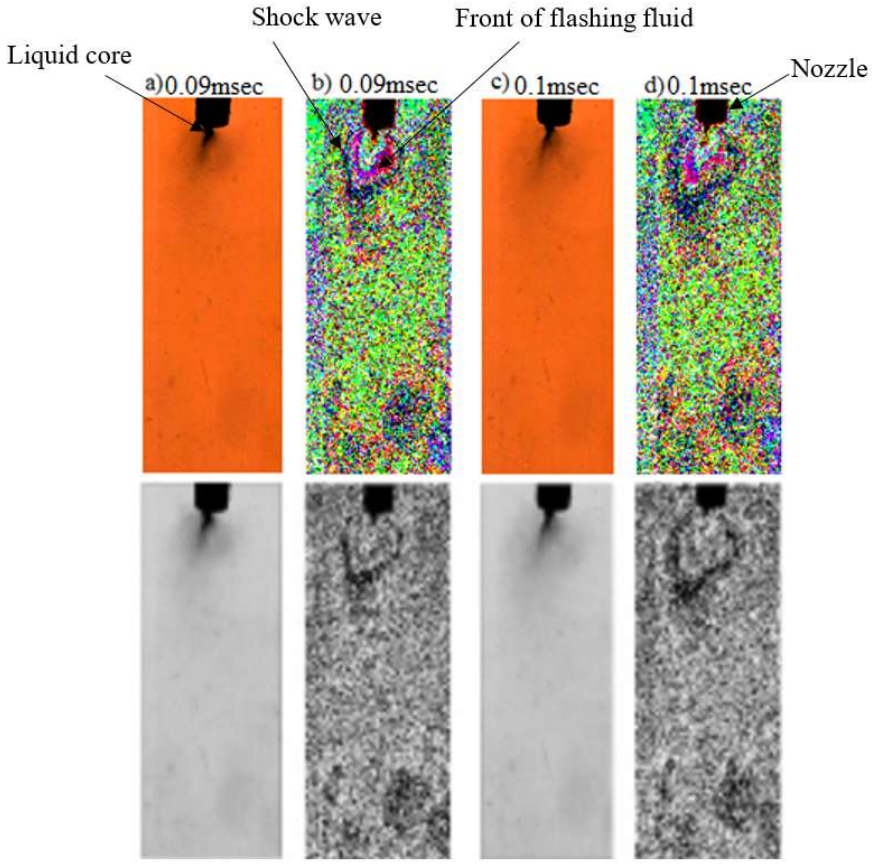

Figure 5.5 Flashing images at P_i = 101325 Pa, T_i = 90 ºC, and P_b = 4000 Pa.

The images presented in Figures (5a & c) show a complete flashing jet at time steps 0.09 ms and 0.1 ms respectively, where the cloud of the many fine droplets enveloping the liquid core is smaller and hence evaporated faster than observed in Figure (5.4). Those pictures were then filtered using the ImageJ filter resulting in Figures (5b & d). The dark spheroidal or ellipsoidal shapes represent the moving shock wave structure enveloping the liquid core and the purple spheroidal shape may represent the front of the incoming flashing fluid acting as a piston generating the moving shock wave as explained by Anderson [148, 149].

The spheroidal or ellipsoidal shape of the shock wave structure is similar to the chocking behavior shock wave structure observed by Simões-Moreira et al. [117], who carried out the experiments and numerical analysis for a flashing jet of iso-octane injected through a short nozzle. However, the resulting shock wave in Figure 8 is a moving shock wave that move ahead of the incoming flashing fluid (piston) and travels further forward into the vacuum chamber until it hits the end wall and gets reflected.

CHAPTER 6

Conclusions

6.1 Conclusion

This dissertation investigates the flashing evaporation phenomenon and resulting shock waves experimentally and numerically when superheated water is injected into a vacuum chamber through a nozzle. The research presents shock waves as one of significant consequences that can be produced in flashing evaporation and utilization of those resulting shock waves in creating useful compression.

A 2D transient numerical Ansys Fluent simulation was utilized to present and prove the occurrence of shock waves generated by a flashing water jets when superheated water is injected through a nozzle into a low-pressure water vapor zone. The results show that at the first time step and due to the sudden pressure drop, intensive fast phase change occurs, and a shock wave is generated directly at the exit of the nozzle (inlet of the vacuum chamber). This shock wave is a moving shock, and it propagates forward through the water vapor in the vacuum chamber, hits the wall at the end of the flashing chamber, reflects from the wall and moves back through the vacuum chamber to the nozzle. The results show that across the moving shock wave, all fluid properties are discontinuous with the pressure, the liquid volume fraction, and the velocity increasing. The density is predominantly determined by the liquid volume fraction. The highest velocity is always found at the evaporation front that moves with supersonic speed following the primary shock wave and is also observed in front of the reflected shock. The increase in the pressure across the shock led to condensation signified by an increase of the liquid water volume fraction. This was particularly strong across the reflected shock wave. The advantage of moving shock waves is that they can carry and transfer energy directly between fluids without using mechanical components like piston or vanes. Therefore, it can be useful to further develop the phenomena's industrial and technological applications such as utilize resulting shock waves in creating useful compression.

The research also experimentally investigated the flashing evaporation phenomenon and resulting shock wave for superheated water injected through a short nozzle into a vacuum chamber. The initial superheated water temperature ranges from 40 °C to 100 °C and the vacuum chamber is filled with saturated water vapor under vacuum pressure ranging between 4000 Pa and 10000 Pa. The results confirm that with increasing superheat of the injected water, the flash evaporation accelerates. If in addition the back pressure in the vacuum chamber is reduced, full flashing occurs, and a shock wave is induced. The generated shock wave travels through the chamber as a moving shock wave, proving experimentally that a moving shock wave can be generated by injecting superheated water into a chamber filled with saturated water vapor under vacuum as described e.g. for the concept of the condensing wave rotor [156, 157, 158, 159, 160, 161, 162]. The significance of this moving shock wave is that it can transfer energy directly between fluids without using mechanical components such as pistons or vaned impellers in technical applications. As is realized in a shock tube for a single time and in a pulse donation engine repeatedly, a wave rotor realizes such process quasi-continuously at high speed in multiple channels arranged in a disk or drum that rotates around an axis moving the channels past ports in stationary end plates to open and close them repeatedly injecting and ejecting fluids to and from the rotor [106, 107, 104, 163, 164].

REFERENCES

REFERENCES

[1] R. Saurel, P. Boivin , and O Le Métayer, "A general formulation for cavitating, boiling and evaporating flows," *Computers and Fluids,* vol. 128, pp. 53-64, 2016.

[2] Z. Zhifu, W. Weitao, C. Bin, W. Guoxiang, and G. Liejin, "An experimental study on the spray and thermal characteristics of R134a two-phase flashing spray," *International Journal of Heat and Mass Transfer,* vol. 55, pp. 4460-4468, 2012.

[3] V. Cleary, P. Bowen, and H. Witlox, "Flashing liquid jets and two-phase droplet dispersion, I. Experiments for derivation of droplet atomisation correlations," *Journal of Hazardous Materials,* vol. 142, pp. 786-796, 2007.

[4] J. C. Lin, "Insights from the risk analysis of a nearby propane tank farm," in *Probabilistic Safety Assessment and Management PSAM 12*, Honolulu, Hawaii, 2014.

[5] B. P. Avksentyuk and V. V. Ovchinnikov, "Dynamics of explosive boiling of drops at the superheat limit," *Journal of Applied Mechanics and Technical Physics.,* vol. 40, no. 16, p. 1070, 1999.

[6] T. Alghamdi, S. T. Thoroddsen, and J.F. Hernández-Sánchez, "Ultra-high speed visualization of a flash-boiling jet in a low-pressure environment," *International Journal of Multiphase Flow,* vol. 110, pp. 238-255, 2019.

[7] J.R. Simões-Moreira and C.W. Bullard, "Pressure drop and flashing mechanisms in refrigerant expansion devices," *International Journal of Refrigeration,* vol. 26, pp. 840-848, 2003.

[8] E. Golliher, A. Licari, and T. Jin, "Testing of a Compact Flash Evaporator System for Exploration," in *38th International Conference on Environmental Systems*, San Francisco, California, 2008.

[9] The Geothermal Communities, "Geothermal Energy for Power Generation," Geothermal Systems and Technologies, Morahalom (Hungary), Galanta (Slovakia), and Montieri (Italy), 2010.

[10] S. Zheng, X. Xie, and Yi Jiang, "Experimental study on the flash evaporation process of LiBr—H2O solution in an absorption heat pump," *ScienceDirect,* vol. 61, pp. 117-126, 2016.

[11] K. Roman, "Experimental investigation of condensation wave structure in steam–water injector," *International Journal of Heat and Mass Transfer,* vol. 91, pp. 594-601, 2015.

[12] C. Lv, Z. M. Zhang, Q. Y. Zhao, T. A. Zhang, X. H. Guo & J. Wang, "Numerical simulation of flash vaporisation in alumina production," *The Canadian Journal of Metallurgy and Materials Science,* vol. 55, no. 4, pp. 463-469, 2016.

[13] M. A. Raj, K. K. Murugavel, T. Rajaseenivasan, and K. Srithar, "A review on flash evaporation desalination," *Desalination and Water Treatment,* vol. 57, pp. 13462-13471, 2016.

[14] K. Holum and C. Frank, Proceedings of the First International Symposium on Water Desalination, Volume 1, Washington, D.C (USA): U.S. Department of Interior, Office of Saline Water, 1965.

[15] S. Choi, "Thermal type seawater desalination with barometric vacuum and solar energy," *ScienceDirect,* vol. 141, pp. 1332-1349, 2017.

[16] A. H. Araghi, M. Khiadani, M. H. Sadafi, and K. Hooman, "A numerical model and experimental verification for analysing a new vacuum spray flash desalinator utilising low grade energy," *Desalination,* vol. 413, pp. 109-118, 2017.

[17] S.A. Elagouz, G.B. Abd El-Aziz, and A.M. Awad, "Enhancing performance of low-temperature desalination using spray evaporation," *Desalination and Water Treatment,* vol. 94, pp. 1-10, 2017.

[18] Stengler, Jana, K. Schaber, and S. Mall-Gleissle, "Experimental study on low temperature desalination by flash evaporation in a novel compact chamber design," *Desalination,* vol. 448, pp. 103-112, 2018.

[19] A. Nannaronea, C. Torob, and E. Sciubbac, "Multi-Stage Flash Desalination Process: Modeling and Simulation," in *The 30th International Conference on Efficiency, Cost, Optimization, Simulation and Environmental Impact of Energy Systems*, San Diego, California (USA), 2017.

[20] A. D. Khawaji, I. K. Kutubkhanah, and J. Wie, "Advances in seawater desalination technologies," *Desalination,* vol. 221, pp. 47-69, 2008.

[21] H. Ludwig and M. Hetscel, "Treatment of distillates and permeates from seawater desalination plants," *Desalination,* vol. 58, pp. 135-154, 1986.

[22] L. Boile, P. Downar-Zapolski, J. Franco, and J.M. Seynhaeve, "Flashing water flow through a safety valve," *Journal of loss prevention in the process industries,* vol. 8, no. 2, pp. 111-126, 1995.

[23] J. Schmidt, "Sizing of nozzles, venturis, orifices, control and safety valves for initially sub-cooled gas/liquid two-phase flow -TheHNE-DSmethod," *Forschung im Ingenieurwesen,* vol. 71, no. 1, pp. 47-58, 2007.

[24] G. Boccardi, R. Bubbico, G. P. Celata, and B. Mazzarotta, "Two-phase flowthrough pressure safety valves. Experimental investigation and model prediction," *Chemical Engineering Science,* vol. 60, pp. 5284-5293, 2005.

[25] N. Ashgriz, Handbook of Atomization and Sprays: Theory and Applications, Springer Science & Business Media, 2011.

[26] R. Reitz, "Modeling atomization processes in high-pressure vaporizing sprays," *Atomisation and Spray Technology,* vol. 3, no. 4, pp. 309-337, 1987.

[27] M. Gorokhovski and M. Herrmann, "Modeling Primary Atomization," *The Annual Review of Fluid Mechanics,* vol. 40, pp. 343-366, 2008.

[28] G. Tryggvason, B. Bunner. A. Esmaeeli, D. Juric, N. Al-Rawahi, W. Tauber, J. Han, S. Nas, and Y.J. Jan, "A front-tracking method for the computations of multiphase flow," *Journal of Computational Physics,* vol. 169, no. 2, pp. 708-759, 2001.

[29] S. M. Ghiaasiaan, Two-phase flow, boiling, and condensation: in conventional and miniature systems, Cambridge University Press, 2017.

[30] B. B. Mikic, W. M. Rohsenow, and P. Griffith, "On bubble growth rates," *International Journal of Heat and Mass Transfer,* vol. 13, no. 4, pp. 657-666, 1970.

[31] H. Kamoun, G. Lamanna, S. Ruberto, A. Komenda, B. Weigand, and J. Steelant, "Experimental investigations of fully flashing jets," in *Space Propulsion*, Berlin (Germany), 2014.

[32] M. S. Plesset, Pasadena, and Calif, "The Dynamics of Cavitation Bubbles," *Journal of Applied Mechanics,* vol. 16, pp. 277-282, 1949.

[33] S. P. Aktershev and V. V. Ovchinnikov, "Dynamics of a Vapor Bubble in a Nonuniformly Superheated Fluid at High Superheat Values," *Journal of Engineering Thermophysics,* vol. 16, no. 4, pp. 236-243, 2007.

[34] B. P. Avksentyuk, V. V. Ovchinnikov, AND V. Ya. Plotnikov, "Self-Supporting Vaporization Front and Third Vaporization Crisis, (Unsteady Processes in Two-Phase Flows)," in *ITF SO AN SSSR*, Novosibirsk (Russia), 1989.

[35] C. H. M. Baltis and C. W. M. van der Geld, "Heat transfer mechanisms of a vapour bubble growing at a wall in saturated upward fow," *Journal of Fluid Mechanics,* vol. 771, pp. 264-302, 2015.

[36] V. P. Carey, Liquid Vapor Phase Change Phenomena: An Introduction to the Thermophysics of Vaporization and Condensation Processes in Heat Transfer Equipment, 2th Edition, New York (USA): CRC Press, 2018.

[37] Jens, Eggers, and E. Villermaux, "Physics of liquid jets," *Reports on progress in physics,* vol. 71, no. 3, p. 036601, 2008.

[38] A. H. Lefebvre and V. G. McDonell, Atomization and Sprays, 2nd Edition, New York (USA): CRC press, 2017.

[39] C. W. M. Van Der Geld and H. Vermeer, "Prediction of Drop Size Distributions in Sprays Using the Maximum Entropy Formalism: The Effect of Satellite Formation," *International Journal of Multiphase Flow,* vol. 20, no. 2, pp. 363-381, 1994.

[40] D. Christophe, "A New Formulation of the Maximum Entropy Formalism to Model Liquid Spray Drop-Size Distribution," *Particle & Particle Systems Characterization,* vol. 23, no. 6, pp. 468-479, 2006.

[41] D. Saury, S. Harmand, and M. Siroux, "Flash evaporation from a water pool: Influence of the liquid height and of the depressurization rate," *International Journal of Thermal Sciences,* vol. 44, pp. 953-965, 2005.

[42] Y. Liao, D. Lucas, E. Krepper, and R. Rzehak, "Flashing evaporation under different pressure levels," *Nuclear Engineering and Design,* vol. 265, pp. 801-813, 2013.

[43] H. Guo, B. Wang, Y. Li, H. Xu, and Z. Wu, "Characterizing external flashing jet from single-hole GDI injector," *International Journal of Heat and Mass Transfer,* vol. 121, pp. 924-932, 2018.

[44] Y. Liao and D. Lucas, "Computational modelling of flash boiling flows: A literature survey," *International Journal of Heat and Mass Transfer,* vol. 11, pp. 246-265, 2017.

[45] Hammitt and G. Frederick, Cavitation and multiphases flow phenomena, New York (USA): McGraw-Hill, 1980.

[46] A. Bouchama, P. Sébastian, and J. P. Nadeau, "Flash Evaporation: Modelling and Constraint Formulation," *Chemical Engineering Research and Design,* vol. 81, pp. 1250-1258, 2003.

[47] W. Cheng, H. Chen, L. Hu, and W. Zhang, "Effect of droplet flash evaporation on vacuum flash evaporation cooling: Modeling," *International Journal of Heat and Mass Transfer,* vol. 84, pp. 149-157, 2015.

[48] L. Liu, B. Qin-cheng, and H. Li, "Experimental investigation on flash evaporation of saltwater droplets released into vacuum," *Microgravity Science and Technology,* vol. 21, pp. 255-260, 2009.

[49] B. Cai, Xi. Tuo, Z. Song, Y. Zheng, H. Gu, and H. Wang, "Modeling of spray flash evaporation based on droplet analysis," *Applied Thermal Engineering,* vol. 130, pp. 1044-1051, 2018.

[50] E. Russo, J. Kuerten, C. W. M. Van Der Geld, and B. J. Geurts, "Modeling water droplet condensation and evaporation in DNS of turbulent channel," *International Journal of Physics,* vol. 318, no. 5, p. 052019, 2011.

[51] B. S. Deb, L. Ghazaryan, J. Bernard, Geurts, H. J.H. Clercx, J.G.M. Kuerten and C.W.M. Van Der Geld, "Effect of evaporation and condensation on droplet size distribution in turbulence," in *Direct and Large-Eddy Simulation VIII*, Dordrecht (Netherlands), Springer, 2011, pp. 201-206.

[52] D. Saury, S. Harmand, and M. Siroux, "Experimental study of flash evaporation of a water film," *International Journal of Heat and Mass Transfer,* vol. 45, pp. 3447-3457, 2002.

[53] T. Gemci, K. Yakut, N. Chigier, and T.C. Ho, "Experimental study of flash atomization of binary hydrocarbon liquids," *International Journal of Multiphase Flow,* vol. 30, pp. 395-417, 2004.

[54] E. Sher, T. Bar-Kohany, and A. Rashkovan, "Flash-boiling atomization," *Progress in Energy and Combustion Science,* vol. 34, no. 4, pp. 417-439, 2008.

[55] Y. Zhang, J. Wang, J. Yan, D. Chong, and J. Liu, "Experimental study on energy transformation and separation characteristic of circulatory flash evaporation," *International Journal of Heat and Mass Transfer,* vol. 99, pp. 862-871, 2016.

[56] Q. Yang, B. Zhao, D. Zhang, Y. Wang, and J. Yan, "Experimental study on heat transfer characteristics in static flash evaporation of aqueous NaCl solution," *International Journal of Heat and Mass Transfer,* vol. 102, pp. 1093-1099, 2016.

[57] D. Zhang, D. Chong, J. Yan, and B. Zhao, "Experimental study on static flash evaporation of aqueous NaCl solution at different flash speed: Heat transfer characteristics," *International Journal of Heat and Mass Transfer,* vol. 65, pp. 584-591, 2013.

[58] Q. Yang, D. Zhang∗, J. Yan, and T. Liang, "Experimental study on energy conversion in static flash evaporation of aqueous NaCl solution," *Desalination,* vol. 430, pp. 56-63, 2018.

[59] D. Zhang, D. Chong, J. Yan, and Y. Zhang, "Study on steam-carrying effect in static flash evaporation," *International Journal of Heat and Mass Transfer,* vol. 55, pp. 4487-4497, 2012.

[60] R. J. Peterson, S. S. Grewal, and M. M. El-Wakil, "Investigations of liquid flashing and evaporation due to sudden depressurization," *International Journal of Heat and Mass Transfer,* vol. 27, no. 2, pp. 301-310, 1984.

[61] B. Mikuza, I. Tiselja, M. Beyerb, and D. Lucas, "Simulations of flashing experiments in TOPFLOW facility with TRACE code," *Nuclear Engineering and Design,* vol. 283, pp. 60-70, 2015.

[62] L. Liu, B. Qin-cheng, W. Liu, Q. Fang-cheng, and B. Xin-gang, "Experimental and theoretical investigation on rapid evaporation of ethanol droplets and kerosene droplets during depressurization," *Microgravity Science and Technology,* vol. 23, pp. 89-97, 2011.

[63] J. Kim and N. Lior, "Some critical transitions in pool flash evaporation," *International Journal of Heat and Mass Transfer,* vol. 40, no. 10, pp. 2363-2372, 1997.

[64] D. Zhang, Q. Yang, T. Liang, and J. Yan, "Experimental study on evolutions of temperature and height of waterfilm during static flash," *International Journal of Heat and Mass Transfer,* vol. 121, pp. 323-332, 2018.

[65] Y. Kltamura, T. Takahashl, and H. Morlmltsu, "Critical Superheat for Flashing of Superheated Liquid Jets," *Industrial and Engineering Chemistry Fundamentals,* vol. 25, no. 2, pp. 206-211, 1986.

[66] K. Adel, El-Fiqi, N.H. Ali, H.T. El-Dessouky, H.S. Fath, and M.A. El-Hefni, "Flash evaporation in a superheated water liquid jet," *Desalination,* vol. 206, pp. 311-321, 2007.

[67] O. Miyatake, T. Tomimura, Y. Ide, M. Yuda, and T. Fujii, "Effect of liquid temperature on spray flash evaporation," *Desalination,* vol. 37, pp. 351-366, 1981.

[68] O. Miyatake, T. Tomimura, Y. Ide, and T. Fujii, "An experimental study of spray flash evaporation," *Desalination,* vol. 36, pp. 113-128, 1981.

[69] O. Miyatake and T. Tomimura, "Enhancement of spray flash evaporation by means of the injection of bubble nuclei," *Journal of Solar Energy Engineering,* vol. 107, pp. 177-182, 1985.

[70] O. Miyatake, T. Hashimoto, and N. Lior, "The relationship between flow pattern and thermal non-equilibrium in the multi-stage flash evaporation process," *Desalination,* vol. 91, pp. 51-64, 1993.

[71] B. Cai, Q. Zhang, Y. Jiang, H. Gu, and H. Wang, "Experimental study on spray flash evaporation under high temperature and pressure," *International Journal of Heat and Mass Transfer,* vol. 113, pp. 1106-1115, 2017.

[72] W. Du, K. Li, S. Wang, and J. Zhao, "Flashing Liquid Jets in Low-Pressure Environment," *Interfacial Phenomena and Heat Transfer,* vol. 1, pp. 173-180, 2013.

[73] X. Jin, H. Zhen, M. Junjun, and Q. Xinqi, "An experimental study on spray transient characteristics in fuel containing CO2," *Atomization and Sprays,* vol. 19, no. 4, pp. 311-320, 2009.

[74] N. Abuaf, B. J. C. Wu, G. A. Zimmer, and P. Saha, "Study of nonequilibrium flashing of water in a converging-diverging nozzle. Volume 1: experimental. No. NUREG/CR-1864-Vol. 1; BNL-NUREG-51317-Vol. 1," Brookhaven National Lab., Upton, NY (USA), 1981.

[75] B. J. C. Wu, N. Abuaf, and P. Saha, "Study of nonequilibrium flashing of water in a converging-diverging nozzle. Volume 2. Modeling. No. NUREG/CR-1864-Vol. 2; BNL-NUREG-51317-Vol. 2," Brookhaven National Lab., Upton, NY (USA), 1981.

[76] S. Mutair and Y. Ikegami, "Experimental study on flash evaporation from superheated water jets: Influencing factors and formulation of correlation," *International Journal of Heat and Mass Transfer,* vol. 52, pp. 5643-5651, 2009.

[77] S. Mutair and Y. Ikegami, "Study and Enhancement of Flash Evaporation Desalination Utilizing the Ocean Thermocline and Discharged heat," *Proceeding of World Academy of Science, Engineering and Technology,* vol. 2, no. 7, pp. 473-481, 2008.

[78] T.H. Nigim and J.A. Eaton, "CFD prediction of the flashing processes in a MSF desalination chamber," *Desalination,* vol. 420, pp. 258-272, 2017.

[79] H. Vu and G. Aguilar, "High-Speed Internal Nozzle Flow Visualization of Flashing Jets," in *11th Triennial International Annual Conference on Liquid Atomization and Spray Systems*, Vail, Colorado USA, 2009.

[80] A. Günther and K.-E. Wirth, "Evaporation phenomena in the atomization of superheated liquids and their impact on the spray characteristics," in *12th Triennial International Conference on Liquid Atomization and Spray Systems*, Nürnberg, Bavaria (Germany), 2012.

[81] D. Ju, C. Wang, X. Qiao, J. Xiao, and Z. Huang, "Internal flow pattern and macroscopic characteristics of a flash-boiling spray actuated through a twin-orifice atomizer with low injection pressure," *Atomization and Sprays,* vol. 26, no. 4, pp. 377-410, 2016.

[82] D. Ju, J. Shrimpton, and A. Hearn, "The effect of reduction of propellant mass fraction on the injection profile of metered dose inhalers," *International Journal of Pharmaceutics,* vol. 391, no. 1-2, pp. 221-229, 2010.

[83] G. B. Wallis, One-dimensional two-phase flow., New York: McGraw-Huill, 1969.

[84] A. Günther and K.-E. Wirth, "Evaporation phenomena in superheated atomization and its impact on the generated spray," *International Journal of Heat and Mass Transfer,* vol. 64, pp. 952-965, 2013.

[85] X. Wang, B. Chen, R. Wang, H. Xin, and Z. Zhou, "Experimental study on the relation between internal flow and flashing spray characteristics of R134a using straight tube nozzles," *International Journal of Heat and Mass Transfer,* vol. 115, pp. 524-536, 2017.

[86] E. M. Peter, A. Takimoto, and Y. Hayashi, "Flashing and Shattering Phenomena of Superheated Liquid Jets," *JSME International Journal,* vol. 37, no. 2, pp. 313-321, 1994.

[87] S. Vandroux, Koenig, and G. Berthoud, "Modelling of a two phase momentum jet close to the breach, in the containment vessel of a liquefied gas," *Journal of Loss Prevention in the Process Industries,* vol. 10, no. 1, pp. 17-29, 1997.

[88] J.C.F. Pereira and X. Q. Chen, "Numerical calculations of unsteady heavy gas dispersion," *Journal of Hazardous Materials,* vol. 46, no. 2-3, pp. 253-272, 1996.

[89] D. Bharathan and T. Penney, "Flash Evaporation From Turbulent Water Jets," *Journal of Heat Transfer,* vol. 106, no. 2, pp. 407-416, 1984.

[90] S. Mutair and Y. Ikegami, "On the evaporation of superheated water drops formed by flashing of liquid jets," *International Journal of Thermal Sciences,* vol. 57, pp. 37-44, 2012.

[91] W. Cheng, W. Zhang, H. Chen, and L. Hu, "Spray cooling and flash evaporation cooling: The current development and application," *Renewable and Sustainable Energy Reviews,* vol. 55, pp. 614-628, 2016.

[92] V. V. Kuznetsov*, I. A. Kozulin, and O. V. Vitovsky, "Experimental Investigation of Adiabatic Evaporation Waves in Superheated Refrigerants," *Journal of Engineering Thermophysics,* vol. 21, no. 2, pp. 136-143, 2012.

[93] W. Cheng, Y. Peng, H. Chen, L. Hu, and H. Hu, "Experimental investigation on the heat transfer characteristics of vacuum spray flash evaporation cooling," *International Journal of Heat and Mass Transfer,* vol. 102, pp. 233-240, 2016.

[94] Z. Zhou, G. Lu, and Bi. Chen, "Numerical study on the spray and thermal characteristics of R404A flashing spray using OpenFOAM," *International Journal of Heat and Mass Transfer,* vol. 117, pp. 1312-1321, 2018.

[95] M. Luo and O. J. Haidn, "Characterization of Flashing Phenomena with Cryogenic Fluid Under Vacuum Conditions," *Journal of Propulsion and Power,* vol. 35, no. 5, pp. 1253-1263, 2016.

[96] C. Wang, R. Xu, Y.Song, and P. Jiang, "Study on water droplet flash evaporation in vacuum spray cooling," *International Journal of Heat and Mass Transfer,* vol. 112, pp. 279-288, 2017.

[97] C. Wang, R. Xu, Y. Song, P. Jiang, X. Chen, and B. Liu, "Study on water flash evaporation under reduced pressure," *International Journal of Heat and Mass Transfer,* vol. 131, pp. 31-40, 2019.

[98] Y. Jin, H. J. Lee, K. Hwang, D. Park, and S. Min, "Flashing injection of high temperature hydrocarbon liquid jets," *Experimental Thermal and Fluid Science,* vol. 90, pp. 200-211, 2018.

[99] Q. Chen , J. M. Kum, Y. Li, and K. J. Chua, "Experimental and mathematical study of the spray flash evaporation phenomena," *Applied Thermal Engineering,* vol. 130, pp. 598-610, 2018.

[100] B. Cai, Q. Wang, S. Yin, H. Gu, H. Wang, H. Zhen, and L. Zhang, "Energy analysis of spray flash evaporation from superheated upward jets.," *Applied Thermal Engineering,* vol. 148, pp. 704-713, 2019.

[101] Y. Wu, X. Zhang, X. Zhang, and M. Munyalo, "Modeling and experimental study of vapor phase-diffusion driven sessile drop evaporation," *Applied Thermal Engineering,* vol. 70, no. 1, pp. 560-564, 2014.

[102] O. Miyatake, "Comparative study of flash evaporation rates," *Desalination,* vol. 96, pp. 163-171, 1994.

[103] A. Mansour and N. Müller, "A review of flash evaporation phenomena and resulting shock waves," *Experimental Thermal and Fluid Science,* vol. 104, pp. 146-168, 2019.

[104] P. Akbari, A. A. Kharazi, and N. Müller, "Utilizing Wave Rotor Technology to Enhance the Turbo Compression in Power and Refrigeration Cycles," in *ASME International Mechanical Engineering Congress & Exposition*, Washington, D.C. (USA) November 16-21, 2003.

[105] P. Akbari, R. Nalim, and N. Müller, "A Review of Wave Rotor Technology and Its Applications," *Journal of Engineering for Gas Turbines and Power,* vol. 128, no. 4, pp. 717-738, 2006.

[106] P. Akbari and N. Müller, "Wave Rotor Research Program at Michigan State University," in *AIAA 2005-3844*, Tucson, Arizona (USA), 2005.

[107] F. Iancu and N. Müller, "Efficiency of shock wave compression in a microchannel," *Microfluidics and Nanofluidics,* vol. 2, no. 1, pp. 50-63, 2006.

[108] T. Kurschat, H. Chaves, and G. E. A. Meier, "Complete adiabatic evaporation of highly superheated liquid jets," *Journal of Fluid Mechanics,* vol. 236, pp. 43-59, 1992.

[109] S. Negro and G.M. Bianchi, "Superheated fuel injection modeling: An engineering approach," *International Journal of Thermal Sciences,* vol. 50, no. 8, pp. 1460-1471, 2011.

[110] J. R. Simões-Moreira and J. E. Shepherd , "Evaporation Waves In Superheated Dodecane," *Journal of Fluid Mechanics,* vol. 382, pp. 63-86, 1999.

[111] J. R. Simões-Moreira, "Oblique evaporation waves," *Shock Waves,* vol. 10, pp. 229-234, 2000.

[112] H. Emmons, Fundamentals of Gas Dynamics, Volum III, Princeton, N.J (USA): Princeton University Press, 1958.

[113] Pasqua, "Metastable flow of freon-12," *Refrigerating Engineering,* vol. 61, pp. 1084-1089, 1953.

[114] Y. Kim and D. O'Neal, "An experimental study of twophase flow of HFC-134a through short tube orifices," *Heat Pump and Refrigeration Systems Design, Analysis, and Applications, AES-ASME,* vol. 29, pp. 1-8, 1993.

[115] R. Reitz, "A photographic study of flash-boiling atomization," *Aerosol Science and Technology,* vol. 12, pp. 561-569, 1990.

[116] J. Simoes-Moreira, "Oblique evaporation waves," *Shock Waves,* vol. 10, pp. 229-234, 2000.

[117] J. R. Simões-Moreira, M. M. Vieira and E. Angelo, "Highly Expand Flashing Liquid Jet," *Journal of thermophysics and Heat Transfer,* vol. 16, no. 3, pp. 415-424, 2002.

[118] E. Angelo and J. R. Simões-Moreira, "Numerical Solution of Highly Expanded Flashing Liquid Jets," *Journal of Thermophysics and Heat Transfer,* vol. 21, no. 2, pp. 379-391, 2007.

[119] J. Liu , J. Chen, and Z. Chen, "Critical flashing flow in convergent-divergent nozzles with initially subcooled liquid," *International Journal of Thermal Sciences,* vol. 47, pp. 1069-1076, 2008.

[120] V. V. Kuznetsov and O. V. Vitovskii, "Evaporation Waves in a Metastable Single-Component Liquid," *Journal of Engineering Thermophysics,* vol. 16, no. 3, pp. 169-174, 2007.

[121] J. A. J. Avila, M. M. Pimenta and J. R. Simoes-Moreira, "Numerical solution of the two-phase expansion of a metastable flashing liquid jet using the dispersion-controlled dissipative scheme," *Wiley InterScience,* vol. 63, pp. 622-637, 2009.

[122] Y. Niu and H. Wang, "Simulations of the shock waves and cavitation bubbles during a three-dimensional high-speed droplet impingement based on a two-fluid model," *Computers and Fluids,* Vols. 134-135, pp. 196-214, 2016.

[123] M. Paudel, J. Dahal, and J. McFarland, "Particle evaporation and hydrodynamics in a shock driven multiphase instability," *International Journal of Multiphase Flow,* vol. 101, pp. 137-151, 2018.

[124] J. Dahal and J. A. McFarland, "A numerical method for shock driven multiphase flow with evaporating particles," *Journal ofComputationalPhysics,* vol. 344, pp. 210-233, 2017.

[125] M.G. Rodio, P.M. Congedo, and R. Abgrall, "Two-phase flow numerical simulation with real-gas effects and occurrence of rarefaction shock waves," *European Journal of Mechanics, B/Fluids,* vol. 45, pp. 20-35, 2014.

[126] Y. Dai, S. Zhang , S. Tao , and D. Hu, "Superposition of two incident shocks in R718 vapor flows," *International Journal of Heat and Fluid Flow,* vol. 65, pp. 159-165, 2017.

[127] Y. Dai, C. Yonghang, Z. Jiupeng, and H. Dapeng, "Superheating and supercharging characteristics of moving shock in wet steam flows," *International Journal of Heat and Mass Transfer,* vol. 86, pp. 351-357, 2015.

[128] M. M. Vieira and J. R. Simões-Moreira, "Low-pressure flashing mechanisms in iso-octane liquid jets," *Journal of Fluid Mechanics,* vol. 572, pp. 121-144, 2007.

[129] A. Attou, L. Bolle, and J.M. Seynhaeve, "Experimental study of the critical fashing fow through a relief line: evidence of the double-choked fow phenomenon," *International Journal of Multiphase Flow,* vol. 26, pp. 921- 947, 2000.

[130] G. Lamanna, H. Kamoun, B. Weigand, and J. Steelant, "Towards a unified treatment of fully flashing sprays," *International Journal of Multiphase Flow,* vol. 58, pp. 168-184, 2014.

[131] A. A. Avdeev, "The Shape of Jets during Discharge of a Superheated Liquid (Structure of Wave Formations and the Reactive Force)," *ISSN 0018-151X, High Temperature,* vol. 54, no. 5, pp. 698-707, 2016.

[132] V. P. Skripov, Metastable liquid, New York (USA): J. Wiley, 1973.

[133] M. Deich, Engineering Gas Dynamics, 3rd revised edition, Moscow (Russia): Energiya, 1974.

[134] Manninen, Mikko, V. Taivassalo, and S. Kallio, "On the mixture model for multiphasse flow," VTT Publication 288, 1996.

[135] C. E. Brennen, Fundamentals of Multiphase Flows, Pasadena, California: Cambridge university press, 2005.

[136] I. Fluent, FLUENT 6.1 User's Guide, Centerra Resource Park: Fluent Inc., 2003.

[137] A. Hossain, J. Naser, K. McManus, and G. Ryan, "CFD Investigation of Particle Deposition and Distribution in A Horizontal Pipe," in *Third International Conference on CFD in the Minerals and Process Industries*, CSIRO, Melbourne, Australia, 2003.

[138] C. Choi ,T. Kwon, and C. Song, "Numerical analysis and visualization experiment on behavior of borated water during MSLB with RCP running mode in an advanced reactor," *Nuclear Engineering and Design,* vol. 237, pp. 778-790, 2007.

[139] K. Hiltunen, A. Jäsberg, S. Kallio, H. Karema, M. Kataja, A. Koponen, M. Manninen & V. Taivassalo, "Multiphase Flow Dynamics Theory and Numerics," *VTT Publications,* vol. 722, 2009.

[140] Bonnie J. McBride, Sanford Gordon, and Martin A. Reno, "Coefficients for calculatiing thermodynamic and transport properties of individual species," NASA TM-4513, 1993.

[141] Schiller, L. and Naumann, "A Drag Coefficient Correlation," *Z. Ver. Deutsch. Ing,* vol. 77, pp. 318-320, 1935.

[142] M. Karimi, G. Akdogan, Kiran H. Dellimore, Steven M. Bradshaw, "comparison of different drag coefficient correlations in the cfd modilling of a laboratory-scale rushton-turbine flotation tank," in *Ninth International Conference on CFD in the Minerals and Process Industries*, CSIRO, Melbourne, Australia, 2012.

[143] G. Dennis, Physics of Shock and Impact, Volume 1, IOP Publishing, 2017.

[144] E. Rathakrishnan, Applied Gas Dynamics, John Wiley & Sons (Asia) Pte Ltd, 2010.

[145] G. D, Physics of Shock and Impact, Volume 1, IOP Publishing, 2017.

[146] C. E. Brennen, Fundamentals of Multiphase Flows, California: Cambridge University press, 2005.

[147] K. S. Werner, "Sound speed in liquid-gas mixtures: Water-air and water-steam," *Journal of Geophysical research,* vol. 80, no. 20, pp. 2895-2904, 1977.

[148] J. D. Anderson, Computational Fluid Dynamics: The Basics with Applications, New York: McGraw-Hill Education, 1995.

[149] J. D. Anderson, Modern Compressible Flow: With Historical Perspective, New York (USA): McGraw-Hill Education, 2004.

[150] W. Ziniu , X. Yizhe, W. Wenbin, and H. Ruifeng, "Review of shock wave detection method in CFD post-processing," *Chinese Journal of Aeronautics ,* vol. 26, no. 3, pp. 501-513, 2013.

[151] H. Kleine, K. Hiraki, H. Maruyama, T. Hayashida, J. Yonai, K. Kitamura, Y. Kondo, and T. G. Etoh, "High-speed time-resolved color schlieren visualization," *Springer-Verlag,* vol. 14, pp. 333-341, 2005.

[152] Fastcam SA4 Hardware Manual, Tokyo (Japan): Photron limited, 2009.

[153] D. Estruch, N. J. Lawson, D. G. MacManus, K. P. Garry, and J. L. Stollery, "Measurement of shock wave unsteadiness using a high-speed schlieren system and digital image processing," *The Review of scientific instruments,* vol. 79, no. 12, p. 126108, 2009.

[154] J. Michael, Hargather, and G. S. Settles, "A comparison of three quantitative schlieren techniques," *Optics andLasersinEngineering,* vol. 50, pp. 8-17, 2002.

[155] J. A. J. Avila, M. M. Pimenta and J. R. Simões-Moreira, "Numerical solution of the two-phase expansion of a metastable flashing liquid jet using the dispersion-controlled dissipative scheme," *Wiley InterScience,* vol. 63, pp. 622-637, 2009.

[156] AA Kharazi, P Akbari, and N Müller, "An Application of Wave Rotor Technology for Performance Enhancement of R718 Refrigeration Cycles," in *2nd International Energy Conversion Engineering Conference, AIAA 2004-5636*, Providence, Rhode Island, 2004.

[157] A. A. Kharazi, P. Akbari, and N. Müller, "Performance Benefits of R718 Turbo-Compression Cycle Using 3-Port Condensing Wave Rotors," in *ASME International Mechanical Engineering Congress and Exposition*, Anaheim, California, 2004.

[158] A. A. Kharazi, P. Akbari, and N. Müller, "Preliminary Study of a Novel R718 Turbo-Compression Cycle Using a 3-Port Condensing Wave Rotor," in *ASME Turbo Expo 2004: Power for Land, Sea, and Air, 381-388*, Vienna, 2004.

[159] A. A. Kharazi, P Akbari, and N. Müller, "Preliminary study of a novel R718 compression refrigeration cycle using a three-port condensing wave rotor," *J. Eng. Gas Turbines Power ,* vol. 127, no. 3, pp. 539-544, 2005.

[160] N. Müller, "Woven turbomachine impeller". United States Patent 60/627,423, 12 November 2004.

[161] A. A. Kharazi, P. Akbari, and N. Müller, "Preliminary study of a novel R718 compression refrigeration cycle using a three-port condensing wave rotor," *J. Eng. Gas Turbines Power ,* vol. 127 , no. 3, pp. 539-544, 2005.

[162] A. A. Kharazi, P. Akbari, and N. Müller, "Implementation of 3-port condensing wave rotors in R718 cycles," *J. Energy Resour. Technol,* vol. 128, no. 4, pp. 325-334, 2006.

[163] M. Hirceaga, F. Iancu, and N. Müller, "Wave rotors technology and applications," in *The 11th International Conference on Vibration Engineering*, Timisoara, Romania, 2005.

[164] F. Iancu, J. Piechna, and N. Müller, "Basic design scheme for wave rotors," *Shock Waves ,* vol. 18, no. 5, p. 365–378, 2008.

[165] Fastcam SA5 Hardware Manual, Tokyo (Japan): Photron limited, 2009.

[166] W Ziniu , X Yizhe, W Wenbin, and H Ruifeng, "Review of shock wave detection method in CFD," *Chinese Journal of Aeronautics ,* vol. 26, no. 3, pp. 501-2013, 2013.

[167] Y. Dai, S. Zhang , S. Tao , and D. Hu, "Superposition of two incident shocks in R718 vapor flows," *International Journal of Heat and Fluid Flow,* vol. 65, pp. 159-165, 2017.